IMPROVING FORCE CONTROL THROUGH END-EFFECTOR VIBRATION REDUCTION AND VARIABLE STIFFNESS JOINT DESIGN

LI RENJUN

NATIONAL UNIVERSITY OF SINGAPORE

2014

IMPROVING FORCE CONTROL THROUGH END-EFFECTOR VIBRATION REDUCTION AND VARIABLE STIFFNESS JOINT DESIGN

LI RENJUN

(B.Eng. (Hons.), NUS)

A THESIS SUBMITTED

FOR THE DEGREE OF DOCTOR OF PHILOSOPHY
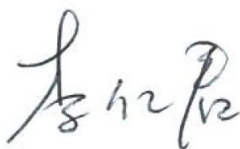
DEPARTMENT OF MECHANICAL ENGINEERING

NATIONAL UNIVERSITY OF SINGAPORE

2014

DECLARATION

I hereby declare that the thesis is my original work and it has been written by me in its entirety. I have duly acknowledged all the sources of information which have been used in the thesis.

This thesis has also not been submitted for any degree in any university previously.

_____

Li Renjun

08 January 2014

Acknowledgements

I would like to express my most sincere gratitude to my supervisor, Associate Professor Chew Chee-Meng for his patience and valuable guidance during the course of my Ph.D. study. His depth of knowledge, insight and untiring work ethic has been and will continue to be a source of inspiration to me.

I would also like to thank the staffs in Singapore Institute of Manufacturing, particularly Dr. Lim Chee Wang, Dr. Vuong Ngoc Dung and Dr. Li Yuanping for their support and help during my study. I want to thank them for their motivation, support, and critique about the work.

I have also benefitted from discussion with many of seniors and colleagues. In particular Wu Ning, Shen Bingquan, Tan Boon Hwa and others in the Control and Mechatronics Lab.

I also would like to thank National University of Singapore for offering me research scholarship and research facilities. I benefitted from the abundant professional books and technical Journal collection at NUS library.

Finally, I would like to devote the thesis to my family for their love and understanding.

Table of Content

Summary

In this thesis, the author proposed two approaches to improve robotic force control performance. Two commercially recognized force control methods were studied and solutions were proposed to resolve the issues in these two methods.

Conventional manipulators typically are designed for repetitively position controlled applications. They are normally constructed using transmission systems, such as gears, to increase the load capacity and position accuracy. Their large inertia and non-back-drivability due to the transmission system make the robots very sensitive to disturbances, especially at high frequencies. In many applications, high frequency disturbances are inevitable due to the relative motion between the end-effector and the environment. Therefore, this research is aimed to study various ways of improving the force control performance.

In this thesis, the author constructed a dynamic model to analyze robotic force control. Two approaches of improving the performance from both manipulator level and joint level were explored in this thesis.

The first method of improving force control performance from the manipulator level involves using a conventional manipulator to carry a high performance end-effector. However, internal vibration has been found in such a system despite of its good performance. Thus, a design and control guideline named Zero Coupling Impedance criterion has been proposed to handle the vibration. The Zero Coupling Impedance criterion aims to decouple the high performance mini manipulator from the conventional macro manipulator so that the performance of the mini will not be limited by the macro.

The second method aims to modify the conventional manipulator design from joint level such that it is suitable for force control. However, many existing variable stiffness joints have non-linear load-displacement relationship, which tends to induce relatively large contact force when high frequency disturbance presents. Therefore, a new variable stiffness joint has been proposed to address the problem. Theoretically, the novel variable stiffness joint has a linear load-displacement relationship, with stiffness ranged from zero to infinity. This guarantees that the joint mechanism could be widely used in all types of applications. Furthermore, designing controller for the proposed variable stiffness actuator can be easy since the system can be a linear system.

Simulation and experiments were performed to verify the effectiveness of the proposed methods. A Mitsubishi PA-10 robot and a linear voice coil actuator were used to form a series macro-mini manipulator. The force control performance during grinding showed that the Zero Coupling Impedance criterion is effective in suppressing the vibration in a series macro-mini manipulator system. Furthermore, a variable stiffness joint using level mechanism has been built and tested. Experiments have shown that the novel variable stiffness joint design using a lever arm mechanism with constrained ends successfully decoupled the stiffness from the output load.

In conclusion, this thesis has provided two approaches to improve force control performance. The Zero Coupling Impedance criterion could be used to improve the performance of a series macro-mini manipulator while the novel joint design provided a possibility to build a new generation manipulator using compliant joint mechanism.

List of Table

List of Figures

Chapter 1

Introduction

1.1 Background

In the past few decades, robots have been widely employed in industries to increase productivity. Conventional industrial applications such as wielding, picking and placing, emphasize positional accuracy and repeatability. Most of the current industrial robot design is suited for this type of tasks, mainly using position and velocity control. Therefore, robots are designed to be rigid to ensure positional accuracy.

In contrast to these conventional non-interactive applications, interactive processes such as grasping, assembling, and machining require the robot to be able to handle the interaction between itself and the objects. In these processes, pure motion control, which controls the positional trajectory, turns out to be inadequate because of the unavoidable modeling error and uncertainties in both environment and robot. Therefore, large contact force may be resulted, especially when dealing with rigid environment. In order to accommodate large force that may be caused by position error during interaction, force control is introduced to replace motion control. Many methods to deal with interaction between robot and environment have been reported in literature[1, 2]. However, most of the industrial manipulators are designed to be rigid to ensure position accuracy in position controlled applications. The ability to handle interaction that is limited by robot structure cannot be easily improved using pure active control methods. Improving force control performance from the structural design perspective has been widely explored. Many different methods have been proposed [3-7], among which, reducing the robot impedance is one of the most effective approach. In this thesis, two methods of improving force control performance will be discussed.

The first method of force control applies the force from the end-effector whose position is controlled by the robot arm. An example of force control using end-effector approach is a series macro-mini manipulator [8], which uses a macro robot to carry a mini robot to deliver the force. The combined macro and mini manipulator system usually has the features of both systems, such as large workspace, small inertia and high control bandwidth [6]. However, the serially coupled system also suffers from one of the main issues of the macro manipulator, namely, the low frequency resonant modes. The low frequency resonant modes normally cause vibration in the robot and therefore, degrade force control performance. Several effective approaches have been developed to suppress the vibration [8-10]. However, these methods may not be easily implemented on commercial industrial manipulators due to control architecture that is closed, i.e., user cannot modify the joint control algorithms. Therefore, more effort needs to be made to eliminate the vibration effect by taking the limitation of the macro manipulator into consideration.

The second method of force control applies force through passive compliant joints. In force control, joint compliance can be realized either through active control or passive mechanisms. Active control methods such as active stiffness control [11], damping control [1] and impedance control [12] regulate the robot behavior based on force sensor measurements to deliver the force required. Force control using this approach usually encounters large contact force when high frequency disturbance is present. On the other hand, passive mechanism approaches that use spring [7] or damper [13] to deliver the force could effectively reduce the large contact force due to high frequency disturbance. Further research on the compliant joints has led to the development of variable stiffness actuators, which can be used in more applications. However, most of the variable stiffness actuators cannot decouple the stiffness from the output load, i.e., the stiffness changes if the output is changed. This makes the controller design more complicated. It may also result in higher contact force due to the change in the stiffness. Furthermore, many of the variable stiffness actuators were designed for a special purpose and may not be used in different applications. For example, in order to make the robot inherently safe when interacting with human, stiffness

should not be too high. This has eliminated the needs of high stiffness. Hence, these types of robot will not be suitable for tasks that need positional accuracy.

This thesis aims to improve force control using both approaches. For the first approach, the dynamics of a series macro-mini manipulator system will be analyzed. The internal vibration problem due to the low frequency resonant modes of the macro manipulator will be addressed. For the second force control approach, robot joints with variable compliance will be studied and a new design will be proposed. The non-linear load-displacement relationship which exists in many works will be properly handled through mechanical design.

1.2 Research Objective and Contributions

Controlling interaction between robot and environment remains a challenge, especially in a rigid environment. The key challenge is to reduce the robot impedance such that the contact force is less sensitive to disturbance. Both force control approaches, through series macro-mini manipulation and through compliant joint mechanism, will result in systems with smaller impedance. The main research gaps in these two approaches are identified as follows:

- For force control through end-effector, most macro-mini manipulator systems suppress the vibration by regulating the impedance of the macro manipulator. However, commercial robot manufacturer may not allow users to modify the robot dynamics arbitrarily. Suppressing vibration from the mini manipulator is necessary.
- For force control through compliant joints, most of the variable stiffness joints are designed to have non-linear load-displacement relationship. It makes controller design more complicated since systems become non-linear when interacting with environment. Furthermore, stiffness range in many designs is also limited. Hence, a robot designed for one application may not be used for another application. A new variable stiffness joint mechanism with linear load-displacement relationship and wide stiffness range needs to be developed. .

3

The main objective of this thesis is to improve force control through modifying robot structures. This objective can be further divided into two objectives:

- Minimize vibration in a series macro-mini system in all postures through controlling mini manipulator only;
- Develop a variable stiffness joint with linear load-displacement relationship and wide stiffness range.

In order to achieve the first objective, the dynamics of a series macro-mini manipulator system will be studied. A criterion named Zero Coupling Impedance will be proposed as a design guideline for series macro-mini manipulators. This criterion describes the condition to eliminate vibration in a series macro-mini manipulator as a general solution to improve the force control performance. A machining process, grinding will be used to demonstrate the advantage of the proposed approach.

The second objective is achieved by a lever mechanism with constrained ends. A novel variable stiffness joint based on a specially designed lever arm mechanism will be presented. The proposed mechanism will decouple joint stiffness from the output load, making the robot easier to control and less sensitive to external disturbance. Its achievable stiffness ranging from zero to infinity will ensure that it can be used in various applications.

The contributions of this thesis are as follows:

- Synthesis of dynamics of a series macro-mini manipulator system using block diagram method;
- Establishment of a Zero Coupling Impedance criterion as a general guideline to design a series macro-mini manipulator system for force control;
- Proposing a novel variable stiffness joint with linear load-displacement relationship and wide stiffness range;
- Developing control schemes for the variable stiffness joint to perform contact tasks.

This thesis will not address problems such as actuator saturation and driving source selection (for example, hydraulic, pneumatic, and electric, etc) for the variable stiffness joint.

1.3 Organizations of the Thesis

The thesis is organized as follows:

Chapter 1 provides a brief introduction to the motivation of the thesis and highlights the main contributions.

Chapter 2 presents the current research in robot force control field. Research work on force control approaches will be discussed.

Chapter 3 presents the proposed Zero Coupling Impedance criterion as a general design guideline for a macro-mini manipulator system. In this chapter, the dynamics of a series macro mini manipulator will be analyzed and mathematical model will be constructed. Instead of regulating the dynamics of the macro manipulator to suppress the vibration, this criterion provides another method by using only the mini manipulator.

Chapter 4 presents the novel variable stiffness joint designed for force control. In this chapter, the design requirement for the variable stiffness joint will be first identified. Then, several variable stiffness joints will be presented. Next, the novel variable stiffness that meets the requirements will be presented. Finally, characterization of the joint will be performed and controller will be designed to demonstrate contact searching process in interaction tasks.

Chapter 5 concludes the thesis with summarizing the results of the work in Chapter 3 and 4. The limitations of the work in this thesis will be presented and directions for future research will be given.

Chapter 2

Literature Review

Control of the physical interaction between the robot and the environment is crucial for the successful execution of manipulation. Most of the current industrial robot design is suited for conventional repetitive tasks, mainly using position and velocity control. Successful execution of manipulation tasks using industrial robot with motion control could be obtained only if the motion was accurately planned. However, planning accurate motion requires not only a good model of the robot, but also a detailed description of the environment, which is usually difficult to obtain. If the robot motion is not planned accurately, large contact force may be generated since industrial manipulator usually are bulky and heavily geared. This drawback could be overcome if a compliance behavior, through either passive or active approach, is ensured during the interaction [14].

In passive interaction control, the trajectory of the robot end-effector is modified by the interaction force due to the inherent structural compliance of the joint, link, and end-effector. It does not require force/torque feedback to close the control loop. Since trajectory of the end-effector is pre-defined and no feedback is used, large contact force may still occur.

In active interaction control, the compliance is mainly ensured by the control system. In this approach, the contact force and/or the motion (position and velocity) can be measured and fed back to the controller to generate online the desired trajectory of the robot end-effector.

However, due to the fact that the commercial industrial robots are usually bulky and heavily geared, force control using this type of robot is slow. Different methods have been adopted to overcome this drawback by modifying the structure of the robots.

In the following section, several active interaction control methods will be introduced and discussed first. Then, two methods of modifying the robot

structure, namely series macro-mini manipulation and re-designing robot using force control actuators will be presented.

2.1 Active Interaction Control

An active interaction controlled system was first implemented in 1960s by Rothchild and Mann on a powered artificial elbow for amputees [1]. A modification to the robot trajectory was calculated from the force sensor feedback and ideal force source was assumed. Numerous effort has been put into this area ever since, and several methods have been developed.

• Active stiffness control performs like a programmable spring through position feedback and/or force feedback [11, 15, 16]. Stiffness is specified in the work space and joint torque command is calculated based on the difference between the desired and actual end effector position. Therefore, the robot becomes compliant according to the user specification.

• Similar as active stiffness control, active damping control works as a virtual damper. It integrates the force feedback and velocity feedback to modify the velocity command [1, 17]. It is commonly used to damp out the disturbance and increase the system stability [18, 19], such as when the robot is searching for contact.

• In impedance control [20], mechanical impedance is defined as force over velocity. This controller is designed to regulate the relationship between force and motion instead of tracking the force trajectory. It is a more general case of force control and can be considered as a combination of stiffness control and damping control [21]. In impedance control, position, velocity and force feedback are used to modify the robot mechanical impedance. It also eliminates the need to calculate inverse kinematics, which is tedious in most cases. It has been successfully implemented in various forms, utilizing different types of sensors. However, impedance control focuses on regulating the mechanical impedance rather than tracking the force trajectory. In order to regulate the contact force in impedance control frame, the desired position and

velocity can be modified based on the system impedance and the desired contact force [22-24].
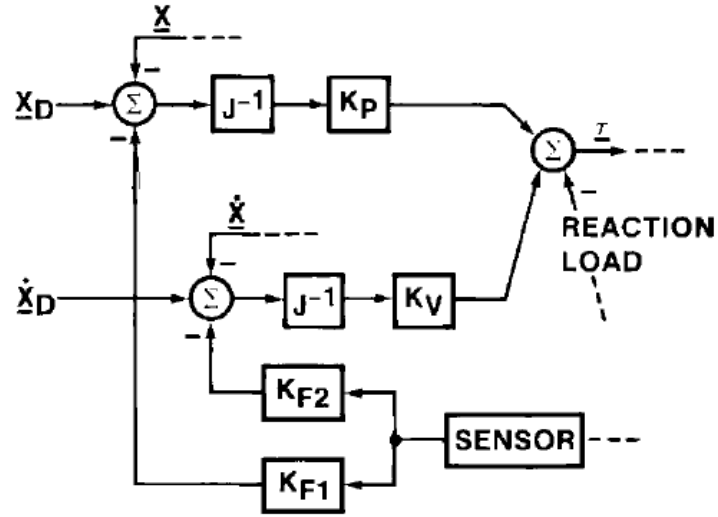
Figure 2.1: Impedance control [1]

- In admittance control, mechanical admittance is defined as velocity over force, which is the inverse of the impedance in definition. The underling concept is to use position controlled robot as a baseline system and modify the admittance of the system to track a force trajectory [25, 26]. Compared with impedance control, admittance control focuses more on the force tracking [27].

- Hybrid position/force control is a combination of conventional position control and force control. The workspace is defined as two orthogonal workspaces for displacement and force separately [28, 29]. Anderson and Spong [30] later proposed hybrid impedance control which provides a designer with more flexibility in choosing the desired impedance.
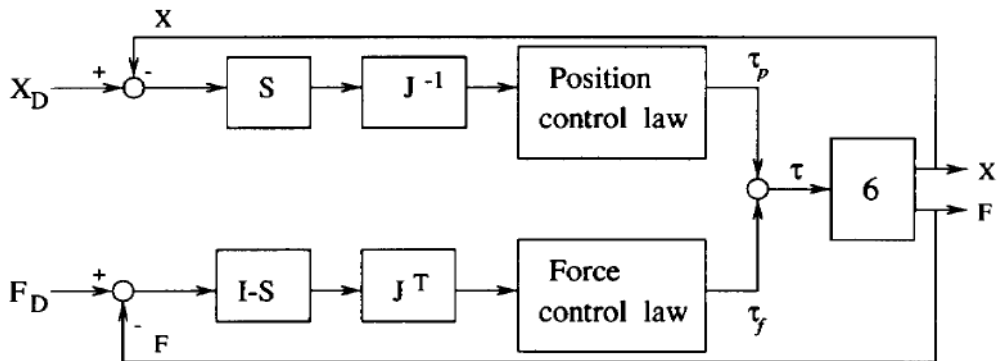
Figure 2.2: Hybrid position/force control [2]

8

In many applications, the environment and the robot dynamics are not known exactly. This raises the challenge of robot force control. Based on the basic control techniques discussed above, some advanced force control techniques have been developed, such as adaptive force control [25, 31, 32] and robust force control [33-35]. Learning algorithm has also been applied to the force control field [36, 37].

Above are the common active force control algorithms. However, researchers have realized that without proper hardware, it is difficult to perform good force control. The system performance is significantly bounded by the mechanical structure due to large inertia, non-linearity and limited energy input, etc. For example, electro-magnetic motor are commonly used as the power source of robot manipulators. Due to their limited power-mass ratio, transmission mechanisms such as gears are usually used to amplify the output torque/force. The transmission mechanism introduces flexibility, friction and non-linearity into the system, which degrades the system bandwidth and stability significantly [38]. Furthermore, many of the above force control methods need to use filter to handle the noise in the feedback signal and also use integral action in control to track the reference. These actions are usually necessary, but they will further decrease the system stability [39]. Therefore, modification to the mechanical structure is necessary.

2.2 Force Control Using Series Macro-Mini Manipulation

Sharon and Hardt [40] proposed the concept of series macro-mini (or macro-micro) manipulation system as a minimal modification to the conventional industrial manipulator system.

As it is shown in Figure 2.3, this system consists of two manipulators, a macro and a mini (or micro) in series to perform force control together. It normally employs a general purpose industrial manipulator as the macro manipulator, to carry a specially designed end-effector, the mini manipulator, to perform force control. The macro manipulator determines the lower bound of the coupled system while the mini manipulator determines the upper bound of the system. This means that the maximum bandwidth of the coupled system will be

determined by the mini manipulator while the minimum bandwidth will be determined by the macro manipulator. In this approach, force control is done by the end-effector carried by the arm instead of the arm itself. Khatib [41, 42] has shown that the impedance of the series macro-mini system is significantly smaller compared to the conventional manipulator. Hence, compared with a single macro manipulator, manipulator in this configuration will be relatively less sensitive to disturbance that is caused by the interaction between the robot and the environment.
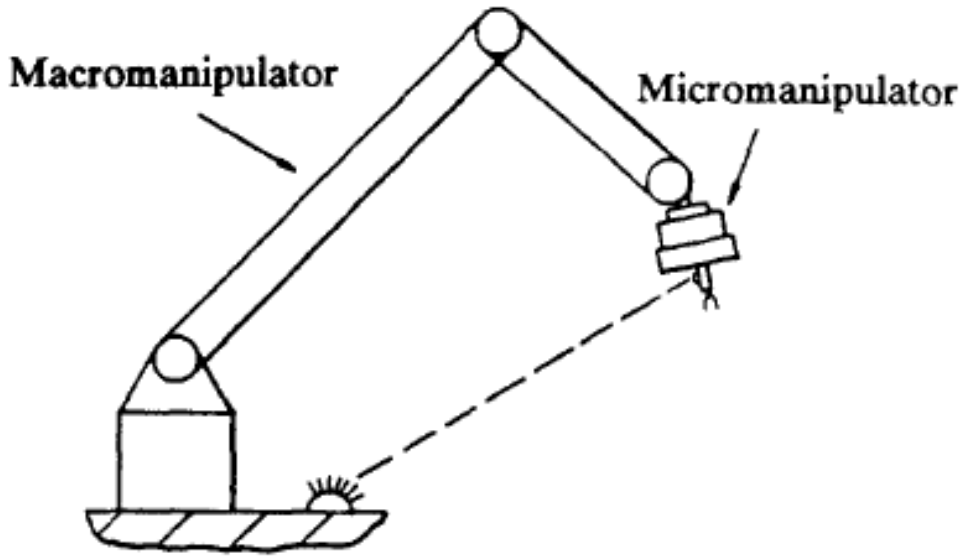
Figure 2.3: Concept of series macro-mini manipulator system[40]

The series macro-mini manipulator system possesses the advantage of both system, such as large work space, low impedance and high control bandwidth. However, it also suffers from the drawbacks of both manipulators, especially the low frequency resonant modes of the macro manipulator. Research on the dynamics of industrial manipulators showed that many industrial manipulators have low resonant frequencies. For example, in an ABB IRB6600 robot, the resonant frequencies in all six joints are around 10 Hz [43]. Vibration in such macro manipulator may be easily induced due to the low frequency resonant modes. Sharon and Hardt [8] proposed a solution to suppress the vibration using impedance matching method, which modifies the impedance of the macro manipulator to minimize the resonant peaks. It was shown that vibration was effectively removed from the system. Several other methods have been proposed to regulate the dynamics of the macro manipulator to

reduce the vibration. In [44], active damping control was applied to the macro manipulator to suppress the vibration. In [45], it used neural network based controller to cancel vibration from both macro and mini manipulator. These two methods could also effectively reduce the vibration in a series macro mini manipulation system. Controllers are designed for the macro manipulator.

The above methods suppress the vibration by regulating the dynamics of the macro manipulator. These solutions are intuitive since the problem of vibration is caused by the macro manipulator. However, many industrial manipulator manufactures do not provide interface for users to modify the robot dynamics arbitrarily due to their control architecture that is closed, i.e. users cannot modify the control algorithms. Another type of approach is to use external sensor to measure the vibration in a global frame [46]. Controllers may be designed in the mini manipulator to suppress the vibration. However, the need of external sensor increases the system complexity and may not be feasible.

Therefore, if no external sensor is used, suppressing the vibration through the mini manipulator is necessary for force control through the end-effector approach. This problem will be discussed in detail and addressed in Chapter 3.

2.3 Force Control Actuators

Another approach of improving force control is generating force through passive mechanisms. Problems that originated from robot large impedance in force control could be effectively addressed by using non-rigid robot joints. Therefore, many researchers have started to develop mechanisms that are suitable for force control tasks.

2.3.1 Series Elastic Actuator (SEA)

In 1995, Pratt and Williamson [7] proposed the concept of Series Elastic Actuator (SEA) suggesting that compliant joint should be used instead of rigid joint in force control. In SEA, as shown in Figure 2.4, an elastic element is placed between the actuator and the output shaft to address the high impedance problem. The elastic element limits the actuator impedance to be

the stiffness of the spring at high frequency. It converts a force control problem into a position control problem. Further improvement has been made to enhance the SEA performance [47-49].

However, the introduction of the compliant element limits the bandwidth of the system and reduces the stability margin greatly. This would be problematic if the tasks require high bandwidth such as in industrial machining. Moreover, the stiffness chosen at the design stage may limit the usage of such joint in different applications. For example, when interacting with stiff environment, it may require the system stiffness to be low such that large contact force may be properly handled. When dealing with soft environment, the system stiffness may be required to be relatively high to provide enough force.
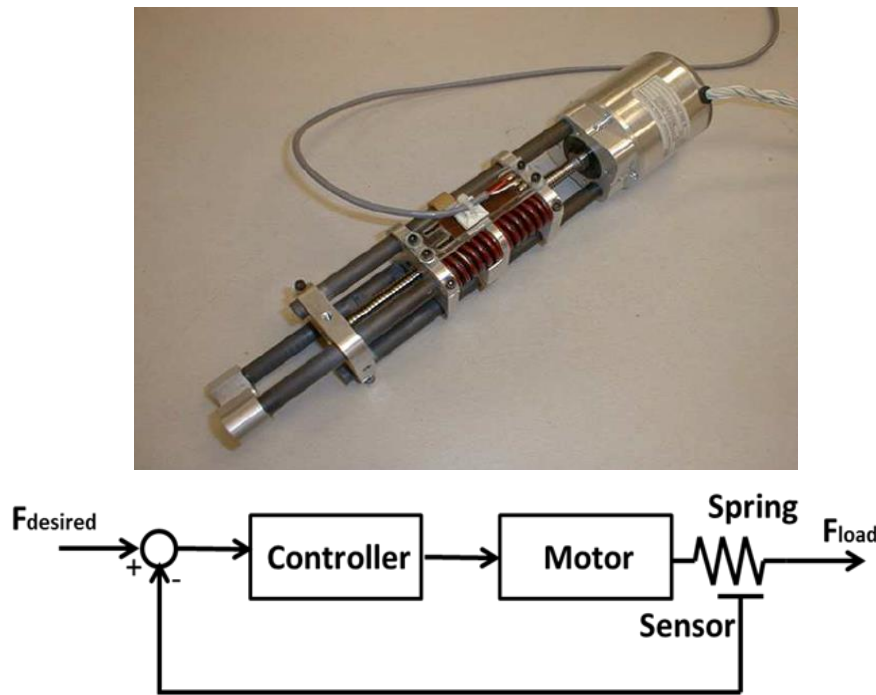
Figure 2.4: Series Elastic Actuator (SEA) [50, 51]

Despite of the limitations of the SEA, the idea of compliant joint has enabled researchers a new way of designing a robot. Many works have been demonstrated in literature to further improve force control performance.

2.3.2 Parallel Actuation

A parallel dual actuator system, Parallel Coupled Micro-Macro Actuator (PaCMMA) was first proposed by Morrell and Salisbury [52]. Then, the concept was further developed by Zinn et al, known as the Distributed Macro-Mini manipulator system (DMM^2) [53].

(a)   (b)
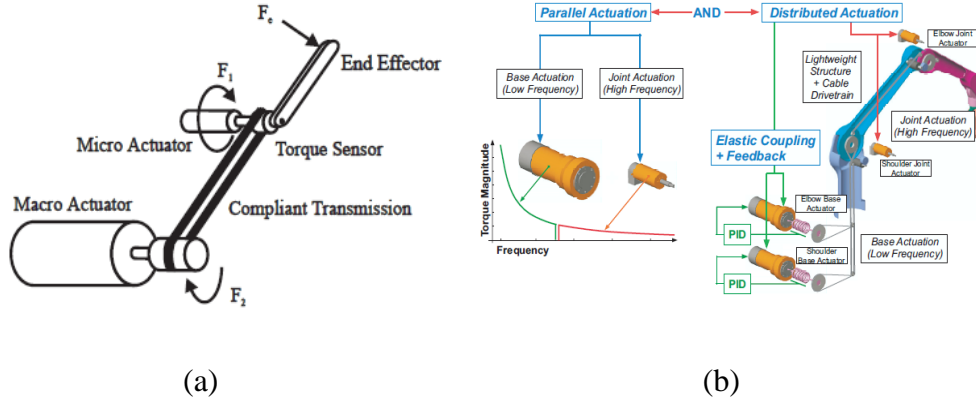
Figure 2.5: (a) Parallel Coupled Macro-Mini manipulator [52]; (b) Parallel-Distributed actuation [53]

The output force in the parallel coupled joint is partitioned into low and high frequency region and is achieved by a macro and a mini actuator, respectively. In both works, the macro actuators have low impedance but slow response. In PaCMMA, a normal motor with gear is used as the macro and a spring is placed in between the macro actuator and the output link to generate compliant transmission, as shown in Figure 2.5(a). The mini manipulator is a direct drive actuator that is connected to the output link in parallel with the macro. In the DMM^2 manipulator system, as shown in Figure 2.5(b), a SEA is used as the macro actuator which has low output impedance but low controllable bandwidth. A smaller actuator with a single stage of gear transmission is used as the mini actuator to ensure low inertia and high bandwidth. It is used to compensate for the phase lag due to the macro actuator to provide high frequency force output.

The overall system could achieve relatively low impedance and high bandwidth. However, the amount of force that the mini manipulator could provide determines its effectiveness. For example, if the maximum force that

13

the mini manipulator can provide is too small, the system is approximately equal to a SEA system.

2.3.3 Series Damper Actuator (SDA)

Series Damper Actuator (SDA), as shown in Figure 2.6, was first proposed by Chew et al [13], using a damper to replace the elastic element in SEA. A rotary magneto-rheological (MR) fluid damper was used in the first prototype to achieve damping effect. When subjected to a magnetic field, the fluid greatly increases its apparent viscosity. Force control is achieved by controlling the velocity of the damper's rotor with respect to the housing.
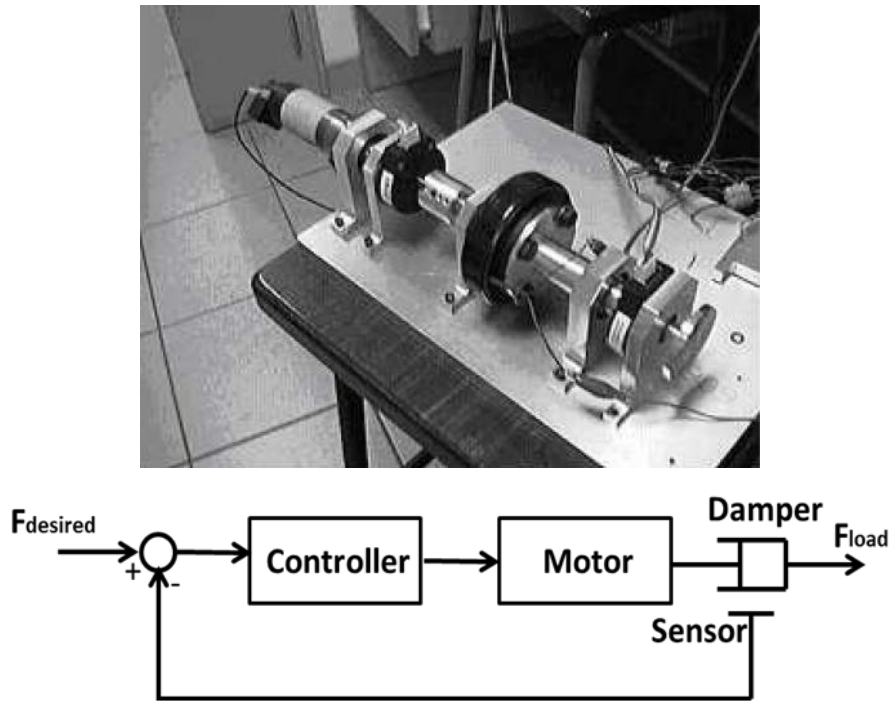
Figure 2.6: Series Damper Actuator (SDA) [13]

SDA has good impact tolerance and could achieve zero force effectively. However, efficiency of the damper should be increased and the non-linearity of the MR fluid damper should be overcome. Furthermore, the ease of controlling the magnetic field makes varying the damping coefficient possible.

2.3.4 Variable Stiffness Actuator (VSA)

The stiffness of a traditional SEA is fixed, which imposes large limitation on the performance of SEA. Therefore, the usage of SEA is limited, especially in

applications that changing stiffness is required. This has led to the research on variable stiffness actuators.

2.3.4.1 Variable Stiffness Mechanism Based on Pretension Non-linear Spring

Variable stiffness actuators usually employ two actuators to control the output torque and the stiffness. Depending on the working principle, the two actuators are used for different purposes. Some variable stiffness joint mechanisms are realized by use of non-linear spring mechanisms and controls the stiffness through pretension of a spring [54, 55].

(a)   (b)

Figure 2.7: (a) Variable stiffness mechanism DLR-VS [54]; (b) Mechanical for Varying Stiffness via changing Transmission ANgle (MESTRAN) [55]

For example, in the work of VS-Joint [54] (as shown in Figure 2.7(a)) the non-linear spring mechanisms are constructed using roller-cam systems. One end of the linear spring is connected to a position controlled motor to deliver the torque required while the other end of the spring is connected to the output link through the roller-cam system. Thus, the non-linear motion relationship between the two ends of the springs creates non-linear stiffness. A secondary motor is then used to vary the stiffness by adjusting the pretension of the spring. Therefore, for the same passive deflection, the stiffness can be controlled. Variable stiffness joint designed based on this method usually has non-linear load-displacement relationship. Hence, the stiffness changes when the output load is changed.

MESTRAN [55] (Figure 2.7(b)) has similar working principle except the shape of the cam is designed in such a way that the stiffness is controlled only by the stiffness motor. This design has decoupled the stiffness from the output load, making controller design easier. However, the accuracy of the cam dimension is critical.

2.3.4.2 Variable Stiffness Mechanism Based on Antagonistic Actuation

Another commonly used configuration, antagonistic actuation also takes the advantage of non-linear spring mechanisms. It is a mimic of the human arm which is driven by two non-linear stiffness actuation mechanisms, the muscles. In this configuration, two non-linear spring mechanism are coupled in parallel to drive the output link together [56-60].
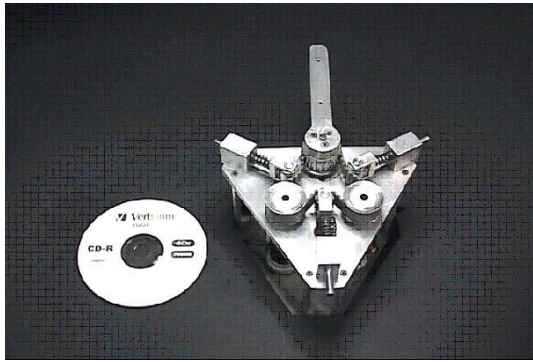
(a)   (b)
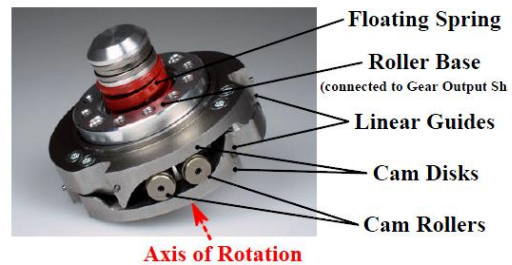
(c)   (d)

Figure 2.8: (a) Prototype of VSA [57]; (b) Prototype of VSA-II [56]; (c) Quadratic series-elastic actuation [58]; (d) DLR Floating Spring Joint [61]

Each non-linear spring mechanism is driven by a position controlled motor. However, most of the antagonistic actuation systems, such as the mechanisms shown in Figure 2.8(a), (b) and (d), also have non-linear load-displacement relationship. This will result in changing of stiffness involuntarily when load changes. In Figure 2.8(a), the non-linear spring mechanism is realized by compressing a linear spring through a belt. The force component along the spring becomes smaller when the spring is compressed. Thus, the output stiffness is changed. In Figure 2.8(b), a four bar linkage is used to form the non-linear spring mechanism. The relationship between the output load and the deflection changes when the four bar linkage moves. In Figure 2.8(d),the design used similar mechanism as in DLR-VS [54] to create non-linear spring mechanism. DLR-VS [54] uses this mechanism with a preset mechanism to adjust the stiffness while VSA-II uses two of this mechanism in parallel for form antagonistic actuation. . In [58] (Figure 2.8(c)) , the authors have demonstrated a new design which have a linear load-displacement relationship. Similar as in VSA-II, roller-cam mechanism is used and a quadratic spring is formed. Hence, a linear load-displacement relationship could be achieved. However, the stiffness range is limited due to finite motion range of the roller on the cam.

2.3.4.3 Variable Stiffness Mechanism Based on Adjustable Mechanical Structure

Another type of variable stiffness joint varies the joint stiffness by adjusting its mechanical structure. In [62, 63], stiffness is modified by adjusting the effective length of a leave spring, as shown in Figure 2.9(a). Hence, the minimum achievable stiffness usually depends on the length of the spring. CompAct-VSA [64] and AwAS-II [65] (Figure 2.9(b) and (c)) adjust the stiffness through controlling the position of the pivot point on a lever arm. In these two designs, the pivot positions are controlled by a secondary stiffness motor. The output shaft is connected to one end of the lever arm while a linear spring is connected to the other end. These works achieved approximated linear load-stiffness relationship, however, within a limited passive deflection

17

range. The advantage of this type of mechanism is the large achievable stiffness range, from zero to infinity.

HDAU joint [66] (Figure 2.9(d)) used two roller-cam mechanisms to change the moment arm length that are connected to springs. It could achieve linear load-stiffness relationship but maximum stiffness is limited due to the finite length of the arm. The achievable stiffness is ranged from zero to a finite value.

(a)

(b)

(c)

(d)
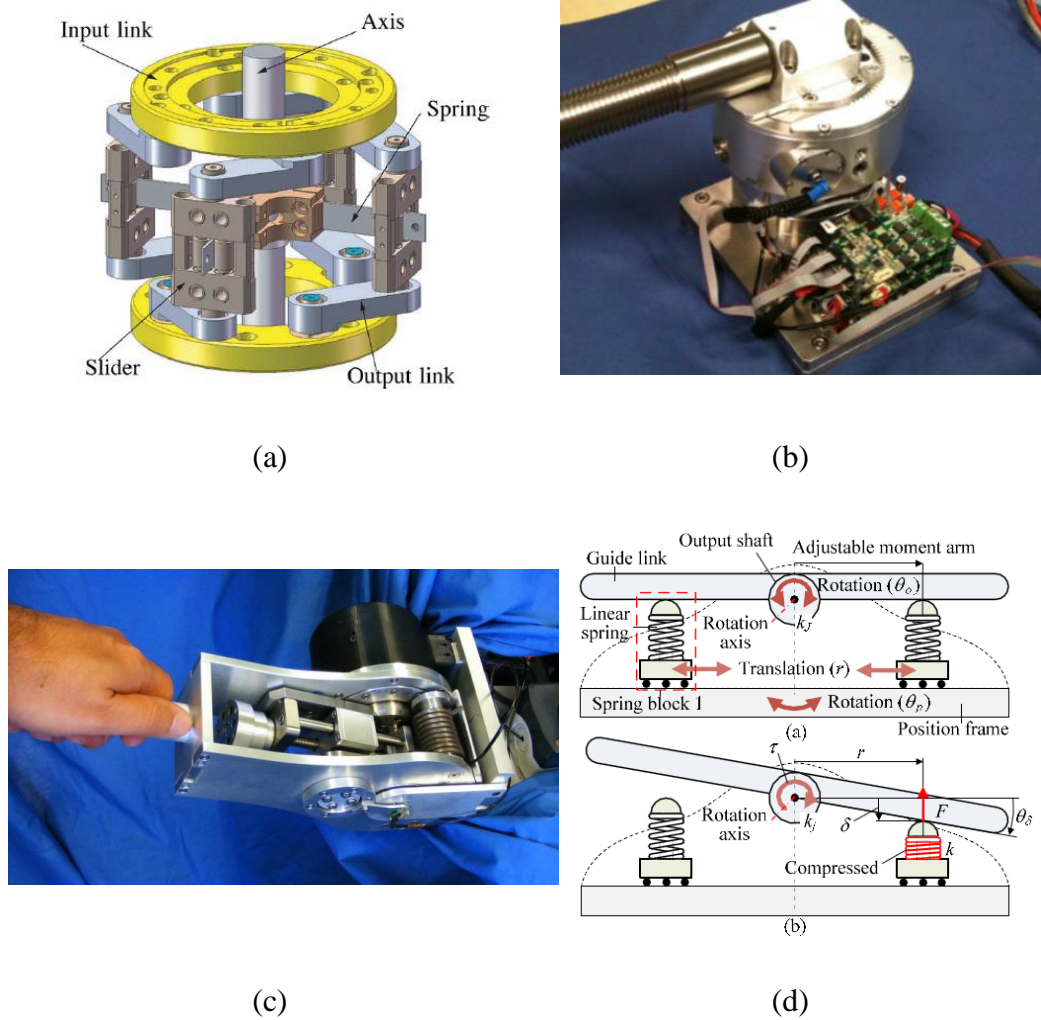
Figure 2.9: (a) CAD drawing of variable stiffness joint using leaf spring [62]; (b) CompAct-VSA [64]; (c) AwAS-II [65]; (d) working principle of HDAU [66]

Many of the variable designs have been successfully demonstrated in the humanoid or human involved applications. Maximum stiffness is usually limited to ensure safety and stiffness does need to be controlled precisely.

18

However, in many interaction processes, a linear load-displacement relationship is very important because high frequency disturbance is usually present. When subjected to high frequency disturbance, non-linear load-displacement relationship may result in larger contact force compared with a joint with linear load-displacement relationship. This will be illustrated further in Chapter 4. Therefore, a new design that is specially designed with linear load-displacement relationship is needed.

2.4 Summary

From the above review, it can be seen that robot force control still remains a challenge. The conventional commercial manipulators are not designed to perform force control. When they are directly used in interaction tasks such as robotic assembly and machining, the closed loop bandwidth is usually low and they are sensitive to disturbance. Modification to the mechanical structure of the conventional manipulator is necessary to bring robot into interaction applications, such as machining. Both force control approaches, through the end-effector and through passive compliant joints, change the traditional industrial manipulator into a force control orientated mechanism. The potential of increasing productivity and improving product quality using these two methods raise the needs to address the problems in these approaches. Therefore, this thesis aims to study both methods and improve both types of systems. More specifically, Chapter 3 will present a method to suppress the vibration in a series macro-mini manipulator system without modifying the dynamics of the macro manipulator; Chapter 4 will present a new variable stiffness joint that modifies the robot dynamics at the joint level to improve force control.

Chapter 3

Force Control Using Serial Macro-Mini Manipulator System

3.1 Introduction

Force control is required in many interactive applications. Amount these applications, robotic machining is one of the most challenging applications. During machining, a robot is constantly subjected to disturbances with different frequency components. Hence, it requires the robot to have both good force tracking and disturbance rejection ability. In robotic machining, the amount of material removed could be controlled by either controlling the motion of the tool, or controlling the force applied by the tool on the workpiece. The main objective of force control in machining is to control the contact force at the interaction point, such that the force between the tool and the workpiece follows the desired value. In this chapter, force control will be discussed in the context of machining.

There are two commonly used methods in commercial robots to perform machining through force control, through the end-effector and through all the joints [67]. Force control through end-effector uses additional mechanisms to deliver the torque while force control through all the joints uses all its joints to provide the output force. It is commonly known that conventional manipulators are not suitable for force control tasks due to poor force control performance caused by large inertia, flexibility in the joints and large friction in the transmission system. Sharon and Hardt [40] proposed the concept of series macro-mini manipulation system which consists of two manipulators in series: a mini manipulator with high bandwidth and low impedance carried by a macro manipulator with large work space. In this example of force control

through end-effector approach, force is delivered to the interaction point by the mini manipulator.

In a series macro-mini manipulator system, force control is carried out by the mini manipulator while the conventional manipulator, i.e. the macro manipulator, controls the position of the mini manipulator. As a result, the force control bandwidth is determined by the high performance mini manipulator and the work space is determined by the macro manipulator. Khatib [41, 42] has shown that the overall impedance of the macro-mini system is significantly lower compared to a conventional manipulator. Therefore, this approach maintains the features of both manipulators with minimal modification to the system.

However, since the non-rigid macro manipulator may start to vibrate even at low frequencies, it may still limits the force control performance of the serially coupled mini manipulator. In this system, the mini manipulator is mounted on a manipulator whose resonant modes are usually at low frequencies, any vibration of the macro manipulator will be transmitted to the contact point. To resolve this constraint, Sharon et al [6, 8], has used an impedance matching method to damp out the vibration in the macro manipulator by modifying the impedance of the macro manipulator. Other researchers have used different methods to control the dynamics of the macro manipulator in order to suppress the vibration [45, 46]. However, these approaches may not be always applicable, especially in industries. Many manipulators used in industries do not allow changes to be made to its basic dynamics due to the closed control architecture. For example, a user could specify a few set points for the robot to follow, but modifying joint stiffness or damping is not allowed since it may lead to unstable or other issues. Furthermore, using mini manipulator to compensate for the vibration is difficult since the resonant modes of the macro manipulator are posture dependent. Therefore, an alternative solution to minimize vibration without modifying the dynamics of the macro manipulator is needed.

In this chapter, a model of a series macro-mini manipulator system will first be constructed and analyzed. Based on the analysis, a design criterion for the

mini manipulator to minimize vibration in the system will be presented. Finally, the effectiveness of the criterion will be experimentally demonstrated.

3.2   Modeling of Series Macro Mini Manipulator Systems

In this section, a general mathematic model of a series macro-mini manipulator system is built to analyze the dynamics of such systems. A multiple Degree-Of-Freedom (DOF) series macro-mini manipulator system shown in Figure 3.1 is used as an example to derive the model. In this system, a mini manipulator is carried by a macro manipulator as its end-effector to perform force control. A machining tool is assumed to be carried by the mini manipulator, with a force sensor in between to measure the force. The tool and the environment are assumed to be in contact. Then，a general mathematic model can be derived to represent the dynamics of the series macro-mini manipulator system.

In this thesis, it is assumed that the end-effector maintains in contact with the surface of the workpiece at all time. In the model, a spring and a damper is used to represent the contact between the robot and the environment. These elements could provide both positive and negative force. However, in practice, the robot end-effector could only be pushed by the environment. Hence, if the contact force is shown to be negative, it indicates the end-effector has left the surface which should be avoided. The dynamics of the robot when the tool leaves the surface will not be analyzed. Furthermore, it is also assumed that the robot is not at singularity.
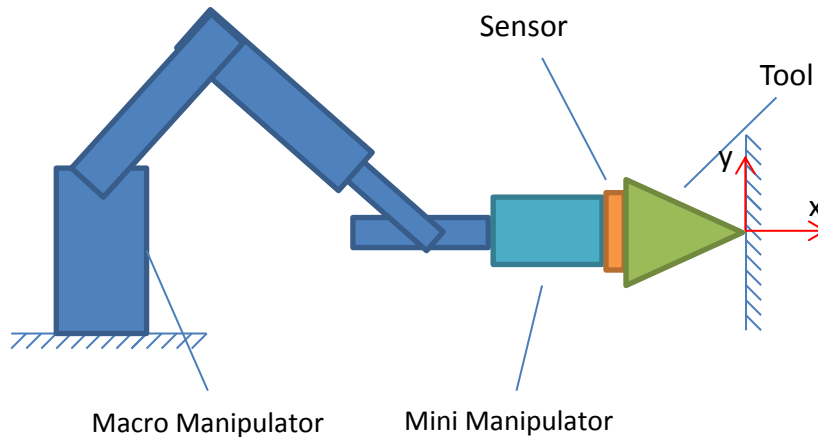
Figure 3.1: A series macro mini system

3.2.1 Lumped Mass-Spring-Damper Representation

In this thesis, linear model is used to present the system near the operating point. The macro manipulator is assumed to be under position control and always stable. Hence, passive mass-spring-damper systems are used to represent the macro manipulator, as shown in Figure 3.2. This linear system model is well suited to our purpose of developing useful insight about how systems behave. In Figure 3.2, several mass-spring-damper blocks (with parameters K_{ri}, M_{ri} and B_{ri}, where $i = 1, 2, \ldots n$) are used to represent the multiple Degree-Of-Freedom macro manipulator while a mass block is used to represent the mini manipulator (with parameters M_m). The force sensor is modeled by a spring-damper (with parameters K_s and B_s).
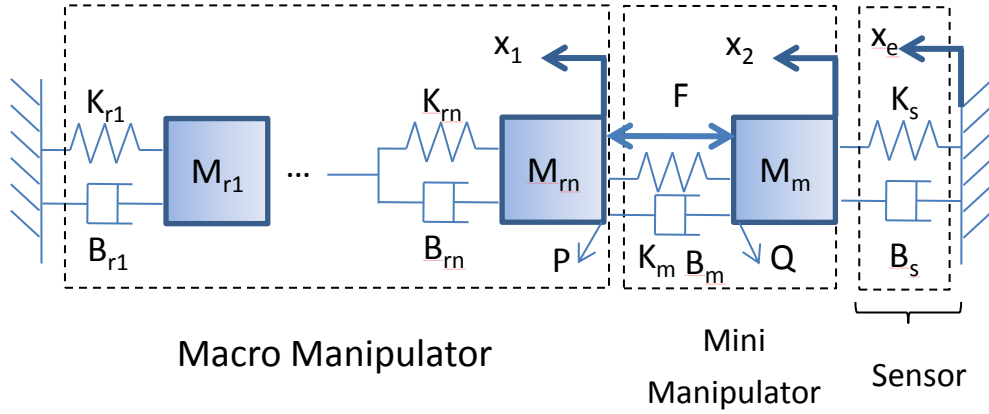
Figure 3.2: Modeling of series macro mini manipulator using lumped mass-spring-damper

3.2.2 Block Diagram Representation

From Figure 3.2, system transfer function could be derived by analyzing each free body diagram. However, the calculation is tedious and it will be difficult to isolate the effect of each component on the system dynamics. Therefore, in the following figure, a block diagram representation of the lumped mass-spring-damper model is constructed.

Figure 3.3(a) shows a single block of mass-spring-damper block. It could be represented in block diagram as shown in Figure 3.3(b). In this system, both F_1 and x_2 can be seen as the input while x_1 and F_2 are the corresponding output. Then, the blocks shown in Figure 3.3(b) can be replaced by their impedance and admittance.

(a)   (b)
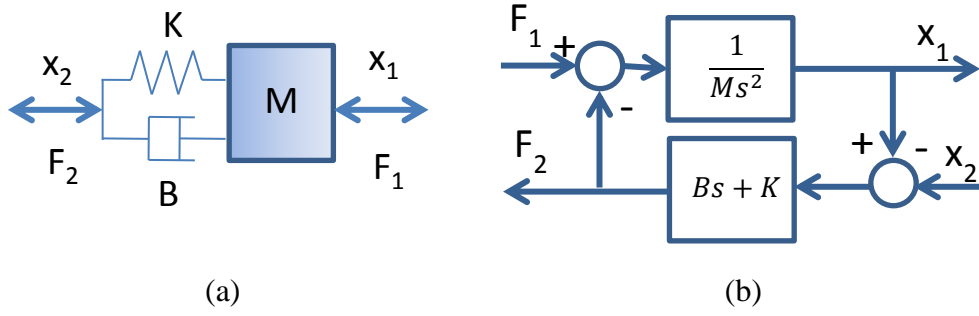
**Figure 3.3: (a) Single block of mass-spring-damper block; (b) block
diagram representation of the single block of mass-spring-damper block**

In this thesis, we define the coupling impedance between two elements as the
ratio of total force $(F(s))$ over the relative motion $(X(s))$, i.e.,

$$Z(s) = \frac{F(s)}{X(s)}$$ (**3.1**)

And similarly, the admittance between two elements is defined as the ratio of
the relative motion $(X(s))$ over the total force $(F(s))$, i.e.,

$$Y(s) = \frac{X(s)}{F(s)}$$ (**3.2**)

Hence, the block diagram shown in Figure 3.3(b) could be represented as in
Figure 3.4:
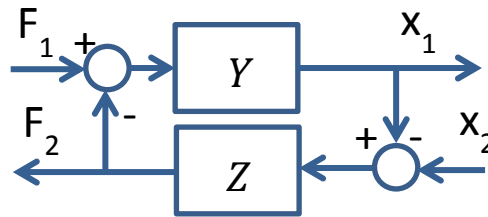
Figure 3.4: Block diagram represented using impedance and admittance

This block diagram represents the interaction between different blocks. Y
represents the admittance of the mass (M) while Z represents the impedance of
the spring (K) and damper (B). The force F_1 represents the force exerted on
the mass at one point while the output from Z that is fed back to Y represents
the reaction force from the spring and the damper acting on another point. The

input and feedback in the block diagram forms force and reaction force on the mass.

If F_1 is the input and x_1 is the output of the system, the block in Figure 3.4 can be seen as an admittance block. Similarly, if x_2 is the input and F_2 is the output of the system, the block can be seen as an impedance block.

This method simplifies the modeling process of a series manipulator. Figure 3.5 shows two mass-spring-damper blocks coupled in series. It could be seen that this block has the same form as a single mass-spring-damper: two inputs F_1 and x_2, two corresponding outputs x_1 and F_2. Hence, it could be further extended into more complex system as shown in Figure 3.6.

(a)   (b)
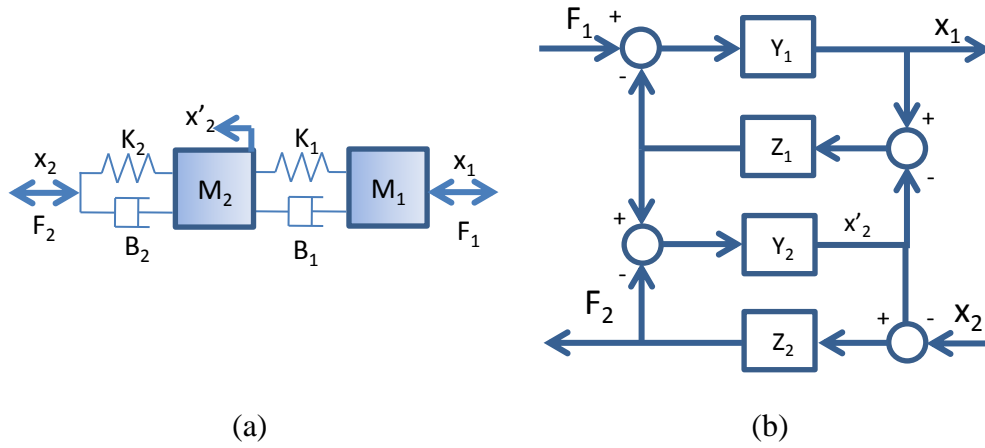
Figure 3.5: (a) two mass-spring-damper blocks in series; (b) block diagram representation

(a)   (b)
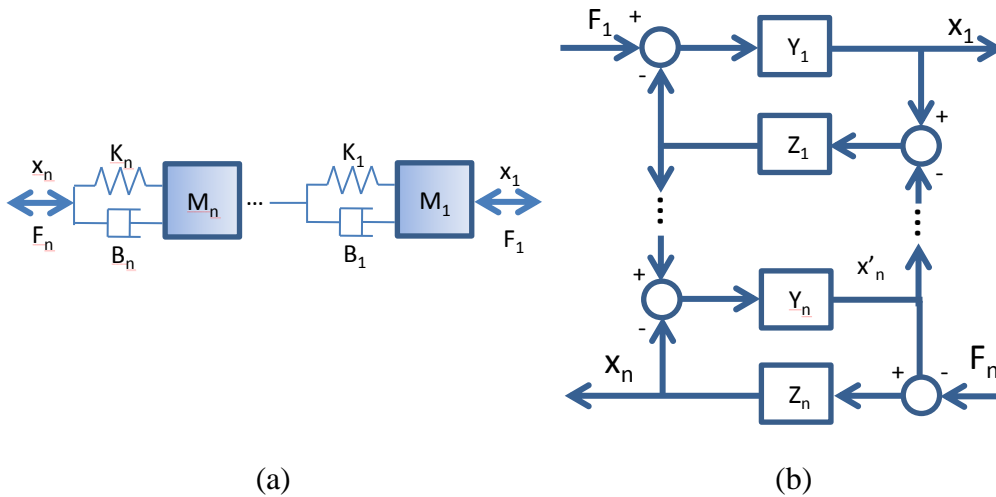
Figure 3.6: (a) *n* mass-spring-damper blocks in series; (b) block diagram representation

The above analysis shows that using this method, a very complex serial robot system can be separated into different sub-systems. The dynamics of each sub-system could be analyzed separately.

Following the above method, the macro-mini manipulator system in the block diagram form is shown in Figure 3.7. The macro manipulator is lumped together and represented by its admittance at point P (in Figure 3.2), Y_1 while the mini manipulator is represented by its admittance at point Q (in Figure 3.2), Y_m. Z_S and Z_m are the impedance of the sensor and the coupling between the macro and mini, respectively. F is the force applied by the mini manipulator while F_c is the contact force.
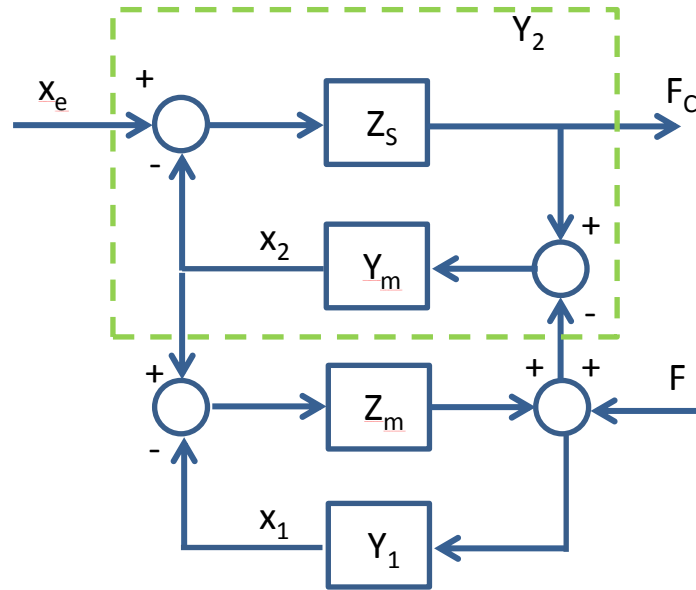
Figure 3.7: Block Diagram representation of the series macro mini system

Based on this figure, the transfer function of a serially connected system can be derived.

Let the contact force be:

$$F_c(s) = (B_s s + K_s)F(s) \tag{3.3}$$

And the impedance of the coupling between the macro and the mini is:

$$Z_m(s) = B_m s + K_m \tag{3.4}$$

26

The system transfer function without feedback between the contact force and the mini actuator output force can be expressed as Equation 3.5. And the contact force due to end point motion can be expressed in Equation 3.6.

$$\frac{F_c(s)}{F(s)} = \frac{Y_m Z_s}{1 + Y_m Z_s + Y_1 Z_m + Y_m Z_s Z_m + Y_1 Y_m Z_m Z_s}$$
$$= \frac{Y_2(s) Z_s(s)}{1 + Z_m(s)(Y_1(s) + Y_2(s))} \qquad (3.5)$$

$$\frac{F_c(s)}{Xe(s)} = \frac{Z_s + Y_1 Z_m Z_s + Y_m Z_m Z_s}{1 + Y_m Z_s + Y_1 Z_m + Y_m Z_s Z_m + Y_1 Y_m Z_m Z_s} \qquad (3.6)$$

where

$$Y_2(s) = \frac{Y_m(s)}{1 + Y_m(s) Z_s(s)} \qquad (3.7)$$

The advantage of using block diagram is to represent the system by its physical components. Later study only needs to substitute the dynamics of each individual system to analyze the coupled system. In this system, the macro and the mini manipulator can be modeled separately. A transfer function $Y_2(s)$ can be used to represent the mini manipulator. This method also provides insights to system. For example, Equation 3.5 shows how the zeros and poles of the macro and mini manipulators contribute to the zeros and poles of the coupled system.

3.3 Zero Coupling Impedance: A Controller to Suppress Vibration from Contact Point

3.3.1 Vibration during Force Control

Industrial manipulators usually have low frequency resonant modes. If the macro manipulator has one or more resonant modes whose frequencies are smaller than the bandwidth of the mini manipulator, the resonant modes of the macro manipulator become the anti-resonant (minimum vibration level) modes in the macro-mini system. In this case, the force control performance of the series macro-mini system is compromised. This is because at the resonant frequencies of the macro manipulator, large magnitude of vibration could be

formed in the macro manipulator and transmitted to the mini manipulator through the coupling between them, reducing the force control bandwidth significantly.

Reduction of the force control bandwidth can also be derived from Equation 3.5. The underdamped poles of Y_1 becomes underdamped zeros in Equation 3.5. Anti-resonant modes appear because these zeros are not perfectly canceled by the poles.

Rewrite Equation 3.5 by representing Y_1 and Y_2 using numerator and denominator:

$$\frac{F_c(s)}{F(s)} = \frac{\frac{N_2(s)}{D_2(s)} Z_s(s)}{1 + Z_m(s)\left(\frac{N_1(s)}{D_1(s)} + \frac{N_2(s)}{D_2(s)}\right)} \qquad (\,3.8\,)$$

$$= \frac{D_1(s)N_2(s)Z_s(s)}{D_1(s)\left(D_2(s) + N_2(s)Z_m(s)\right) + N_1(s)D_2(s)Z_m(s)}$$

where,

$$Y_1(s) = \frac{N_1(s)}{D_1(s)}$$

$$Y_2(s) = \frac{N_2(s)}{D_2(s)}$$

If there exists at least one pair of under damped poles in the macro manipulator (Y_1), i.e.,

$$D_1(s) = D_1'(s)R(s) = D_1'(s)(s^2 + 2\xi\omega_n s + \omega_n^2), and\ \xi < \frac{\sqrt{2}}{2}$$

where,

$$R(s) = D_1'(s)(s^2 + 2\xi\omega_n s + \omega_n^2)$$

It can be seen that the under damped poles in the macro manipulator becomes a pair of under damped zeros in the coupled system.

Since the mini manipulator is chosen with higher resonant frequency, $D_2(s)$ does not consists of $R(s)$. Assume the coupling element do not have a

resonant mode near ω_n. Therefore, the under damped poles in Equation 3.8 will not be cancelled. This under damped pole will become an anti-resonant mode in the coupled system.

This could be demonstrated by using a simple system as follows. A 1-DOF macro manipulator with large inertia and low damping ratio and stiffness and ($M_r=100$, $B_r=100$ and $K_r=10000$) is coupled in series with a 1-DOF mini manipulator with small inertia and high stiffness ($M_m=1$, $B_s=100$, and $K_s=10000$). The coupling between the macro and mini manipulators is assumed to be only friction ($K_m=0$ and $B_m=100$). i.e.,

$$Y1(s) = \frac{1}{100s^2 + 200s + 10000}$$

$$Y_2(s) = \frac{1}{s^2 + 100s + 10000}$$

$$Z_m = 100s$$

$$Z_s = 100s + 10000$$

In the 1-DOF macro manipulator, there is a pair of underdamped poles at ($-0.5 \pm 9.99i$), which results a resonant mode near 10 rad/s. When the macro manipulator is coupled with the mini manipulator, the transfer function between the input force and contact force can be calculated based on Equation 3.5. The bode plot of the coupled system is shown in Figure 3.8, together with the bode plot of the macro and the mini manipulator. It could be seen in the coupled system that, an anti-resonant mode at *10 rad/s* is in the system. This is at the same frequency as the resonant mode in the macro manipulator. The anti-resonant mode is formed because a pair of underdamped zeros ($-0.5 \pm 9.99i$) are contributed by the poles of Y_1 and are not canceled.
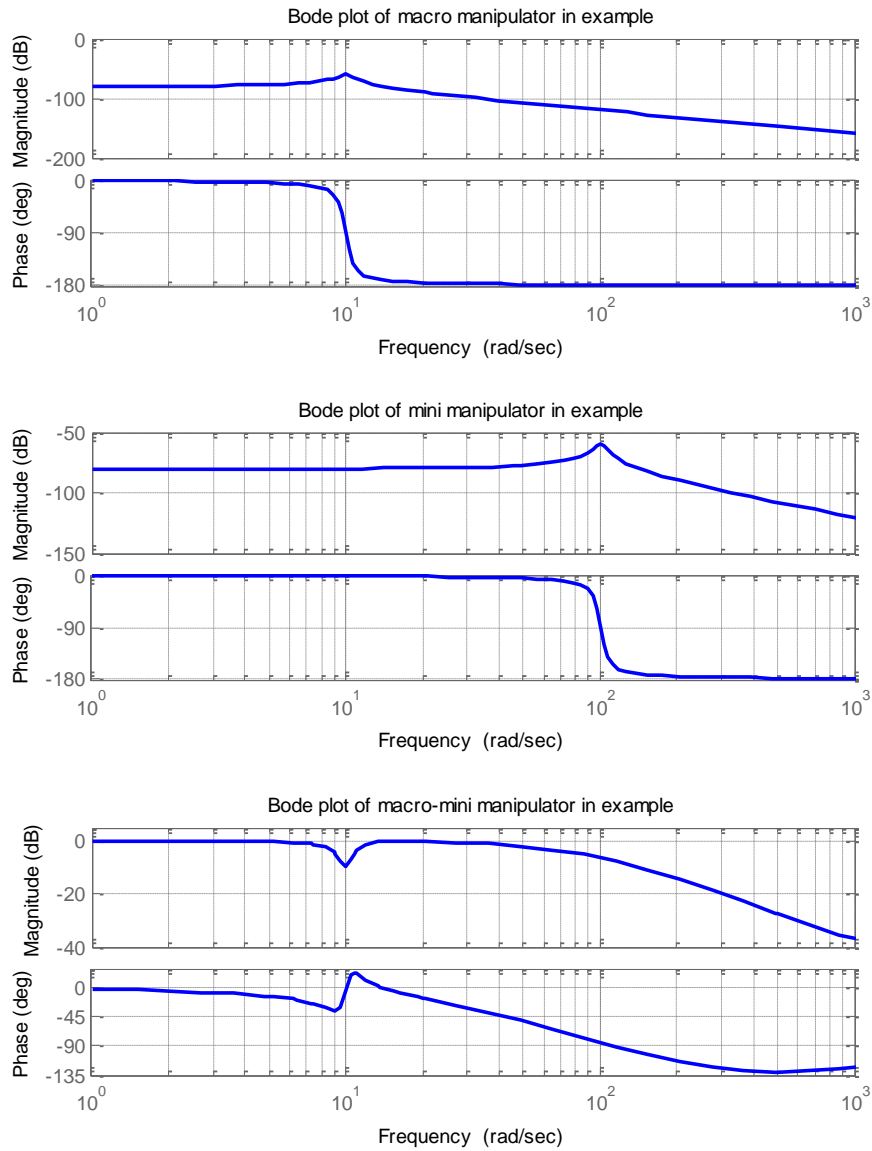
Figure 3.8: Bode plot of the simple series macro-mini manipulator

Therefore, it can be seen that the system bandwidth has been compromised due to the anti-resonant mode.

Although the example is demonstrated using a simple system, this problem also exists in more complex systems such as multiple DOF robots. A few methods to solve this problem can be found by examining Equation 3.5. Since the problem is actually caused by the resonant modes of the macro manipulator, it is intuitive to solve this problem by removing the resonant

modes from it. Sharon [8] has used impedance matching method to modify the damping ratio at joint level to reduce the vibration in the macro manipulator. Although this method has been proven to be effective, realizing this solution in industrial manipulators may not be feasible. The closed control architecture in industrial manipulators makes it difficult to change its basic dynamics. Moreover, the effective compliance changes with the robot posture, making the controller design more complicated since the frequency of the resonant mode varies with the posture. Therefore, an alternative solution to this problem is proposed.

Instead of changing the dynamics of the macro manipulator, Equation 3.5 also suggests the anti-resonant mode can be removed by choosing a proper Z_m. Therefore, a new approach to eliminate the anti-resonant mode is presented in the following section.

3.3.2 Zero Coupling Impedance Criterion

From the above analysis, a new method named Zero Coupling Impedance criterion is proposed to remove the effect of internal vibration from the contact point. The Zero Coupling Impedance criterion is stated as below:

Assume in the macro manipulator, the resonant frequencies change with the posture and its dynamics cannot be controlled. Then,

- Any force feedback controller at the mini manipulator will not remove the anti-resonant modes;
- The anti-resonant modes can be removed if the coupling impedance between the macro and mini is zero.

The following analysis will show the system dynamics with feedback to prove the first point in the criterion. Normally, the tip position of the macro manipulator is calculated based on encoders at all the joints. Error due to the flexibility of the joint transmission (gearbox) and the link will not be counted. Hence, accurate x_1 is not available without external sensor. In this study, it is assumed that a force sensor and an encoder are used to measure the contact force and the relative position between the macro and mini, respectively. Then,

the coupling impedance between the macro and mini is the sum of the mechanical impedance $Z_m(s)$ and the controller impedance $Z_c(s)$.

In order to fully utilize all types of sensor feedback, let the controller be:

$$F(s) = F_e(s)H(s) + Z_c(s)X(s) \qquad (\textbf{3.9})$$

where $F_e(s) = F_{cd}(s) - F_c(s)$, $X(s) = X_1(s) - X_2(s)$ and $F_{cd}(s)$ is the desired contact force. $H(s)$ is the controller of force feedback. This simple controller does not lose generality because it utilizes feedback from both sensors. The block diagram of the closed system is shown in Figure 3.9.
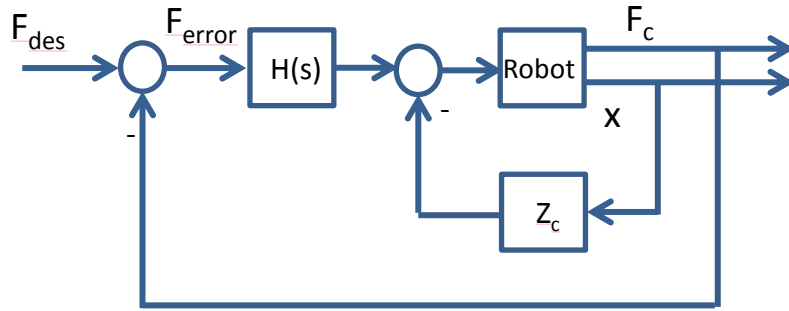
Figure 3.9: Closed loop block diagram

Then the system transfer function of the series manipulator system with feedback is:

$$\frac{F_c(s)}{F_{des}(s)} = \frac{Y_2(s)Z_s(s)H(s)}{1 + Z(s)(Y_1(s) + Y_2{}'(s))} \qquad (\textbf{3.10})$$

where $Z(s) = Z_m(s) + Z_c(s)$ and $Y'(s) = Y_2(1 + \frac{Z_s(s)H(s)}{Z(s)})$.

Comparison between Equation 3.5 and 3.10 shows $Y_1(s)$ will always be in the denominator regardless of the controller $H(s)$ chosen. Only dynamics of the mini manipulator $Y_2(s)$ and the coupling impedance $Z(s)$ are changed by the controller $H(s)$.

Although controller $H(s)$ could be adjusted to compensate for $Y_1(s)$, it is impractical to measure $Y_1(s)$ at all robot configurations. Furthermore, adjusting $H(s)$ as the robot posture changes will make the controller non-linear. Hence, this proves that a controller with contact force feedback cannot eliminate the

32

vibration problem. The second point of the Zero Coupling Impedance criterion could be proven as follows.

If the Zero Coupling Impedance criterion is satisfied, i.e.:

$$Z(s) = 0 \qquad \qquad (\textbf{3.11})$$

Then Equation 3.10 becomes:

$$\frac{F_c(s)}{F_{des}(s)} = Y_2(s)Z_s(s)H(s) \qquad \qquad (\textbf{3.12})$$

where Y_1 is removed from the dynamic equation. Therefore, anti-resonant mode will not exist anymore and no vibration will be transmitted from the macro to the mini. The system behaves as if the mini manipulator is mounted on a rigid platform and the model can be further simplified, as shown in Figure 3.10. As a result, all the advantage of the mini manipulator remains and the work space is enlarged by the macro manipulator.
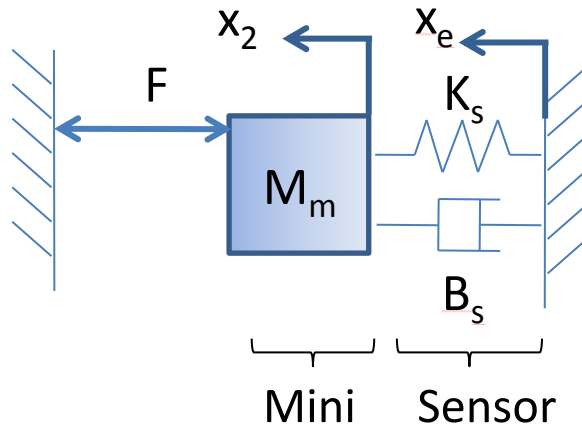
Figure 3.10: Series macro mini system model with Zero Coupling Impedance criterion fulfilled

3.3.3 Verification of Zero Coupling Impedance Criterion

In this section, the Zero Coupling Impedance criterion is verified through both simulation and experiment. A real series macro-mini manipulator system is built for experiments. To make simulation more meaningful, the system model of the system will be used in simulation.

3.3.3.1 System Identification

To verify the Zero Coupling Impedance criterion, a 7-DOF Mitsubishi PA-10 manipulator is used as the macro manipulator and a linear voice coil actuator is used as the mini manipulator. In the following paragraphs, system identification for both systems will be shown.

- **Mini Manipulator Identification**

The system model of the voice coil actuator was attained by mounting the actuator to a rigid table. Since the contact force response to the input force is interested, a force sensor was used to measure the contact force exerted on the environment. To characterize to mini manipulator, both step input and chirp (sinusoidal with constant magnitude but increasing frequency) input have been used and the corresponding output force was measured. Then, Fast Fourier Transform (FFT) was applied to both input and output for both experimental results. The mini manipulator system response plot $F_c(s)/F(s)$ in frequency domain is shown in Figure 3.11 by the solid blue line.
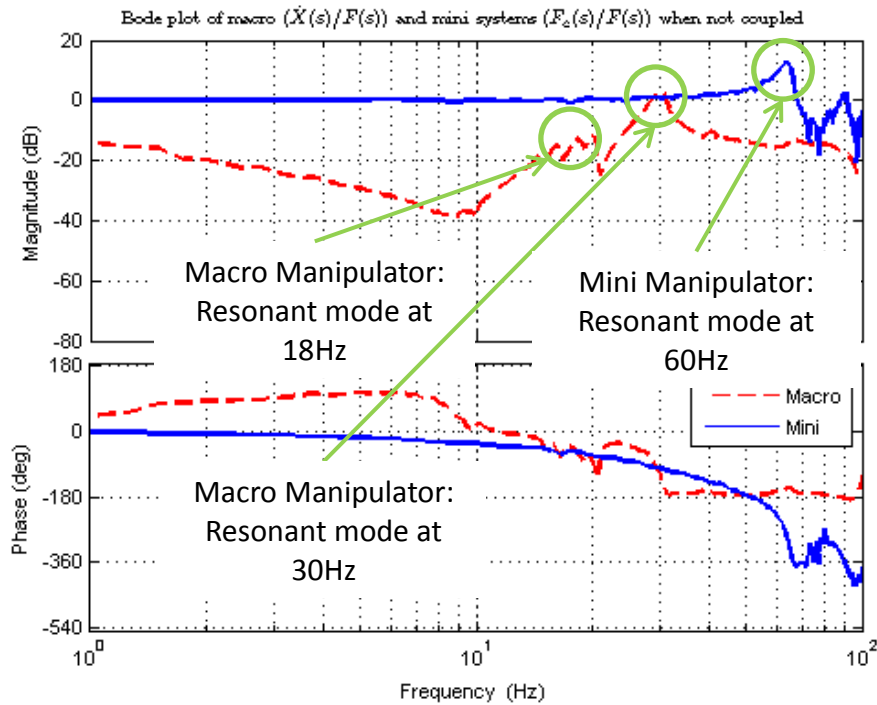
Figure 3.11: Bode plot of individual macro and mini system response when they are not coupled

34

It is shown in Figure 3.11 that the mini manipulator has one pair of dominant poles (at *64Hz*). Then, the mass of the moving part on the mini manipulator was measured separately. All the moving parts of the mini manipulator weighs *0.82Kg*. Therefore, assuming $B = 0$ and estimate the damping ratio through curve fitting, the transfer function of Y_2 could be calculated as follow:

$$Y_2(s) = \frac{1.347 \times 10^5}{1.347 \times 10^5 (s^2 + 162.1s + 1.642 \times 10^5)} \quad (\textbf{3.13})$$

with $Z_s(s) \approx 1.347 \times 10^5 s, M_m = 0.82$.

- **Macro Manipulator Identification**

To identify the dynamic model of the PA-10 robot, the system resonant modes of the PA-10 manipulator was obtained through modal testing. Since the system response to an impulse force from the end point is interested, force exerted on the end point and the resultant motion was analyzed in frequency domain.
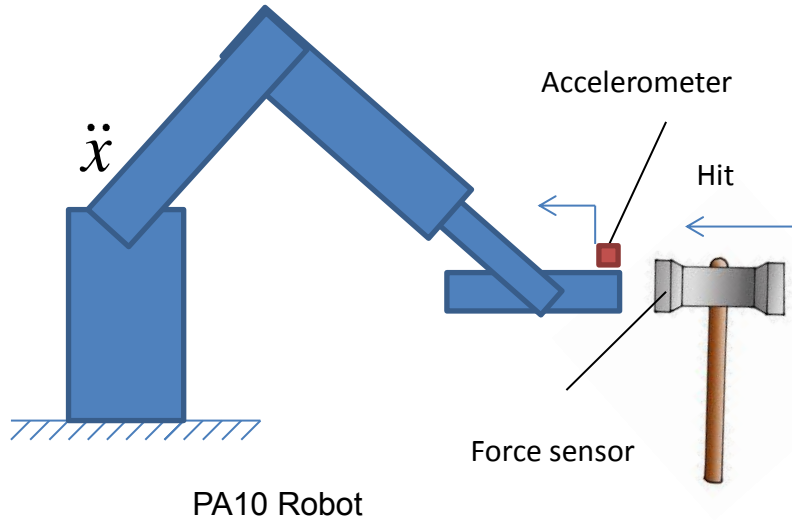
Figure 3.12: Modal test for identifying resonant modes in PA-10 robot

The manipulator was set into position control mode and given a fixed set position. In the modal testing as shown in Figure 3.12, a hammer was used to generate an impulse force and the resultant acceleration of the end point is measured by an accelerometer. Then, Fast Fourier Transform (FFT) was applied to both input and output. In Figure 3.11, the dash red line shows the

35

system response of macro manipulator acceleration to force ($\ddot{X}(s)/F(s)$) in frequency domain. Then, the stiffness of the manipulator was obtained by measuring the manipulator deflection at steady state caused by a constant force. Thus, the gain of the transfer function of the PA-10 robot was calculated from the above data.

From Figure 3.11, it can be seen that the macro manipulator has two pairs of dominant poles (at *18Hz* and *30Hz*) and one pair of zeros (at *21Hz*). Other poles and zeros appear at higher frequencies are not considered since they are higher than the mini manipulator's natural frequency. The mini manipulator becomes a filter for the macro manipulator at high frequency. Therefore, a fourth order system will be sufficient to represent the dynamics of the macro manipulator (PA-10 robot) that is coupled in series with the mini manipulator.

Therefore, choosing proper damping ratios for all the poles and zeros by curve fitting, the admittance of the macro manipulator could be calculated as shown in Equation 3.14.

$$Y_1(s) = \frac{0.436(s^2 + 10s + 17410)}{(s^2 + 10s + 12778)(s^2 + 35s + 35531)} \qquad (\textbf{3.14})$$

3.3.3.2 Simulation Study

Using the above models and assuming non-zero coupling impedance ($Z_m = 150s$), simulations are performed to study the dynamics of the series manipulator system. The bode plot of the mini manipulator and the macro-mini manipulator system contact force due to input force ($F_c(s)/F(s)$) are shown in Figure 3.13.

The solid blue line represents the bode plot ($F_c(s)/F(s)$) of the mini manipulator while the dash red line represents the bode plot ($F_c(s)/F(s)$) of the macro-mini manipulator system. In the bode plot of the macro-mini manipulator system, it is found that curve shape of the mini manipulator remains unchanged at high frequency when it is coupled with the macro. However, anti-resonant modes in the macro-mini system are found below the mini manipulator's bandwidth. It is observed that two anti-resonant modes (at

18Hz and *30Hz*) appear at the same frequencies as the resonant modes of the macro manipulator. These anti-resonant modes attributed by the resonant modes of macro indicate the vibration is transmitted from the macro to the mini through the coupling element.
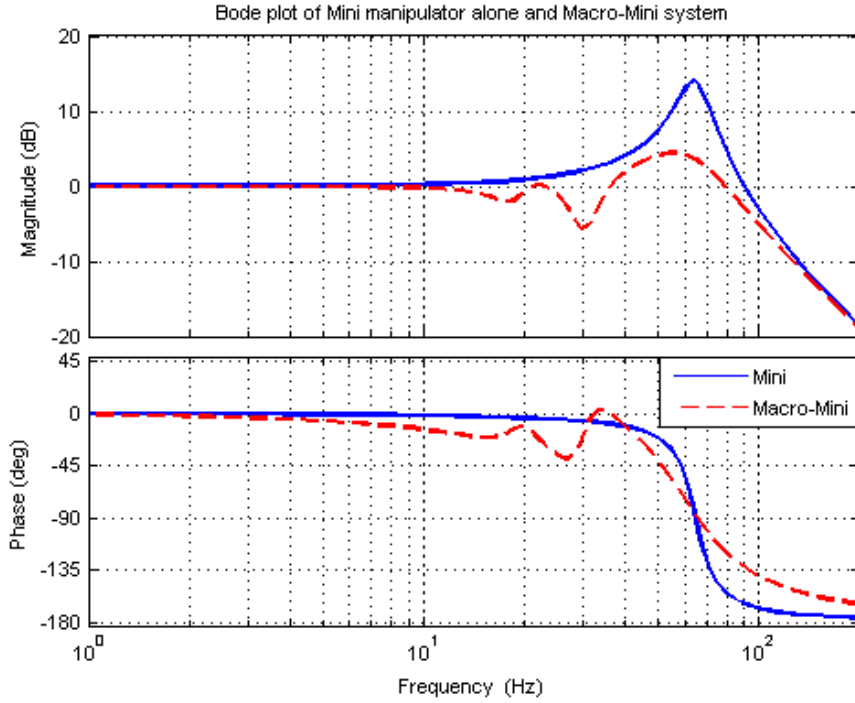
Figure 3.13: Bode plot of the series manipulator system $(\mathbf{F_c}(\mathbf{s})/\mathbf{F}(\mathbf{s}))$

This effect can be critical during machining. Contact may not be retained and chattering would occur. Force control performance in machining applications will be compromised. This can be explained by looking at the impedance of the series manipulator system. Equation 3.6 is the system impedance and it is represented in bode plot as shown in Figure 3.14. It shows that both systems have the same impedance at high frequency, but the system impedance at low frequency is lower if the coupling impedance is zero.

Large impedance usually results in higher contact force. For example, if a machining task requires the end-effector to exert a constant force of *20N* and to move along the surface of a work piece which is sinusoidal shape with magnitude of *1mm*. This is equivalent to the end-effector vibrating at a

magnitude of *1mm* due to the spindle or disturbance. Figure 3.15 shows the contact force when the contact point is moving along work piece's surface with increasing speed. The speed of the moving end increases linearly, resulting in disturbances with increasing frequency.
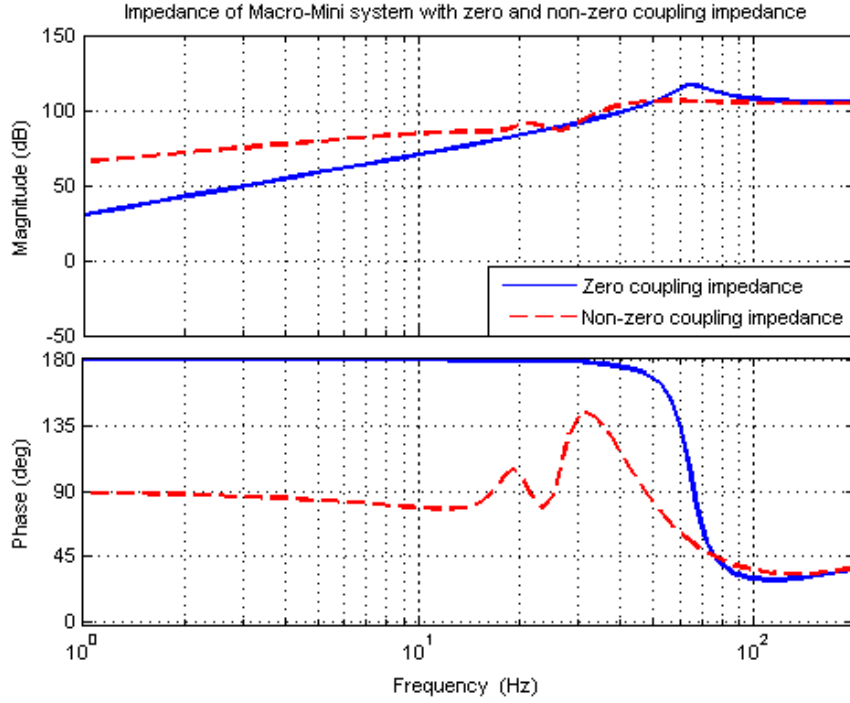
Figure 3.14: Impedance of Macro-Mini with zero and non-zero coupling impedance, $F_c(s)/X_e(s)$

The top curve shows the contact force when Zero Coupling Impedance criterion is applied while the bottom one shows the same but when the coupling impedance is non-zero. Compare the two simulations, the contact force is better maintained around *20N* in the system with Zero Coupling Impedance, especially at low frequency. Large contact force is observed near the anti-resonant mode. Since the contact surface can only push the end point of the manipulator, negative contact force simply indicates loss of contact. It is also observed that the negative force occurs at *23Hz* with the criterion satisfied, *6Hz* higher than that of a system without satisfying the criterion.
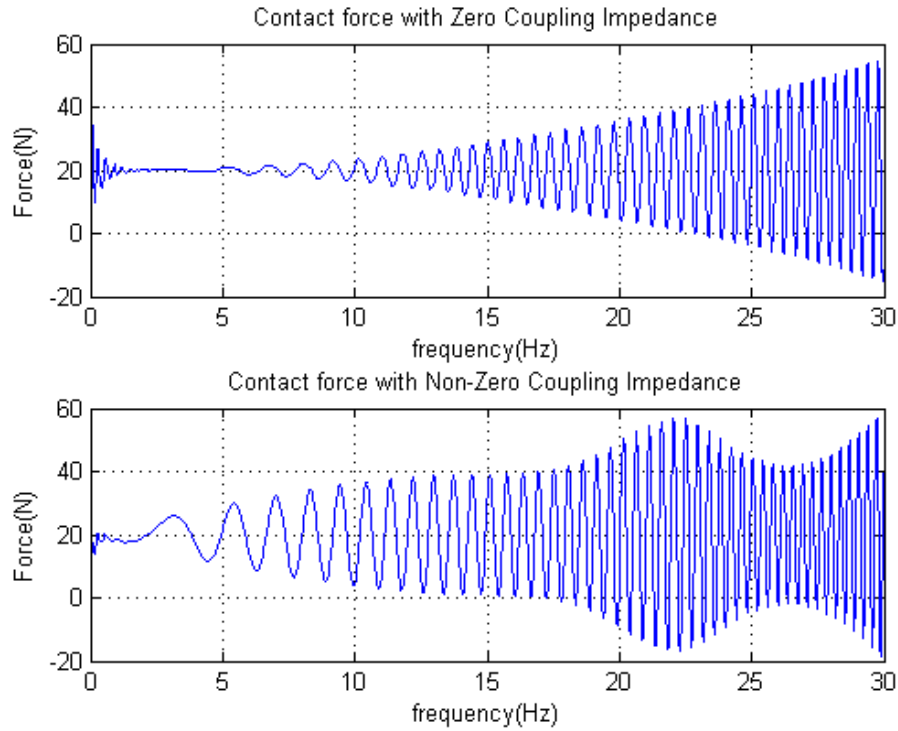
Figure 3.15: Contact force when contact end is moving with increasing frequency

3.3.3.3   Experiment Study

To validate the Zero Coupling Impedance criterion, experiments using a Mitsubishi PA-10 manipulator and a voice coil actuator were conducted as shown in Figure 3.16. The system was controlled using C programming language under RTX, a real-time software environment in Windows. The sampling rate is *1KHz*.

The voice coil actuator with a force sensor attached is mounted at the end point of the PA-10 robot. During the experiment, the PA-10 robot was in position control mode and a fixed point command was given to the robot.

In this experiment, two controller gains were used in order to compare the system dynamics with and without satisfying the Zero Coupling Impedance criterion. In the mini actuator, no force feedback was used since it has no effect on the anti-resonant mode. Only the relative position/velocity between

the macro and mini was fed back to the controller. The force applied from the voice coil actuator is expressed as:
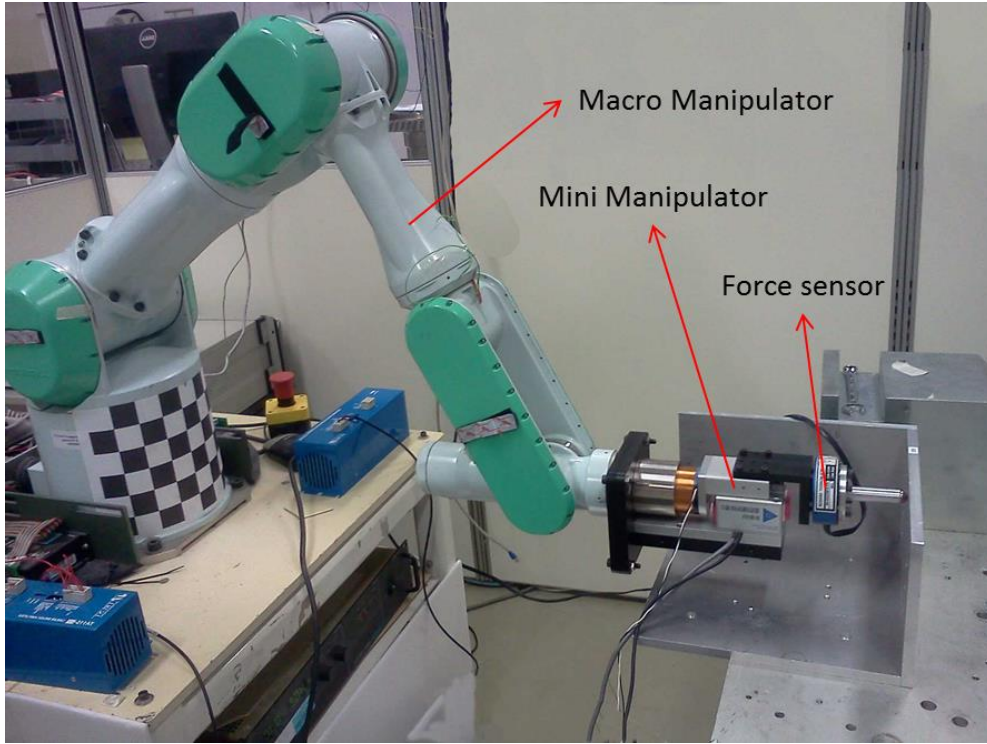
Figure 3.16: Series macro-mini manipulator experiment setup

$$F = F_{des} + Z_c(s)X(s)$$

<div align="right">(3.15)</div>

where $Z_c(s) = Ds$. Therefore, the coupling impedance between macro and mini becomes:

$$Z(s) = Z_m(s) + Z_c(s) = (B + D)s$$

And the mechanical impedance of the voice coil Z_m is assumed to be zero since the friction is negligible. Hence, the total coupling impedance becomes the controller impedance, i.e.

$$Z(s) \approx Z_c(s) = Ds$$

Figure 3.17 shows the system frequency response with and without satisfying the Zero Coupling Impedance criterion. The result shows two anti-resonant modes when $D = 150$ and no anti-resonant mode when $D = 0$, which match well with the simulation result shown in Figure 3.13.

Therefore, both simulation and experiment has proven the effectiveness of the Zero Coupling Impedance criterion in eliminating vibration from the mini manipulator.

The above analysis was performed based on the system model obtained at a fixed posture. However, this analysis does not lose generality because the Zero Coupling Impedance Criterion is independent from the dynamics of the macro manipulator. Therefore, this method could be applied for all robot postures.
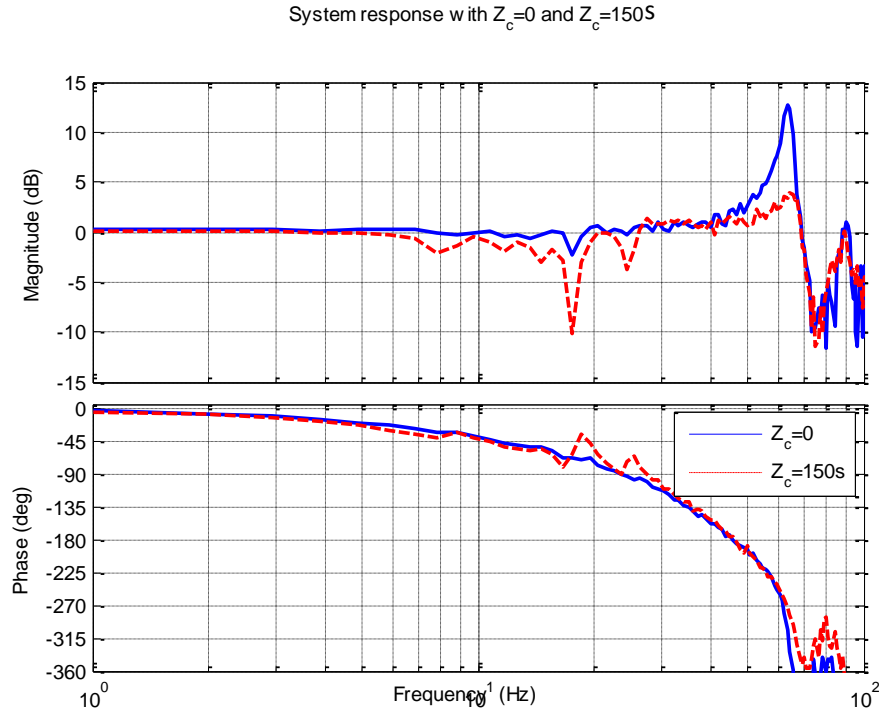
Figure 3.17: Frequency response of a series manipulator system with different coupling impedance

In the following section, a controller design for force will be presented with the Zero Coupling Impedance criterion satisfied.

3.3.4 Controller Design for Force Control

As is shown in Equation 3.9, the controller $H(s)$ does not affect the anti-resonant modes. Only the impedance part of the controller $Z_c(s)$ affects the

anti-resonant modes. If $Z_c(s)$ has satisfied the Zero Coupling Impedance, any controller could be used to optimize the force control performance.

In this thesis, a Linear Quadratic Gaussian (LQG) controller is used as the controller for force control and the details of LQG controller design in shown in Appendix. There are several reasons for choosing LQG controller for force control. First and the foremost, in order to satisfy the Zero Coupling Impedance criterion, the damping factor B_m needs to remain zero, which imposes instability issues in controlling this system. In order to maintain stability, enough damping between the robot and the workpiece should be guaranteed. Conventional PID control requires differentiation of the force sensor feedback, which is noisy in most cases. Passing the force feedback through a low pass filter also degrades the system stability. Therefore, a LQG controller which includes a Kalman filter will be useful. Secondly, the system is simple and the model has been well identified and verified in previous sections. The model based controller LQG requires accurate system model. In the previous subsection, the system was identified and verified through experiment. Therefore, designing this controller is simple. Thirdly, this model based controller provides a better inside view of the system by estimating the system states. The Kalman filter in the system is basically an observer which estimates the system states.

Although LQG controller was used in the experiment, it does not mean only LQG should be used together with the Zero Coupling Impedance criterion. Any model based controller with observer can be used. Other controllers such as PID could also be applied to this system if the force signal has little noise or proper filter is used.

Figure 3.18 shows the system step response with accurate tracking and small overshoot. Figure 3.19 shows the system response to a chirp signal input. The contact force tracked the reference signal accurately and the phase lag is small.
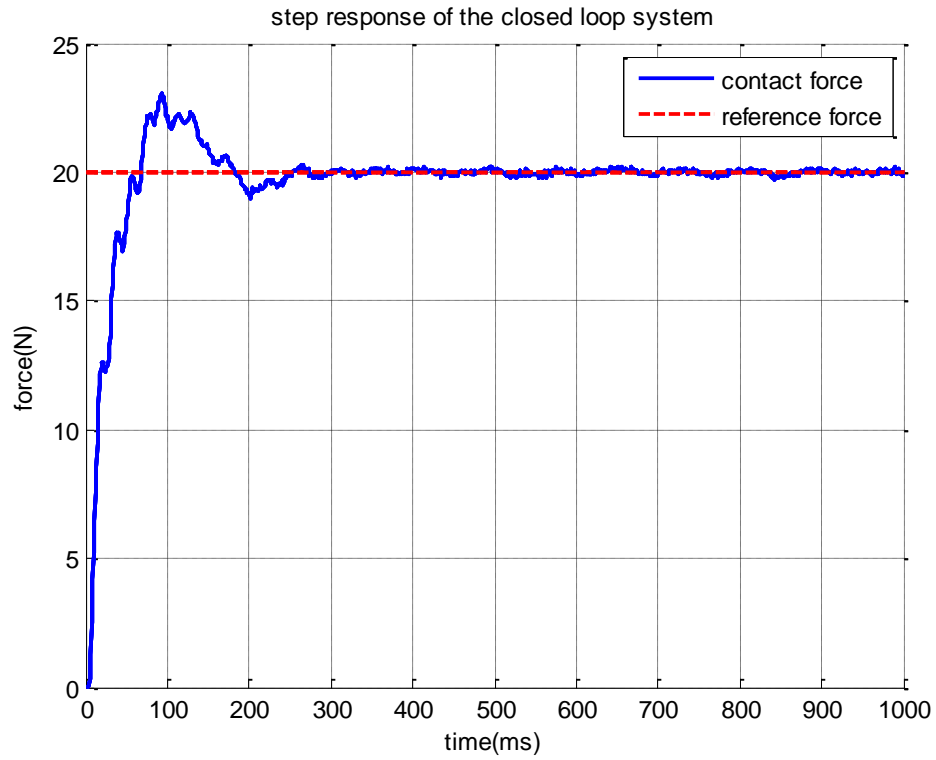
Figure 3.18: Step response of the system with feedback
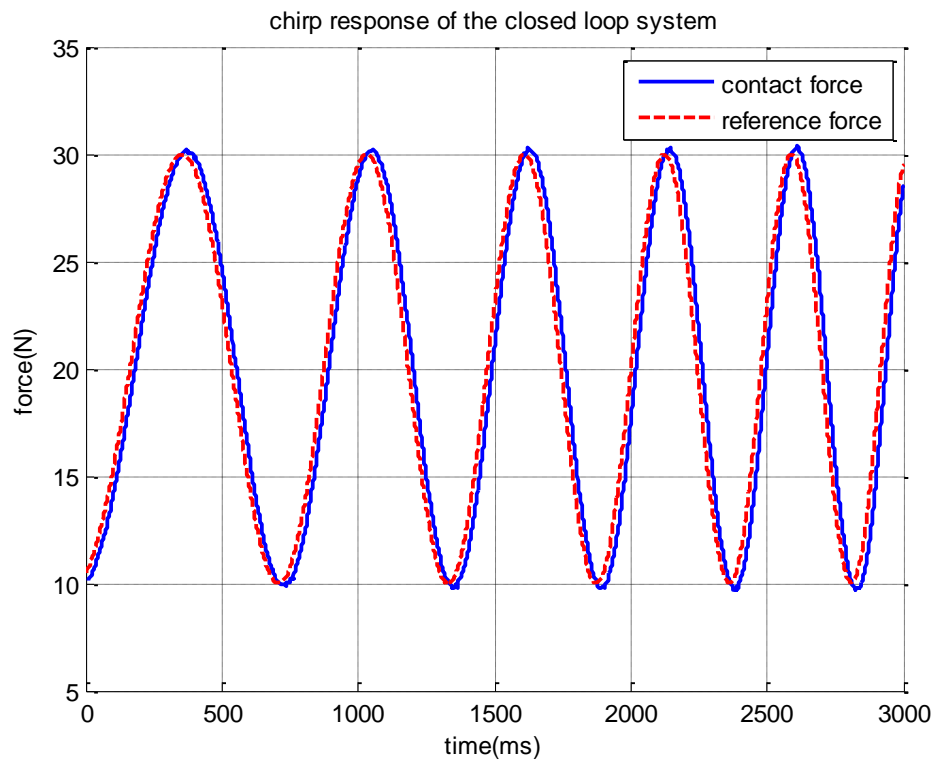
Figure 3.19: Force tracking of a chirp signal of the system with feedback

With the above controller, a pneumatic spindle was mounted onto the mini manipulator to perform grinding task, as shown in Figure 3.20. The pressure supplied to the spindle was 3 bar and the machining tool used was a grinding stone. The workpiece used was a titanium plate with sharp edge.

In this experiment, the macro manipulator carried the mini manipulator to a position that is 1cm away from the surface. During this process, the mini manipulator was under position control and a fixed position with respect to its base was given as the reference point. Then, the position of the macro manipulator was stopped and its reference position remained unchanged. Subsequently, the mini manipulator start to move with a small constant speed until it hit the workpiece. Upon making contact, it was switched to force control and a contact force of *2N* was set as the reference. The force measured by the sensor is shown in Figure 3.21. The result shows promising performance in grinding. The fluctuation in the force signal is mainly due to the sensor noise and the oscillation of the spindle.
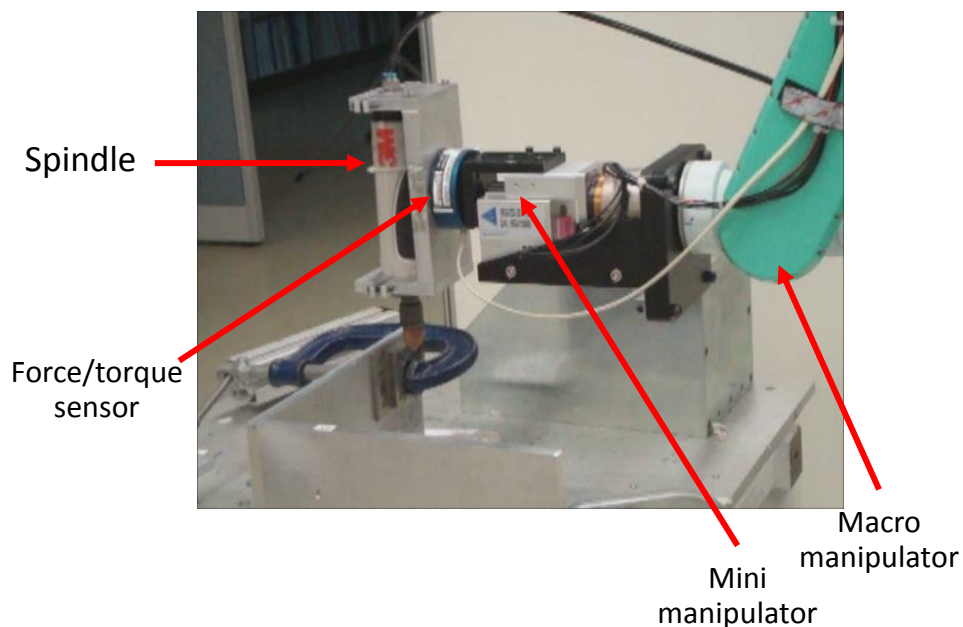
Figure 3.20: Grinding using series macro mini manipulator
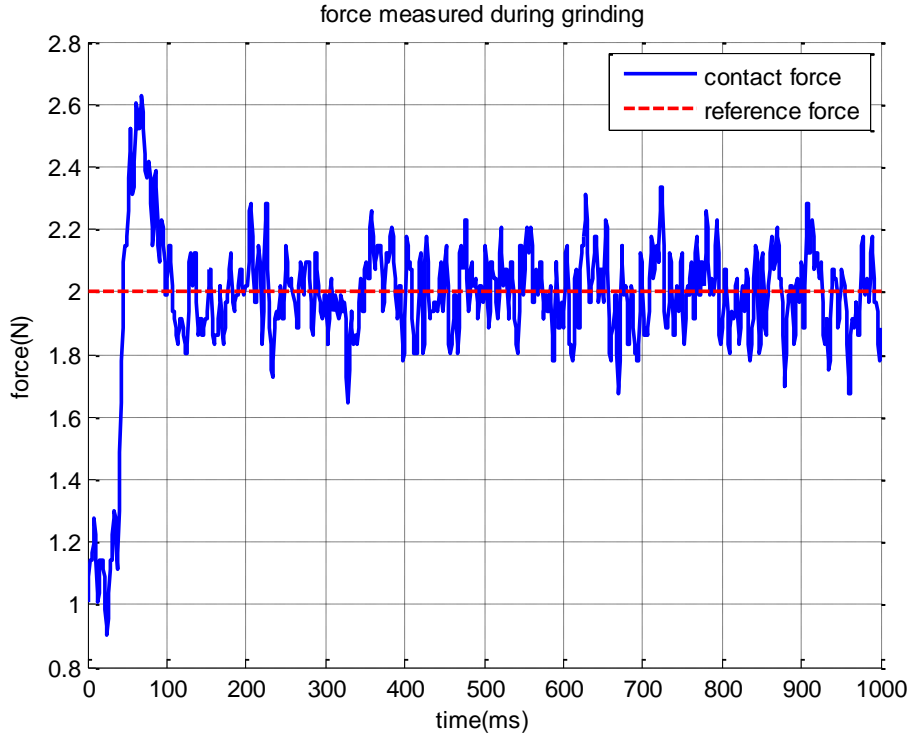
Figure 3.21: Force reading during machining

3.4 Zero Coupling Impedance: A Design Guideline for Series Macro-Mini System

Previous sections have shown that the Zero Coupling Impedance criterion is an effective method of eliminating the effect of vibration in a series macro-mini system on the contact point. It is independent from the robot posture and does not require an accurate system model from the macro manipulator.

In this chapter, in order to verify the results, a direct drive actuator was used as the mini manipulator whose mechanical impedance is close to zero. As it is commonly known that a direct drive actuator has many features that are helpful in improving force control performance, such as small friction, fast response. However, this does not mean only direct drive motors should be used as the mini manipulator. The coupling impedance in Equation 3.10 refers to the total sum of the mechanical impedance and the controller impedance. Actuators that do not have zero mechanical impedance could still be used in a series macro-mini system by compensating its mechanical impedance through

active control. For example, a normal electro-magnetic motor coupled with gears could be used as the mini manipulator, too.

In order to compensate the mechanical impedance using active control, two conditions need to be satisfied.

- The dynamics of the coupling mechanism manipulator need to be well identified;
- The actuator should not be saturated.

The first condition is easy to understand. The coupling impedance needs to be identified so that it could be canceled. This condition needs to be considered when designing the mini manipulator. The coupling element chosen between the macro and the mini should be as simple as possible so that the dynamics remains linear and easy to be identified through experiment.

The second condition states that the requirement of the power rating of the actuator to cancel the impedance of the coupling mechanism. It is impossible to cancel the mechanical impedance completely due to the finite power rating of the actuator. However, it will be enough if the bandwidth of the system with feedback is higher than the resonant modes of the macro manipulator.

For example, a macro and a mini manipulator are coupled by a component with impedance $Z_m = B_m s$. The controller only has limited bandwidth to compensate for the impedance Z_m, as shown in Figure 3.22. It shows that the mechanical impedance could only be canceled below the bandwidth of the controller at about *100Hz*, above which, the impedance is unchanged.
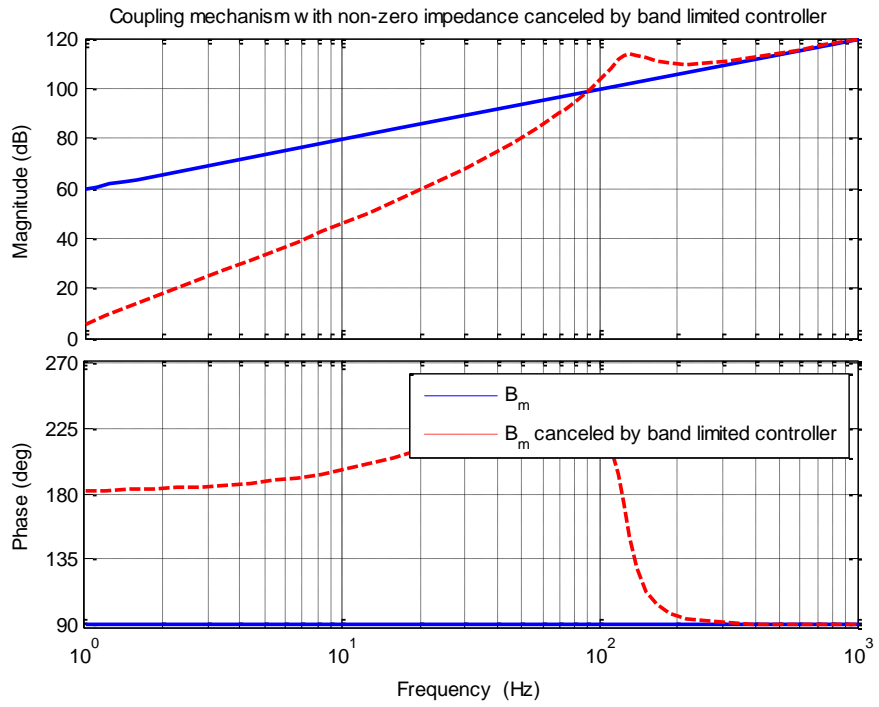
Figure 3.22: Coupling mechanism canceled by band limited controller
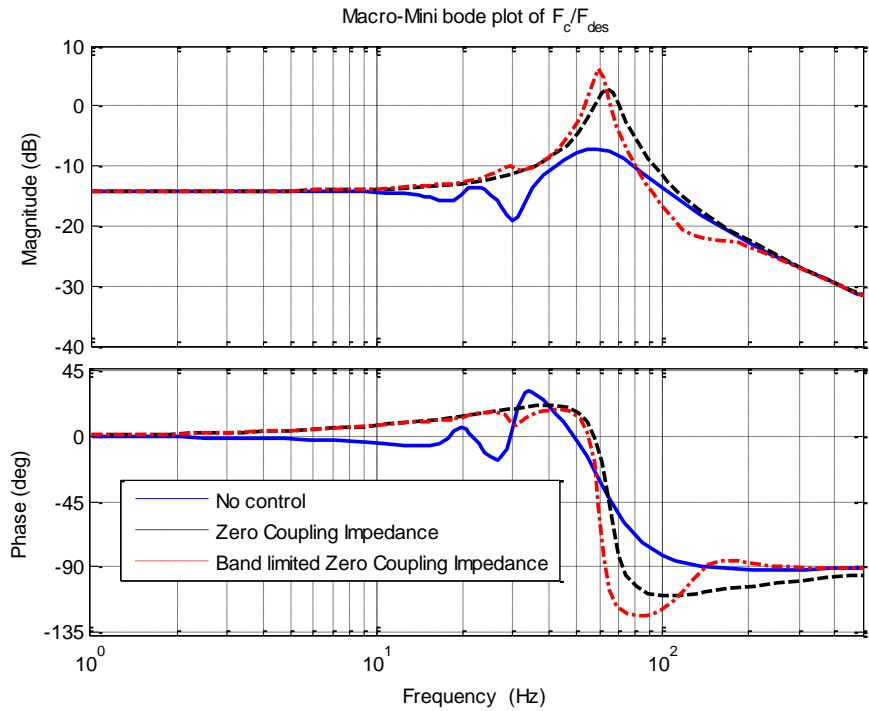
Figure 3.23: Macro-Mini bode plot when coupling impedance is (a) not canceled; (b) completely canceled; (c) canceled by band limited controller

Figure 3.23 shows the bode plots of system, $F_c(s)/F_{des}(s)$ under different conditions. The solid blue line shows that without canceling the coupling impedance, anti-resonant modes appears in the bode plot. The black dashed line shows the system bode plot if the Zero Coupling Impedance criterion is perfectly satisfied. As it has been shown before, the two anti-resonant modes are removed from the system. The red dotted line shows the system bode plot when the coupling impedance is canceled by a band limited controller. The curve shows that the anti-resonant modes are removed, too. Hence, it indicates that the Zero Coupling Impedance criterion could be implemented even using a power limited actuator and could be applied in a variety of mini manipulator systems.

3.5 Summary

Conventional manipulators are designed for repetitive position controlled tasks. Their large impedance and slow response make them not suitable for force control applications, especially in machining tasks. With a specially designed mini manipulator, high performance force control using the conventional manipulator with simple control becomes possible. In this chapter, a series macro mini manipulator system has been studied.

A general mathematical model has been developed to study the dynamics of a series macro-mini manipulator system. In this system, the vibration due to low resonant modes of the macro manipulator is identified as the main limiting factor of the force control performance. Methods such as changing the dynamics of the macro manipulator to suppress the vibration are not applicable to commercial manipulators. Therefore, a new method that regulates the impedance of the coupling element between the macro and the mini manipulator is proposed. In this chapter, the Zero Coupling Impedance criterion has been proposed as a design guideline for a series macro-mini manipulator system to improve force control performance, and is verified by both simulation and experiment. Then, a LQG controller has been designed for force control. Finally, a spindle was used to perform grinding using this system and promising result in force control has been demonstrated.

The Zero Coupling Impedance criterion provides a guideline when using a series macro-mini manipulator to perform force control. This criterion advises on choosing the coupling mechanism between the macro and the mini manipulator and also on designing a controller to optimize the chosen mini manipulator such that the macro manipulator will not degrade the system performance. In all, this method resolves the limitation on the series macro-mini manipulator system.

Chapter 4

A New Variable Stiffness Joint for Force Control

4.1 Introduction

Traditional industrial manipulators were designed to be rigid to improve repeatability, accuracy and avoid large vibration. However, when a robot is interacting with environment, large contact force could be induced if the end-effector is not placed accurately. In Chapter 3, series macro-mini manipulation has been discussed as a solution to resolve the problem. In this approach, no modification has to be made to the conventional manipulator. Only an additional module is added to perform force control. Promising results have been demonstrated using robot in this configuration. In this chapter, the other approach, force control through all robot joints will be discussed as an alternative solution to improve force control. The objective is to re-design the conventional manipulator from joint level to suit force control such that no additional end-effector module is needed.

The work of Series Elastic Actuator (SEA) [7] showed that robots with compliant joint could overcome the drawback due to large impedance of the conventional stiff manipulator. Force could be controlled at each joint by converting the force control problem into a simple position control problem. Inspired by SEA, many variable stiffness mechanisms were built to further improve force control performance and to resolve the limitation of SEA due to the fixed spring compliance.

For example, VS-Joint [54] used non-linear spring mechanism to generate the compliance. The stiffness is determined by the stiffness preset motor and the output load. Mechanisms using antagonistic actuation such as VSA [57] use two motors to drive the output in parallel through non-linear springs. Stiffness

50

is controlled by the input motors and the output load. These types of variable stiffness joints have one property in common: stiffness is dependent of the output load. This property creates non-linear load-displacement relationship and therefore complicates the system and controller design with non-linear stiffness. Furthermore, larger contact force may be induced by disturbance from the end-effector. In [66], the authors also pointed out that linear load-displacement relationship is convenient for controller design. Several mechanisms such as the HDAU [66] and CompAct-VSA [64] have achieved linear load-displacement relationship approximately, however, only in small ranges.

This raises the need for developing a variable stiffness joint that has linear load-displacement relationship in a large working range. This joint should also cover wide stiffness range to execute a variety of tasks.

This chapter is organized as follows. In section 4.2, the design requirements for the proposed joint are identified and explained. Section 4.3 illustrates the working principle of the proposed variable stiffness joint mechanism. Subsequently, the mechanical design to realize the concept is presented in section 4.4. Section 4.5 shows the characterization of the prototype that is built according to the proposed concept. Then, the controller design for force control is demonstrated in section 4.6. Finally, a summary of this chapter is drawn in section 4.7.

4.2   Design Requirements

The aim of the new variable stiffness joint design is to improve force control performance such that a robot equipped with the proposed joint mechanism is easy to control and can be widely adopted in different applications. Besides variable stiffness, more specific requirements need to be identified before proposing a design. Based on the tasks, a general manipulation process could be divided into four phases.

The first phase is the robot approaching the workpiece from a distance. In this phase, the robot moves relatively fast to minimize the processing time and position control will be used. The second phase is searching for contact. After

the robot end effector has been placed near to the surface of the workpiece in the first phase, robot will slow down to search for contact. To avoid large impact, force control could be used in this phase and low stiffness should be used. The third phase is the manipulation phase, where force control is employed. Finally, the last phase is after work is done, robot will leave the surface. Position control or force control could be used in this phase. The entire process may be repeated for many times in some applications.

According to the above procedures, three properties that the novel joint should possess are derived and listed as below. The reasons for having each property will be explained.

Three properties of the proposed variable stiffness joint are:

- Linear passive load-displacement relationship (in theory);
- Adjustable stiffness ranging from zero to infinity;
- High resolution in low stiffness range.

It is clear that any mechanism has a finite stiffness due to many factors, such as the material and the mechanical structure. The objective of this thesis is to propose a mechanical design with zero to infinity stiffness in theory. Therefore, in the following of the thesis, infinity stiffness is only referred to as the theoretical value.

4.2.1 Linear Passive Load-Displacement Relationship

The passive linear load-displacement relationship is important for many interactive applications. This property is often missing in most of the variable stiffness designs. Usually, the stiffness of the variable stiffness joints is designed in such a way that the stiffness increases when joint load is increased [54, 56, 58, 59, 61]. However, the increasing stiffness will be problematic when disturbance is present. In this situation, the importance of the linear load-displacement property can be explained by a scenario described as follows.

Assuming a compliant robot is carrying a spindle for grinding and a constant contact force is desired. However, fluctuation in the end-effector position is

inevitable due to the high turning speed of the spindle. Simulation studies have been performed to compare the performance of robots with different stiffness characteristic, a linear load-stiffness relationship and a non-linear load-displacement relationship. As shown in Figure 4.1, the solid blue curve shows the stiffness of the VS-Joint [54] when preset spring is compressed by 1/3 of its maximum deflection while the red line shows a normal compliant joint with a constant stiffness. Both joint has the same stiffness at deflection angle of 10°.
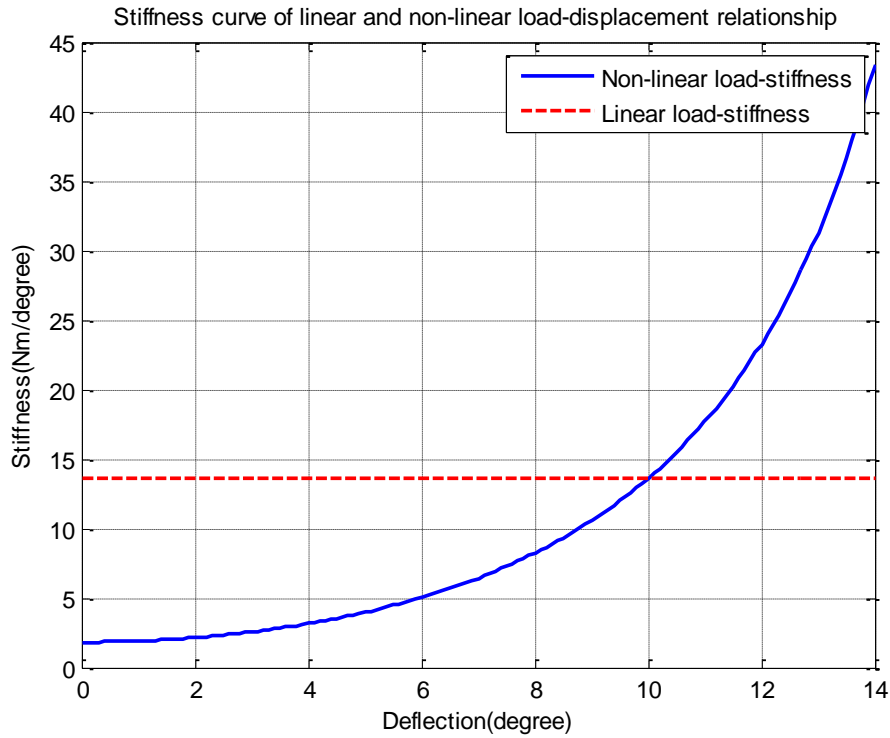
Figure 4.1: Stiffness curve of joint with linear and non-linear load-displacement relationship

Figure 4.2 shows the simulation results of the contact force when both joints are subjected to the same position disturbance from the end-effector. In this simulation, the disturbance is assumed to be a sinusoidal signal with constant magnitude but increasing frequency. It is observed that both the nominal value and the magnitude of the vibration in the contact force are much higher in the joint which has non-linear load-stiffness relationship, as shown in Figure 4.2. This has indicated that joint with the same stiffness, joint has non-linear load-displacement relationship is more sensitive to contact point disturbance.

Furthermore, a non-linear load-displacement relationship results in non-linear systems, making controller design more complicated. Therefore, linear load-stiffness relationship has been chosen as the most important requirement that the joint should meet.

(a) (b)
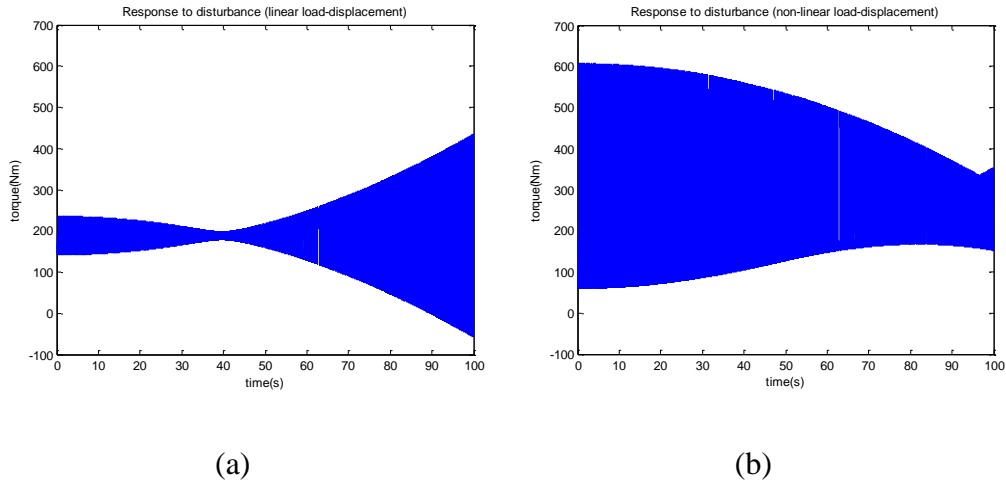
Figure 4.2: Contact force due to sinusoidal disturbance: (a) VS joint with linear load-displacement relationship; (b) VS joint with non-linear load-displacement relationship

4.2.2 Adjustable Stiffness Ranging from Zero to Infinity

The second requirement is needed because in the process of manipulating an object, the robot will require different stiffness to be set in the joints during different phases of the operation. When the robot is carrying the tool to approach the workpiece, very high stiffness is desired to avoid vibration in the robot when it moves at high speed. Ideally, the stiffness should be infinity such that the tool can be accurately positioned at a point that is close to the workpiece. However, moving the tool to the surface of the workpiece using position control with high stiffness is risky since small error in placing the end-effector or the workpiece location will result in large force. Hence, when the end-effector is near the workpiece, the robot will switch to force control mode to search for contact. In this phase, low stiffness is preferred to avoid large force during impact (contact). When the tool is in contact with the workpiece, stiffness may need to be adjusted again depending on the tool and

54

the material of the workpiece. Soft tools such as brush may require high stiffness while hard tool such as grinding stone may need lower stiffness.

Therefore, the second requirement is needed to ensure the robot has the capability to adjust its stiffness within a large range.

4.2.3 High Resolution in Low Stiffness Range

The third requirement is a complementary property to the second one. In variable stiffness mechanisms, stiffness is adjusted by changing the mechanical properties of the joint. Any mechanism used to adjust the stiffness will have limited motion range. It should only take finite motion range to achieve zero to infinity stiffness. Therefore, the stiffness resolution needs to be compromised. As stiffness needs to be controlled more precisely at the lower stiffness range, resolution in the high stiffness region has to be sacrificed to achieve faster stiffness control. Furthermore, this would be useful when the robot needs to switch from force control mode to position control mode rapidly.

4.3 Working Principle

Based on the above requirements, a novel stiffness joint mechanism is proposed. The fundamental working principle of the joint relies on a lever arm with constrained ends. In this joint, when the lever rotates about the pivot point, the motions of the end points are constrained such that the force exerted on both ends of the lever have a constant ratio when the location of the pivot is fixed.

In this joint, the input to the system is controlled by a geared motor (output motor) under position control to deliver the output torque. The position of the pivot on the arm is controlled by a lead screw that is driven by a secondary motor (stiffness motor) to adjust the output stiffness.

In the following, a lever arm without constraint will be shown first to illustrate the purpose of adding the constraint. Limitations of using a un-constraint lever mechanism will be shown. Then, the proposed lever arm mechanism with constrained ends will be introduced to resolve limitations.

55

4.3.1 Lever Arm Mechanism without Constrained Ends
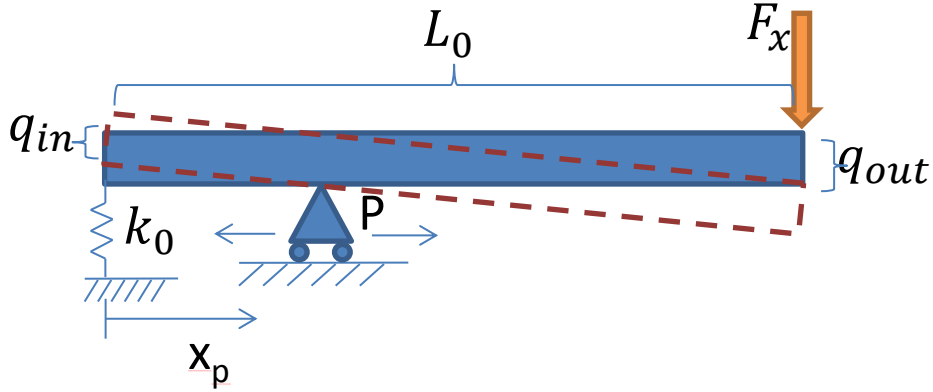
Figure 4.3: Basic working principle of the lever based variable stiffness joint

A schematic diagram of a lever mechanism without constrained ends is shown in Figure 4.3. In this figure, a linear spring with stiffness k_0 is connected to one side of the lever while the load F_x is exerted on the other side of the lever. From this diagram, it can be observed that the stiffness seen by the load F_x is solely dependent on the pivot position (point P) when the arm rotates for a small angle (typically smaller than 5°). However, if the output deflection is large, the stiffness will not be independent from the output load. Furthermore, Figure 4.3 only shows a simple concept by assuming the forces from the output and the spring are always exerted at fixed points and in the same direction. These assumptions are made in some of the variable stiffness joint works, but they may not be realized without a proper design.

(a)   (b)
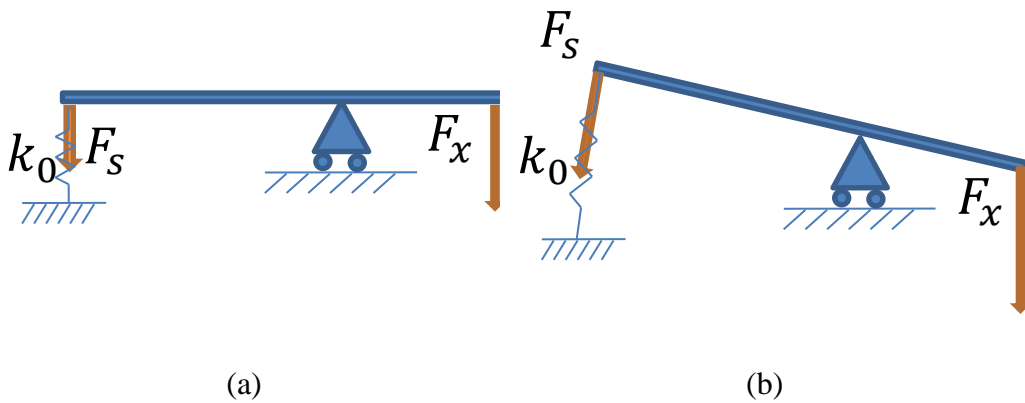
Figure 4.4: Force direction changes as lever arm rotates

For example, in Figure 4.4, F_s and F_x represent forces from the spring and the load, respectively. One end of the spring is fixed on the ground while the other end is fixed on one point of the lever. As the lever is rotated by the load F_x, the direction of the spring force will not be parallel with the load anymore. This will result in non-linear load-displacement relationship as shown in Figure 4.4(b).

Furthermore, the example in Figure 4.4 uses linear force to represent the load to demonstrate a problem in using a normal lever arm mechanism. When converting force to torque, force acting point and direction may vary when the lever rotates. Thus, a modified lever arm mechanism with constrained motion on both ends is proposed.

4.3.2 Lever Arm Mechanism with Constrained Ends
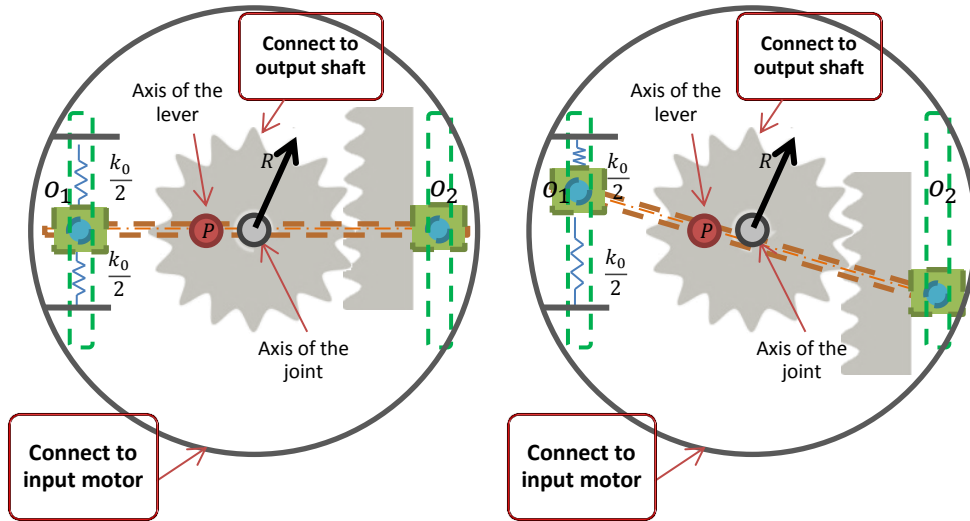
Figure 4.5: Schematic diagram of the working principle

Figure 4.5 shows the proposed mechanical structure of the novel variable stiffness joint. In this joint design, the lever arm mechanism is formed by several in linear guides. Sliders on the linear guides are used to determine the force acting point. Another two linear guides, as shown in the figure, are used to constrain the force acting points and direction on the lever. The output load τ is transmitted to the lever through a rack-pinion mechanism. The pinion pushes the slider on the linear guide down by q_{out} when the output shaft turns by angle θ. The lever rotates about its axis P by angle α, moving the slider on

the other side the lever by q_{in}. Thus, the spring will be effectively compressed by q_{in} due to the output torque τ. The springs are pre-compressed such that both springs will always be in compression. The output motor controls the equilibrium position of the springs, and thus, the equilibrium position of the joint. The position of the pivot point x_p is controlled by the stiffness motor through a lead screw.
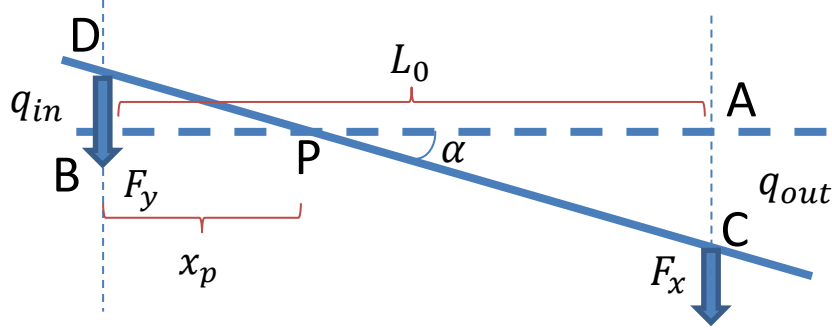
Figure 4.6: Simplified diagram of the proposed variable stiffness joint

To further illustrate the design, the schematic diagram in Figure 4.5 is represented by a simplified diagram as shown in Figure 4.6. In this figure, the pivot is fixed at point P, with distance x_p from the spring. L_0 denotes the effective length of the lever arm. F_x and F_y represent the output force and spring force, respectively.

The keys to ensure linear load-displacement relationship are described in the following paragraphs.

Firstly, the rack-pinion mechanism ensures linear relationship between rotatory motion and linear motion. As shown in Figure 4.7, when the pinion gear rotates by θ, the rack gear will move down by q_{out}. Before moving, assume the centre point of the rack is in contact with the pinion gear at point A. After the gear rotates by angle θ, the previous contact point moves to point B along the arc while the centre point of the rack moves to point C. Assuming there is no backlash between the rack and pinion, arc AB will have the same length of AC.

Hence, $q_{out} = R\theta$, where R is the radius of the pinion gear.
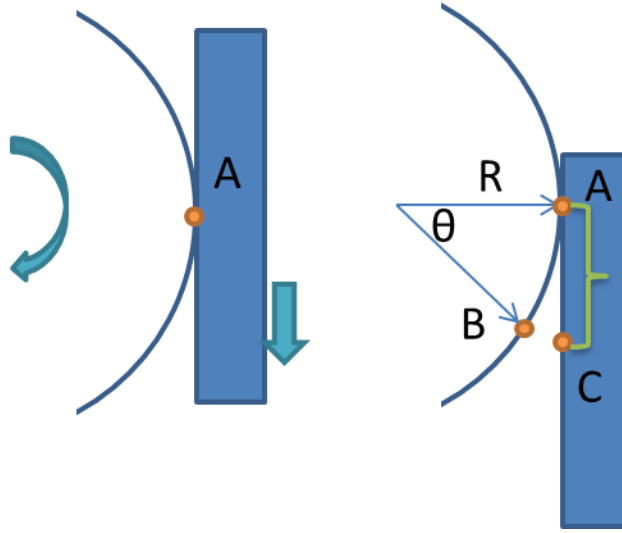
Figure 4.7: Linear motion and angular motion

Secondly, it can be seen that both the output force (F_x) and the spring force (F_y) will always act along the linear guides that are used to constrain the lever mechanism. Therefore, the force acting directions are always parallel on both side of the lever.

Thirdly, the two triangles $\triangle BPD$ and $\triangle APC$ will always be similar to each other, i.e., $\triangle BPD \sim \triangle APC$ always holds, regardless of the lever rotation angle α. This implies that the ratio of two sides of the lever arm will be independent from the deflection angle of the joint. It is worth to notice that the length of the arm changes when the lever rotates. This change will be taken care by the mechanical design, which will be explained in the next section.

These are the keys to generate the linear load-stiffness relationship. Let the output torque be τ and radius of the pinion be R and assume the joint deflection angle due to the load τ is θ, and then the rotational stiffness of the joint K can be calculated as follows:

$$K = \frac{\tau}{\theta}$$

(**4.1**)

$$q_{out} = R\theta$$

(**4.2**)

$$F_x(L_0 - x_P) = F_y x_p$$

(**4.3**)

$$\frac{q_{in}}{q_{out}} = \frac{x_P}{L_0 - x_P} \tag{4.4}$$

$$\tau = F_x R \tag{4.5}$$

Substitute Eq. (4.1)-(4.4) into Eq. (4.5), we have:

$$K(x_p) = k_0 R^2 \left(\frac{\gamma}{1-\gamma}\right)^2 \tag{4.6}$$

where $\gamma = \frac{x_p}{L_0}$.

Equation 4.6 shows that the stiffness is independent from the joint deflection angle θ. Hence, linear load-displacement relationship is guaranteed and the first design requirement is satisfied.

This equation also shows that the stiffness is determined by the radius of the pinion, stiffness of the spring, length of the lever and the position of the pivot. The first three are constant and are determined during design while the last one is controlled by a motor. Let $k_0 = R = 1$ and $\gamma \in [0, 1]$, function $K(x_p)$ could be plotted as in Figure 4.8. As observed in the figure, the stiffness could change from zero to infinity, which satisfies the second requirement.

Furthermore, differentiating Equation 4.6 with respect to x_p gives the sensitivity of the stiffness when the pivot is moved by the stiffness motor, as shown in Equation 4.7.

$$\frac{dK}{dx_p} = k_0 R^2 \frac{2\gamma}{(1-\gamma)^3} \tag{4.7}$$

The sensitivity as a function of the pivot location is plotted in Figure 4.9. It could be seen that at low stiffness (γ is small), large change in the pivot location only causes small change in stiffness, indicating high stiffness resolution. As the stiffness increases, the stiffness resolution decreases. Hence, the third requirement is fulfilled.
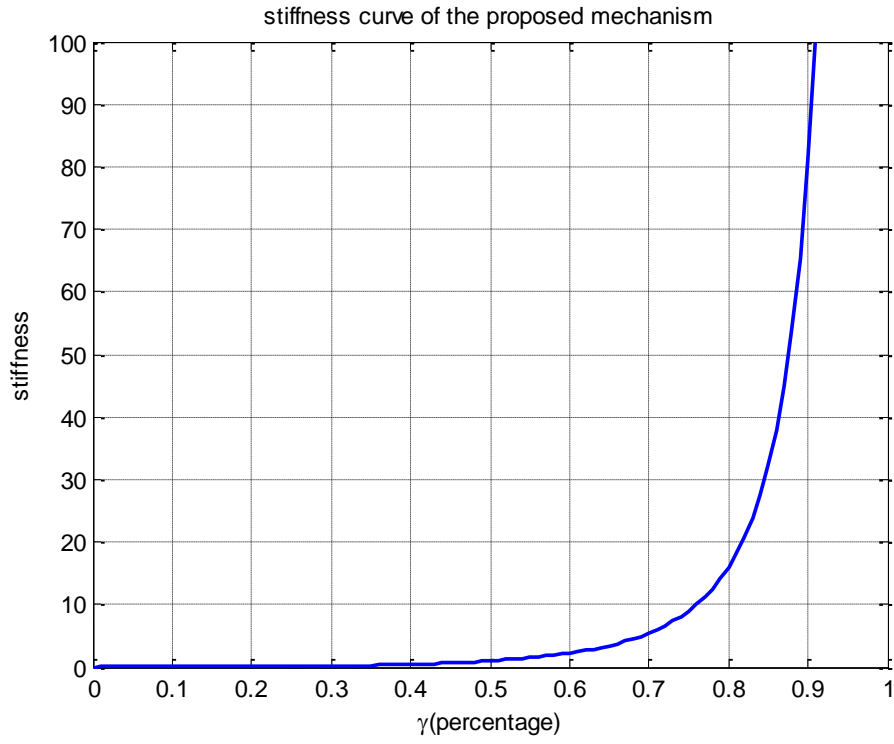
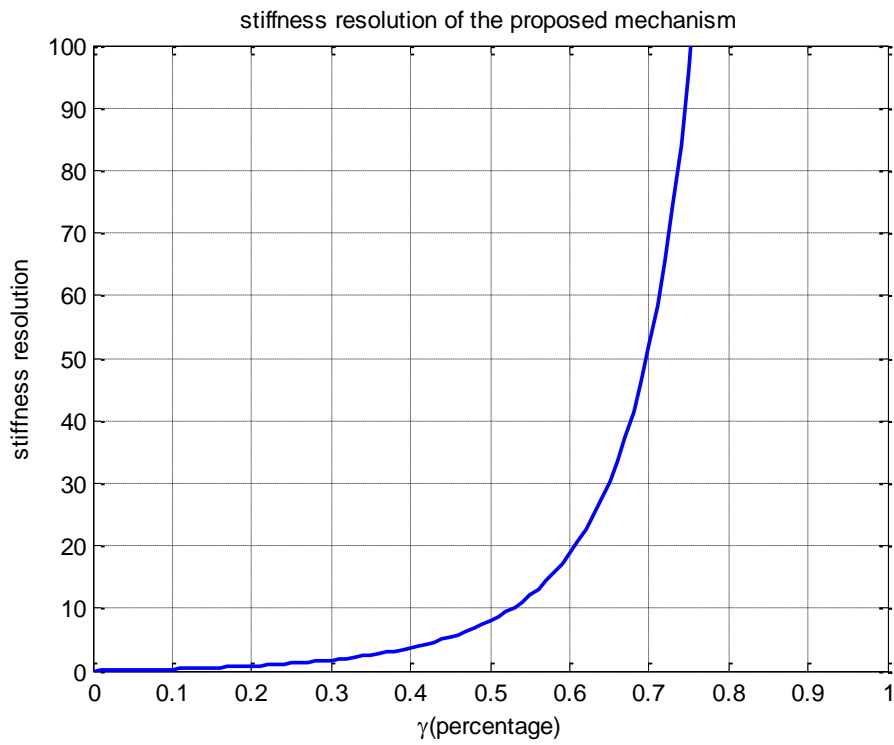**Figure 4.8: Stiffness curve of the proposed mechanism when *k_0=R=1***

Figure 4.9: Stiffness resolution of the proposed mechanism when *k_0=R=1*

The above analysis shows that all the three design requirements are satisfied using the proposed working principle. Characteristics of the mechanical realization of the working principle will be shown in following sections.

4.4 Mechanical Design

Figure 4.10(a) shows the 3D views of the joint design from the CAD software. The input shaft is connected to the output motor to deliver the output torque. The output torque is transmitted to the output shaft through the variable stiffness mechanism in between as shown in the following three sub-figures. Figure 4.10(b) shows the top part of the joint. The output shaft transmits the torque to the rack through the pinion gear. Both shaft of joint O_1 and joint O_2 move along the linear guide. Four pre-compressed springs (as shown in Figure 4.10(b)) of stiffness $\frac{k_0}{4}$ are connected to the left slider in parallel, resulted in total stiffness of k_0. Figure 4.10(c) shows the lever mechanism constructed using four sets of linear guide and slider. The axis of joint O_2 is fixed onto the lever mechanism while the axis of joint O_1 can slide along the linear guides. This makes joint O_1 a 2-DOF joint (rotational and prismatic) and joint O_2 a 1-DOF joint (rotational). This is to adjust the length of the lever arm when it rotates from AB to CD, as shown in Figure 4.6. The position of the pivot of the lever mechanism in Figure 4.10(c) is controlled by the lead screw as shown in Figure 4.10(d). The location of the nut on the lead screw is controlled by the stiffness motor, which drives the lead screw via the pulley belt system.

Most of the parts are fabricated using aluminum while the shafts are made of stainless steel since they are taking the majority of the load.
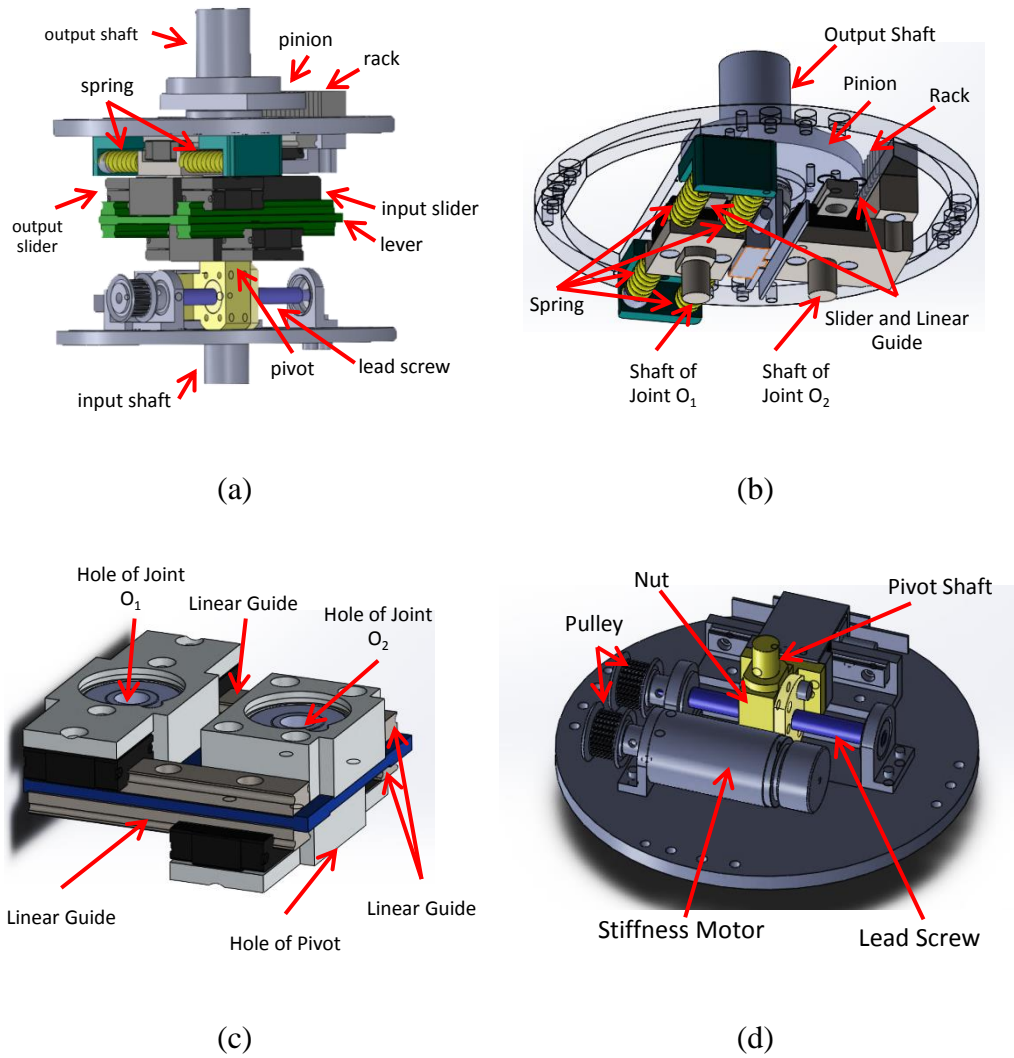
Figure 4.10: 3D views of the joint design. (a) overview; (b) spring and rack-pinion; (c) lever mechanism; (d) pivot mechanism

4.5 Characteristics of the Joint

4.5.1 Key Parameters

The key parameters of the joint are shown in Table 4.1. The input inertia refers to the total inertia of the parts that are rigidly connected to the output input motor, such as the casing frame, the lead screw and the stiffness motor, etc. The output inertia refers to the total inertia of the moving parts such as the lever arm and the sliders that are connected to the lever arm. The input and output inertia are approximated based on inertia value of each individual parts obtained from the CAD software. Since moving the pivot point will change the internal configuration, the output inertia with respect to the pivot point is

shown in Figure 4.11. Minimal inertia is obtained by moving the pivot to the center of the lead screw. This is because a beam has minimum inertia about its axis center of mass and the mass of different parts are evenly distributed on both sides of the lever.

<div align="center">

Table 4.1: Key Parameters of the Joint

</div>

Description	Symbol	Value
Input Inertia	I_1	$1.66 \times 10^6\ gmm^2$
Output Inertia	I_2	$2.92 \times 10^5 \sim 3.85 \times 10^5 gmm^2$
Spring Constant	k_0	$18N/mm$
Non-rotated Lever Length	L_0	$36mm$
Pinion Radius	R	$30mm$
Maximum Spring Deflection	q_{max}	$5mm$

<div align="center">

Figure 4.11: Joint output inertia vs. Pivot position

64

</div>

4.5.2 Joint Deflection Range

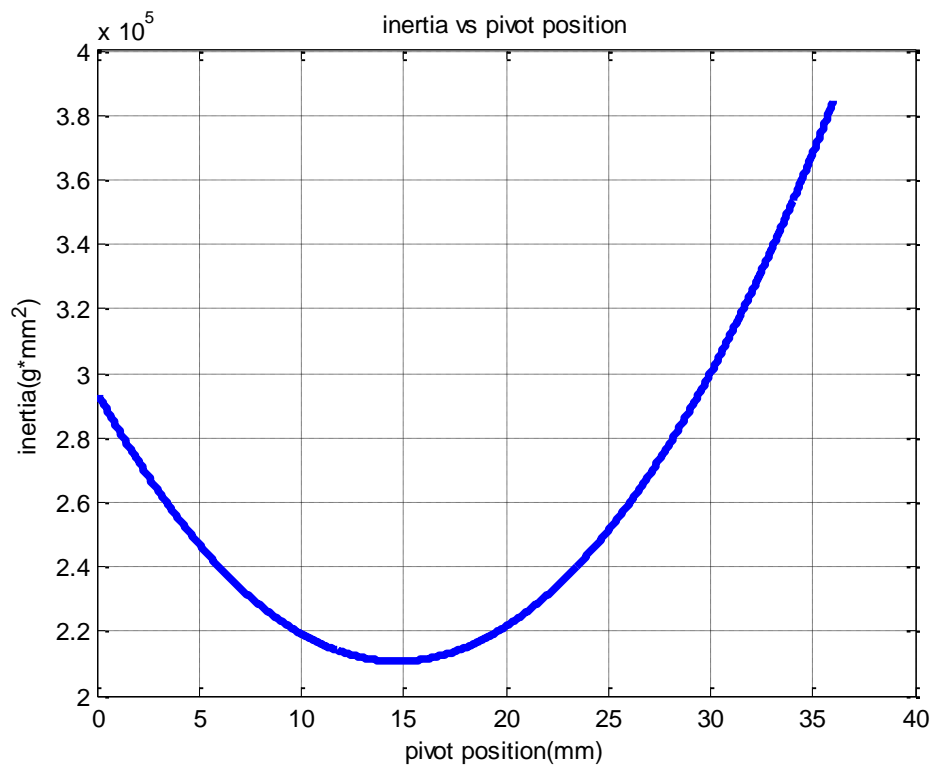In the novel design, motion ranges of the sliders are restrained in a certain range on both sides of the lever arm. As shown in Figure 4.12, the spring compression limit represents the maximum spring deflection while the linear guide motion limit represents the limited motion range imposed by the finite length of the linear guide. Therefore, the joint maximum allowable deflection changes with the pivot position. For example, as shown in Figure 4.12(a), when the pivot is close to the spring side, joint O_2 hits the limit first, resulting in the maximum output angle. Hence, when the pivot is close to the spring, i.e., when the joint stiffness is low, the output link can always reach the maximum angle. In Figure 4.12(b), spring limits will first be hit when the pivot is far from the spring. Hence, the motion range becomes smaller.

(a)   (b)
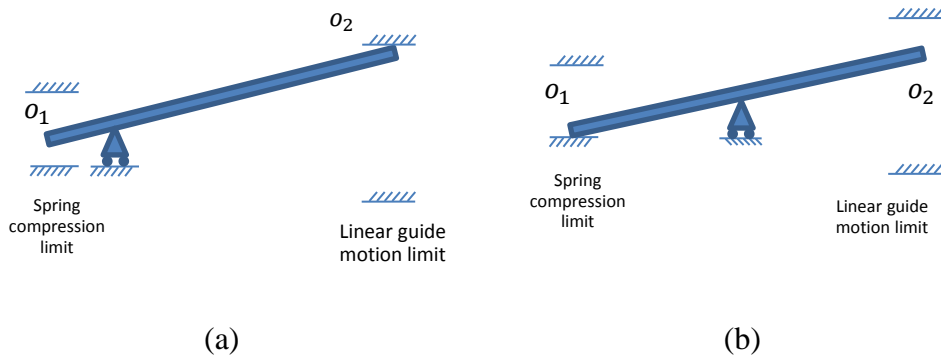
Figure 4.12: Output limit due to motion limit at both ends. (a) motion range limited by linear guide motion limit at O_2, θ_{max}=30°; (b) motion range limited by spring compression limit at O_1, θ_{max}<30°.

Figure 4.13 shows the maximum allowable deflection with respect to the pivot position. The joint is designed in such a way that when the pivot is approximately within *10mm* distance from the spring, the maximum allowable joint deflection can reach $\pm 30^o (\pm 0.525\,rad)$. If the pivot is moved more than *10mm* from the spring side, the maximum allowable joint deflection will be reduced.
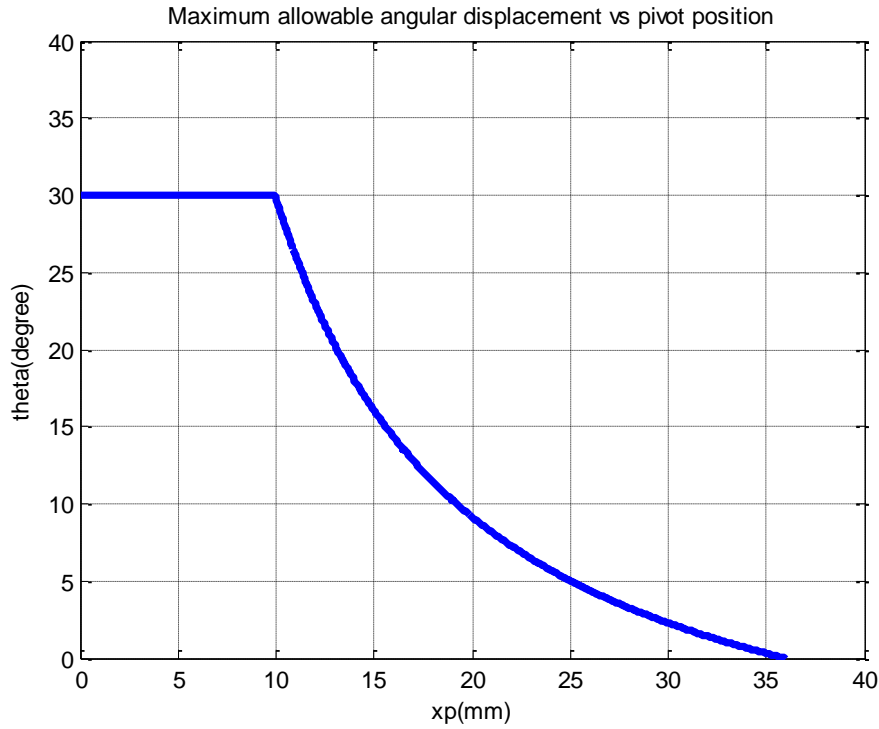
Figure 4.13: Joint maximum allowable deflection vs. Pivot position

4.5.3 Stiffness Characteristic

Figure 4.14 shows the stiffness characteristic curve with respect to the pivot position using the spring chosen in Table 4.1. It shows that the stiffness changes from zero to infinity as the pivot moves away from the spring. The second design requirement has been satisfied.

As the pivot moves further away from the spring, the slope of the stiffness curve increases. This implies that the stiffness will be more sensitive to position error in placing the pivot. Therefore, the stiffness resolution will be higher when the pivot is closer to the spring. The third design requirement has been satisfied, too.

In practice, the spring stiffness needs to be chosen based on the application such that both higher resolution and large allowable joint deflection can be obtained in the typical operating range.
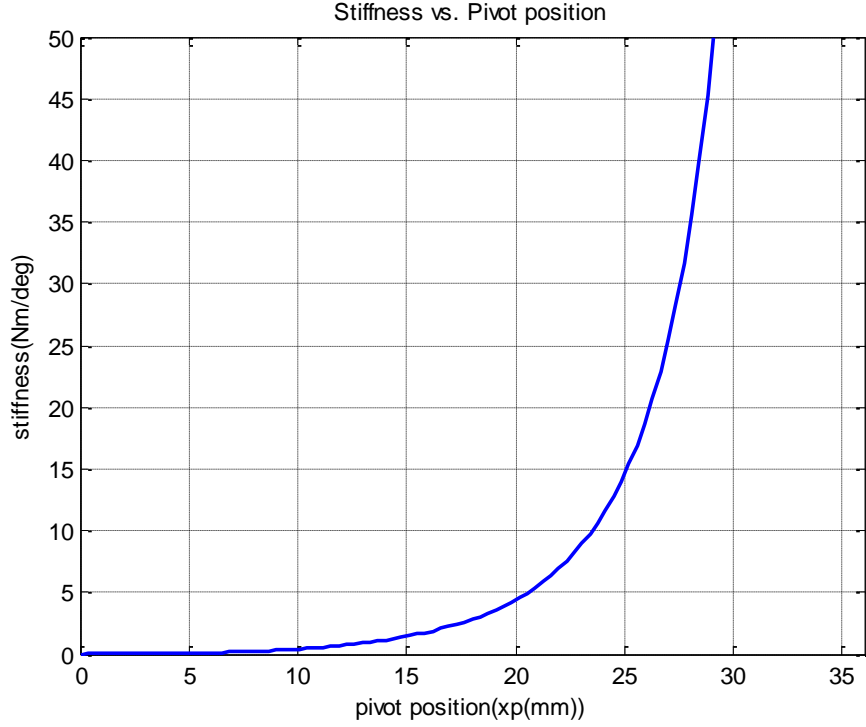
Figure 4.14: Joint stiffness vs. Pivot position

4.5.4 Characteristics Identification

In this section, experimental results are shown to verify the characteristics of the novel variable stiffness joint based on a prototype. Particularly, the load and joint displacement relationship are identified. The experimental setup is shown in Figure 4.15.

In the prototype, a Faulhaber DC brush motor is used to provide the output torque. It is coupled with a planetary gear with gear ratio of *1:38*. The motor without gear could provide stall torque of *1.09Nm*. A rotary optical encoder with resolution of *500count/round* is connected to the motor before the gear. A small Maxon DC brush motor with stall torque of *0.0246Nm* is coupled with a planetary gear of ratio *1:84*. The output of the gear shaft is connected to a lead screw with pitch *1mm* through a pulley-belt system. The two pulleys have the same diameter. A linear optical encoder with resolution *0.5μm/count* is used to measure the position of the pivot. And another linear encoder with the same resolution is used to measure the output slider (the slider that is connected to the rack) displacement. Based on the displacement of the output slider and the

diameter of the pinion, the joint deflection angle can be calculated. A 6-axis force/torque sensor is connected to the output shaft to measure the output load.
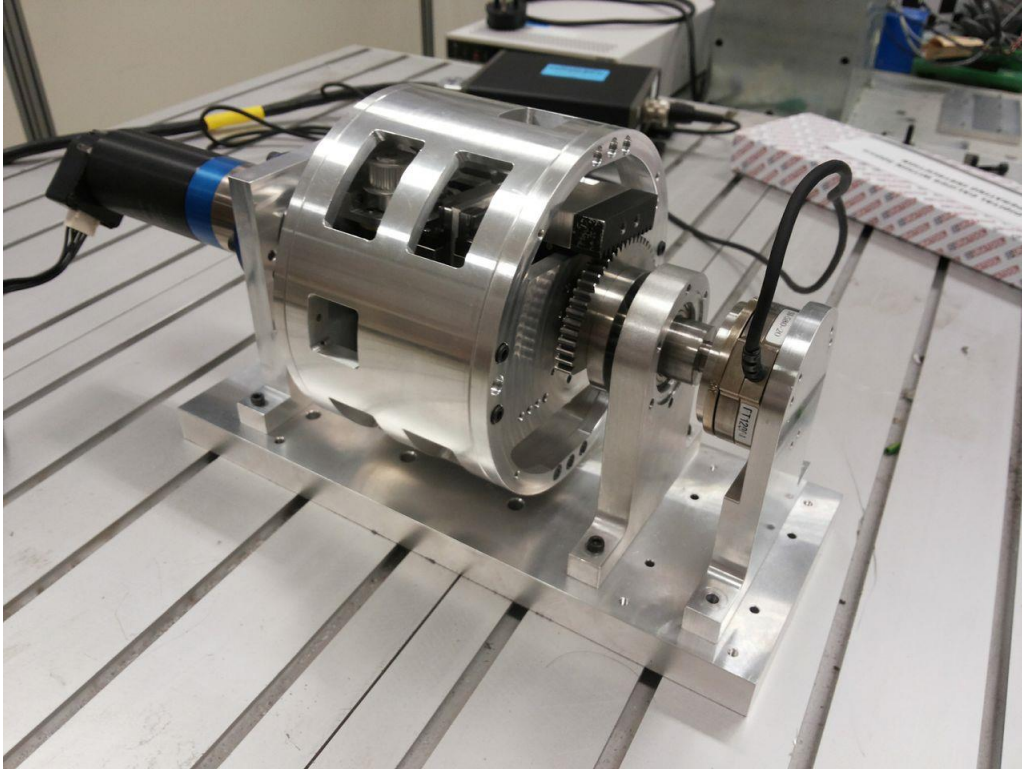
(a)

(b)   (c)   (d)

Figure 4.15: System identification experiment setup (Fixed end). (a) first prototype with fixed end; (b) base of the joint, with the pivot control mechanism; (c) lever mechanism; (d) top of the base, with rack-pinion and springs

Figure 4.15(a) shows the first prototype with fixed end. The input shaft of the variable stiffness joint is connected to a position controlled motor and the output shaft is connected to a link. The link is fixed while identifying the load

68

and joint displacement relationship. Figure 4.15(b) shows the base of the joint with the pivot control mechanism. The stiffness motor is connected to the lead screw through the belt and pulley to control the pivot position. PID controllers are designed and tuned for both motors to control the respective positions. Figure 4.15(c) shows the lever mechanism while Figure 4.15(d) shows the top of the joint where sprints are mounted onto.

The following experiments were conducted using QNX system, which is a real-time system running in Windows. Simulink was used to program the system and the system was running at *1KHz*.

Figure 4.16 shows the result of linearity test of the variable stiffness joint. As it has been identified in the design requirement, the load-displacement relationship should remain linear for all pivot positions.

Experiments were conducted by fixing the pivot at different positions to verify the load-displacement relationship. In the experiment, the output motor's desired position was changed from zero to the maximum allowable joint deflection in both positive and negative direction slowly. The output torque at steady state was measured at each joint deflection angle. Therefore, only the spring dynamic was excited. The stiffness motor's position remained unchanged when the output motor moved. The joint deflection and the torque were measured during the process. Then the experiment was repeated ten times with pivot placed at the same location. Finally, the entire procedure was repeated another four times with the pivot at another four different locations.

The result shows good linearity for all the five pivot positions, from low stiffness to high stiffness. It also exhibits backlash and hysteresis which will be discussed in the following figure.
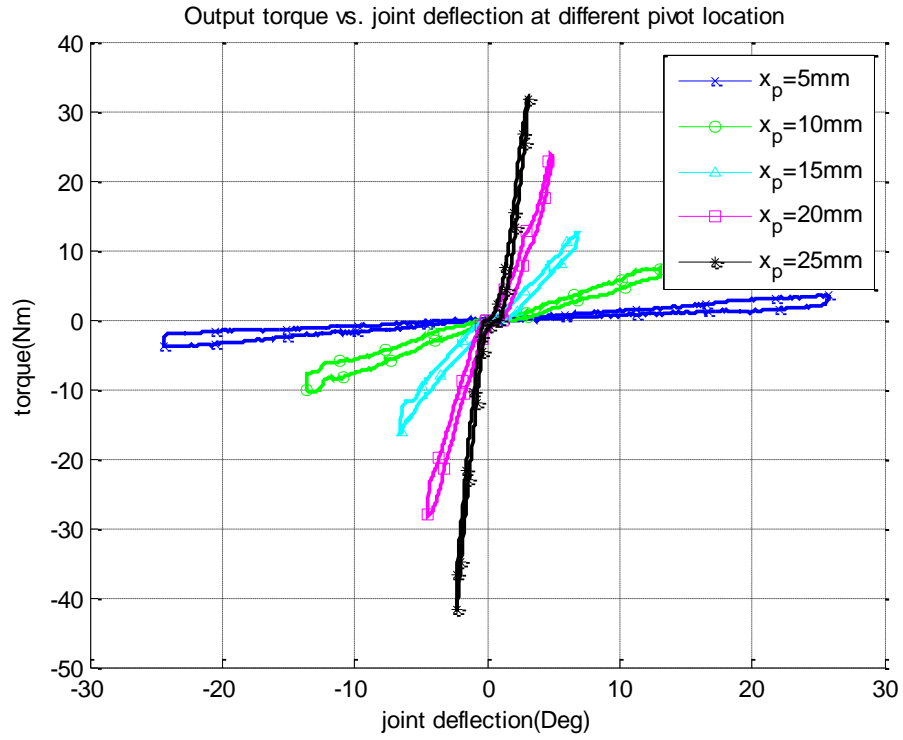
Figure 4.16: Output torque vs. Joint deflection at different pivot location
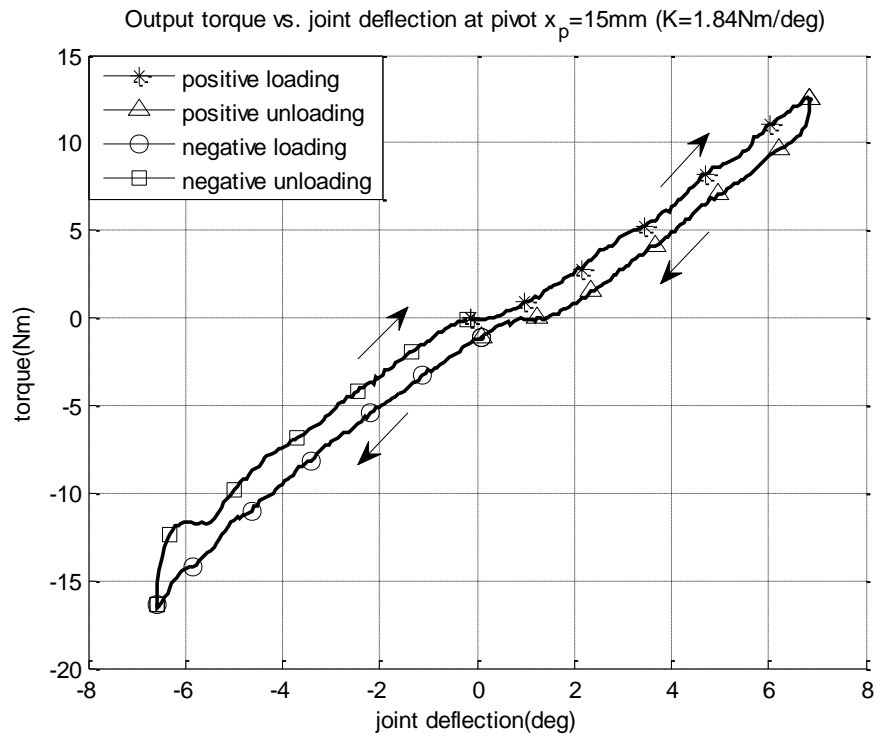
Figure 4.17: Output torque vs. Joint deflection at pivot x_p=15mm (K=1.84Nm/deg)

70

Figure 4.17 shows when the pivot is at $x_p = 15mm, K = 1.84Nm/deg$. Backlash and hysteresis are shown when the joint is loaded and unloaded in both positive and negative direction. This backlash is mainly contributed by the clearance between moving parts in the joints, especially between the rack and pinion mechanisms. Therefore, the amount of backlash remains similar (approximately 1°) for all different pivot locations. This problem could be solved by choosing better tolerance between moving parts when designing each component. In the first prototype, the tolerance chosen between each moving component is large so that the joint could be dismantled to investigate any potential problems. The main source of the hysteresis is due to the backlash of the output motor and the friction. When the joint was changed from loading to unloading, the backlash results in lack of output torque from the motor when the motion direction changes. Thus, the output torque dropped significantly compared to the joint deflection. This problem could be solved by using a heavily geared motor.
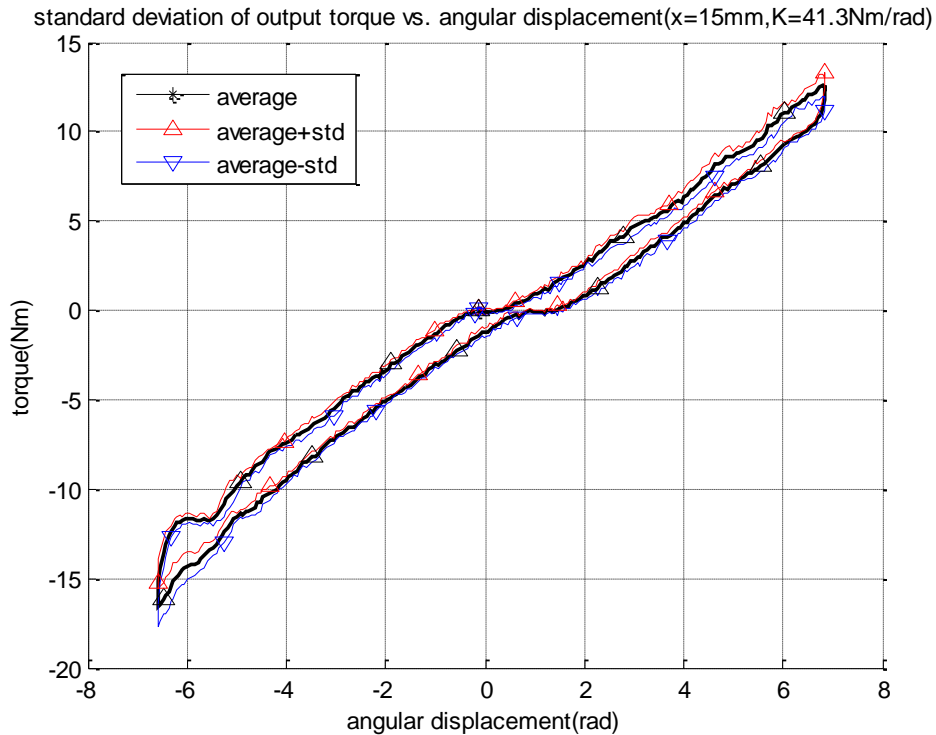
Figure 4.18: average and standard deviation of output torque vs. angular displacement...(x=15mm,K=1.84Nm/deg)

71

Figure 4.18 shows the average of the torque-displacement curve plus and minus the standard deviation of the ten trials. In Figure 4.18, the "average" line represents the average torque calculated from all the ten experimental results against the displacement. The "average+std" and "average-std" are the average summed with plus and minus the standard deviation, representing the error in all ten trials. It shows the repeatability is good, indicating the result is reliable.

Figure 4.19 shows the relationship between the stiffness and the pivot position. In this experiment, the output deflection angle was fixed at different values but the pivot was moving. The pivot position started to move from $x_p = 0mm$ slowly such that at each pivot position, only the steady output torque was measured. It stopped at $x_p = 25mm$ since output torque had become very large even for small joint deflection. The experiment was repeated for ten times with different output deflection. In Figure 4.19, the "average" line represents the average stiffness calculated from all the ten experimental results. The "average+std" and "average-std" are the average stiffness summed with plus and minus the standard deviation, representing the error in all ten trials.
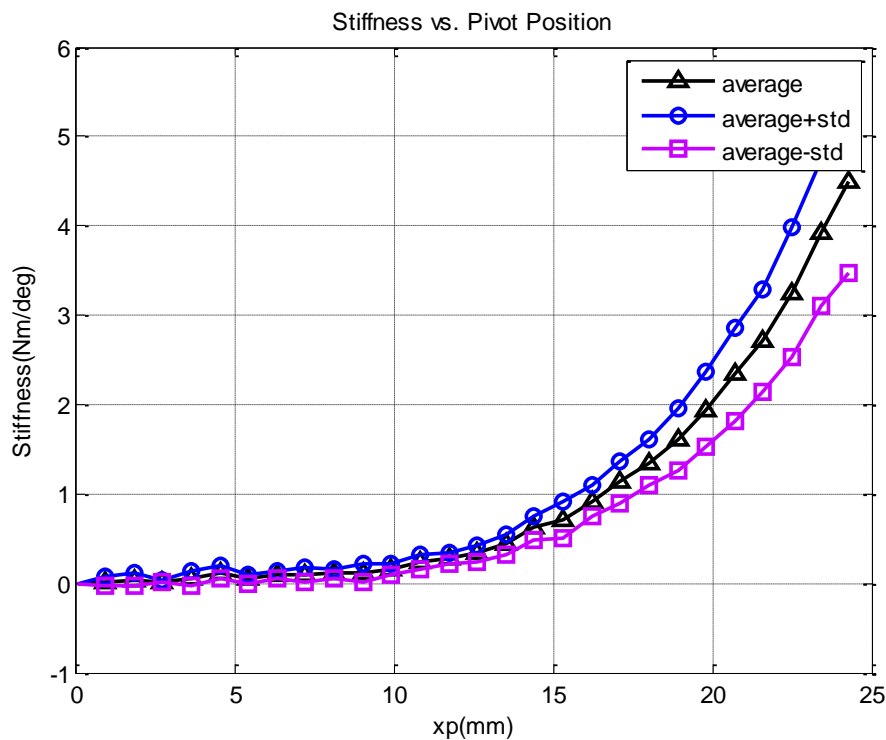
Figure 4.19: Stiffness vs. Pivot Position

Figure 4.19 exhibits a fine stiffness resolution when the pivot is close to the spring. The stiffness increases rapidly as the pivot moves towards the other side of the lever, which implies that the second and third design requirements have been met.

In this prototype, a small Maxon DC motor is used to control the position of the pivot. At full speed, the pivot travel from one end to the other within *12s*, i.e., the stiffness can be varied from zero to infinity (or infinity to zero) within *12s*. This speed can be increased if a more powerful motor is used to control the pivot position.

4.5.5 Output Frequency Response

In this section, the frequency response test results are shown. To exam the dynamic of the system, especially the passive joint deflection response to the output load, an impact test was performed. In this experiment, a hammer was used to hit the output link of the joint while the input motor is servoing at a fixed position. The input torque of the variable stiffness mechanism was measured by the joint torque sensor while the output joint deflection was measured by the encoder. An example of the time domain data when the pivot is at *xp=10mm* (*K=0.557Nm/deg*) is shown in Figure 4.20.

The frequency response between the input and output was obtained through FFT. Figure 4.21 shows the frequency response of the joint deflection to the impact force. It shows that the system first resonant mode became higher when the stiffness of the system increased.
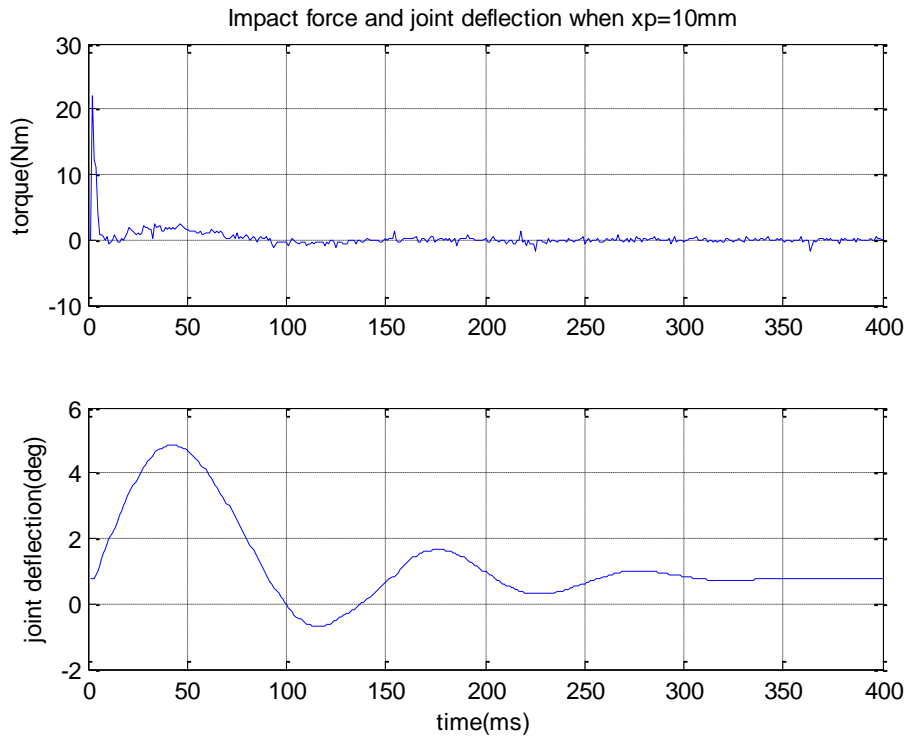
Figure 4.20: Impact force and joint deflection when x_p=10mm
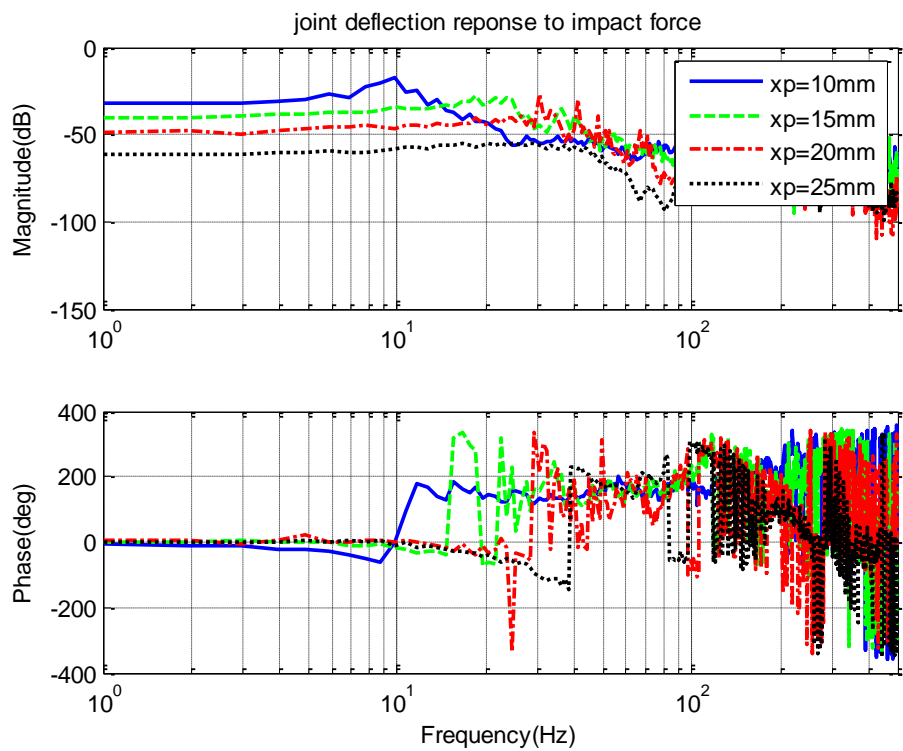
Figure 4.21: Joint deflection frequency response to impact force

4.6 Force Control Using the Joint

In this section, force control generally includes torque control at joint level. To test force control performance, the output shaft is connected to a link that could move freely. Then, controllers are designed to regulate the contact force and adjust the stiffness. Next, an experiment is conducted to simulate the machining process. Finally, a control scheme that results in fast response and low impact force is demonstrated.

4.6.1 Controller Design

As shown in Figure 4.22, both output motor (Motor$_1$) and stiffness motor (Motor$_2$) are under position control by Proportional-Integral-Differential (PID) controllers. The PID controller gains are tuned for output motor and stiffness motor separately. A torque sensor is used to feedback the contact force to form a closed loop system. A second order Butterworth low pass filter is used to filter the noise in the torque sensor. A controller H is employed to generate position command for the output motor based on the force feedback.
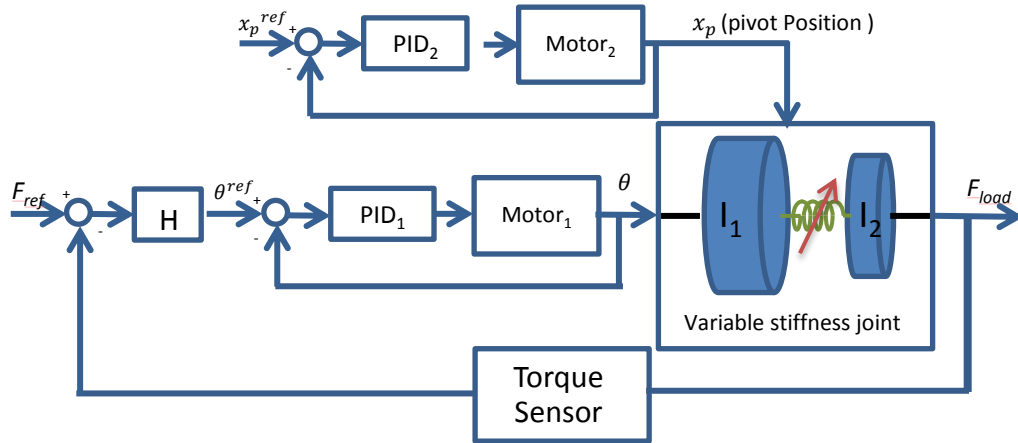
Figure 4.22: Controller diagram of the variable stiffness joint

In the variable stiffness joint, the system dynamics changes when the stiffness is different. Therefore, the controller gain needs to be adjusted accordingly so that the system remains stable.

In this experiment, the controller gains of the output motor are tuned for different stiffness with the pivot at $x_p = 5, 10, 15, 20, 25 \ mm$. Then a lookup

table is built to interpolate any pivot position in between. Another PID controller was used to form the closed loop force control. The PID controller for force control loop is implemented in digital incremental form so that bumpless transfer could be achieved when controller gains are changed. Hence, no significant change in position command is generated.
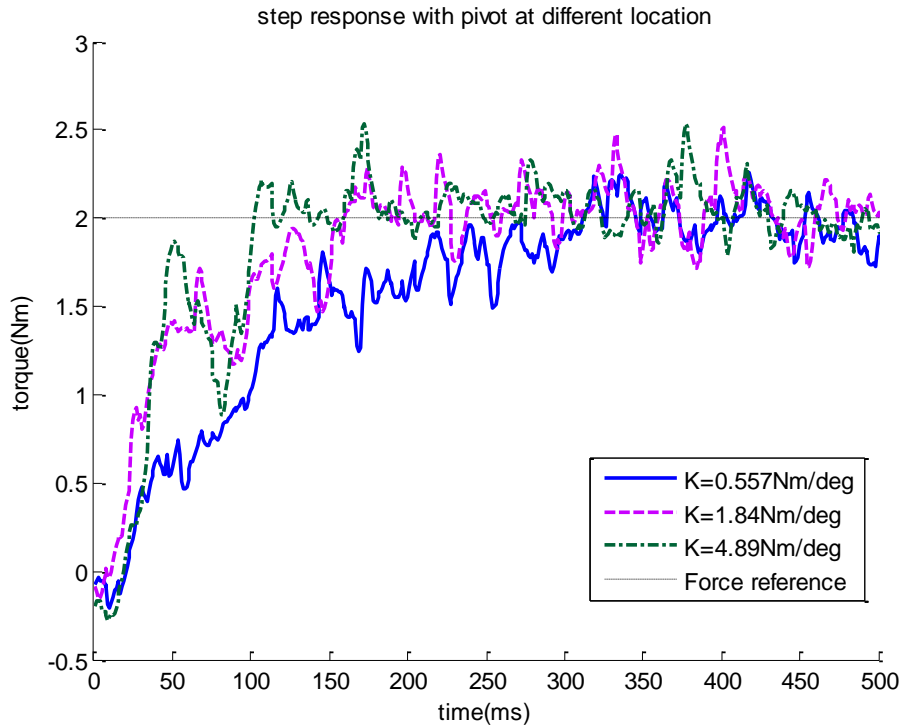
Figure 4.23: Step response with different joint stiffness

Figure 4.23 shows the step response of the system with 3 different stiffness values when force feedback is used. The PID controller gain for each stiffness value was tuned such that the system could response faster when a step input is given. The result in Figure 4.23 shows that higher joint stiffness resulted in faster response. There are several reasons that lead to this result. First of all, a system with higher stiffness has a higher natural frequency. In order to compress the spring to deliver the same output force, the motor of this system needs to travel for a smaller distance. Secondly, in order to increase the response speed of the softer system, large controller gains are required. However, this would make the system less stable. Thus, if response speed is crucial, higher stiffness should be used so that higher bandwidth could be

achieved. In Figure 4.23, it shows that system with stiffness K=4.89Nm/deg has the fastest response.

4.6.2   Searching for Contact Experiment

Although higher stiffness results in faster response, it raises problem when high frequency disturbance is present. For example, the following experiment simulates a common scenario in manipulating an object: searching for contact. As shown in Figure 4.24, the joint start moving towards the surface distance away from the contact surface. The challenge of this task is to avoid large contact force throughout the entire process, especially during impact.
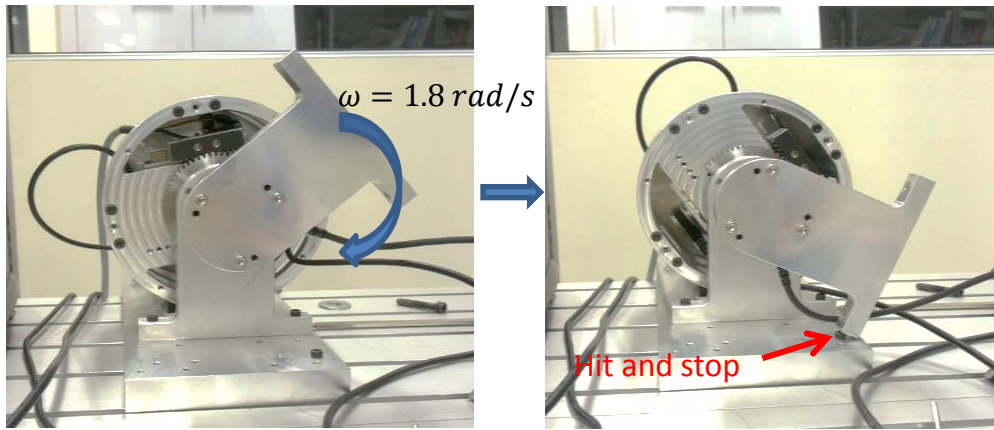
Figure 4.24: Experiment setup (moving end)

In this experiment, the joint starts at a high velocity to demonstrate approaching the workpiece from far away. When the end point is close to the surface, the joint speed will decrease to avoid high speed impact. Upon making contact, the robot will switch to force control. The flow chart of the process is shown in Figure 4.25, where θ is the joint angular deflection and F is the force measured by the force sensor. $\theta_{threshold}$ and $F_{threshold}$ are thresholds to detect contact. If either the angular deflection or the contact exceeds the corresponding threshold, controller will be switched from position control to force control.
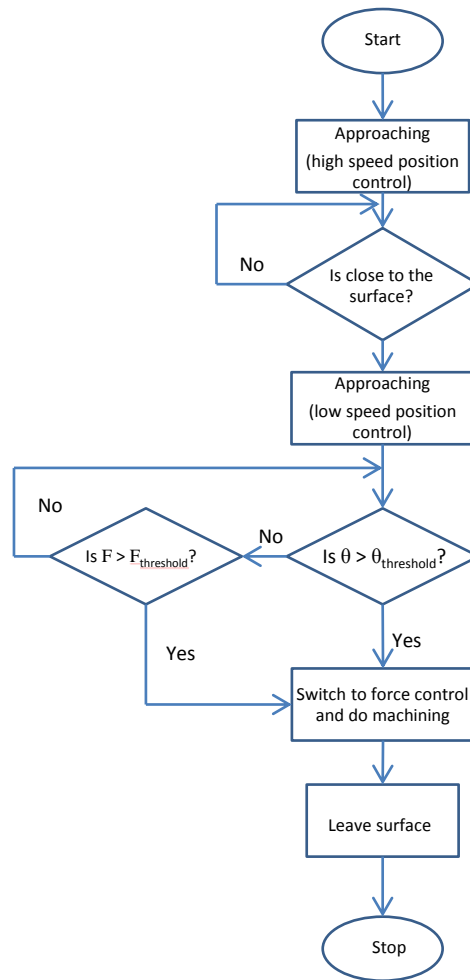
Figure 4.25: Flow chart of from non-contact to force control

Figure 4.26 shows the contact force before and after the end-effector makes contact with the surface when the stiffness is large ($K=4.89Nm/deg$). The result shows large amount of overshoot and vibration after contact and the whole system takes very long time to settle down. The contact force has decreased below zero indicating that the end point has lost contact with the environment and chattering occurred. This is dangerous when interacting with the environment because the unstable behavior will result in unevenly distributed force over the working area. Moreover, tools or workpiece may be broken due to chattering. Hence, this must be avoided during machining.
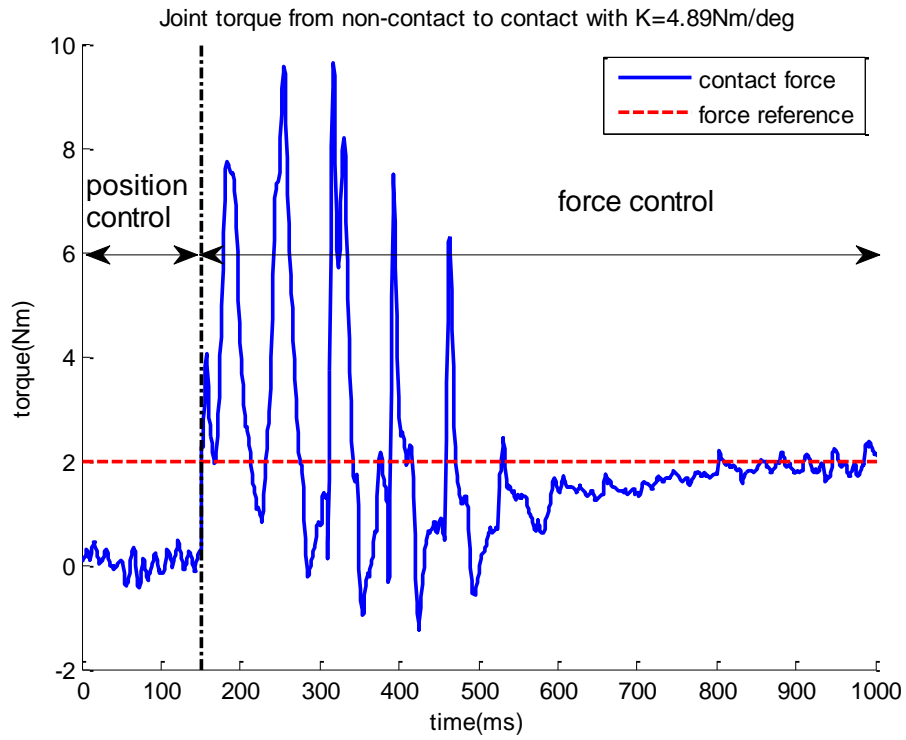
Figure 4.26: Contact force during impact with K=4.89Nm/deg
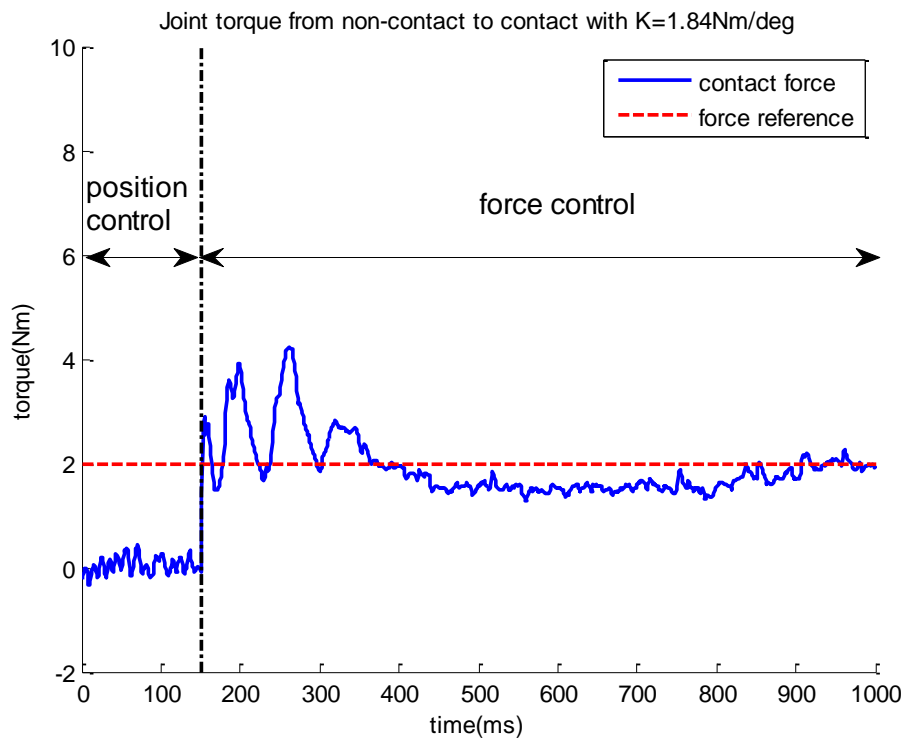
Figure 4.27: Contact force during impact with K=1.84Nm/deg

79

Figure 4.27 shows the contact response when the stiffness was set to *K=1.84Nm/deg*. In this test, although overshoot and vibration is still present, both amplitudes are smaller than that when the stiffness is higher at *K=4.89Nm/deg*. No chattering occurred since the contact force remained positive all the time.
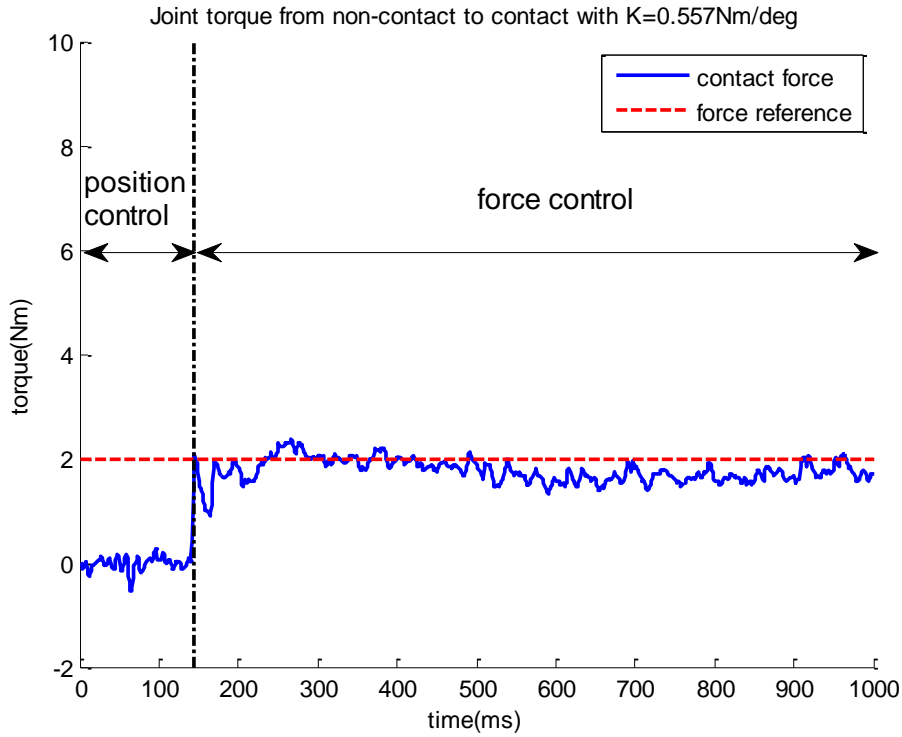
Figure 4.28: Contact force during impact with K=0.557Nm/deg

Figure 4.28 shows the force in the contact response when the stiffness was set to *K=0.557Nm/deg*. In this test, no overshoot or vibration existed, implying a good transmission between position control and force control. No chattering occurred since the contact force remained positive all the time.

The above experiments show that a stiffer joint has poorer disturbance rejection ability but higher bandwidth, while a softer joint has better disturbance rejection ability but lower bandwidth. Hence, when designing a traditional SEA, a tradeoff between bandwidth and disturbance rejection ability has to be made. However, in a variable stiffness joint, the stiffness could be controlled at different phase of the contact process such that both disturbance rejection ability and high bandwidth can be achieved simultaneously.

Figure 4.29 shows a control strategy that utilizes the feature of adjustable stiffness in different phases of the contact process. In this figure, the solid blue line shows the force measured by the sensor while the green dotted line shows the pivot position, x_p. Before contact, the stiffness was set to be low ($K=0.557Nm/deg$, $x_p=10mm$) so that no overshoot or vibration was observed during the impact. Upon detecting contact by following the scheme in Figure 4.25, the pivot was moved towards the other end of the lever such that the stiffness became higher ($K=1.84Nm/deg$, $x_p=15mm$).
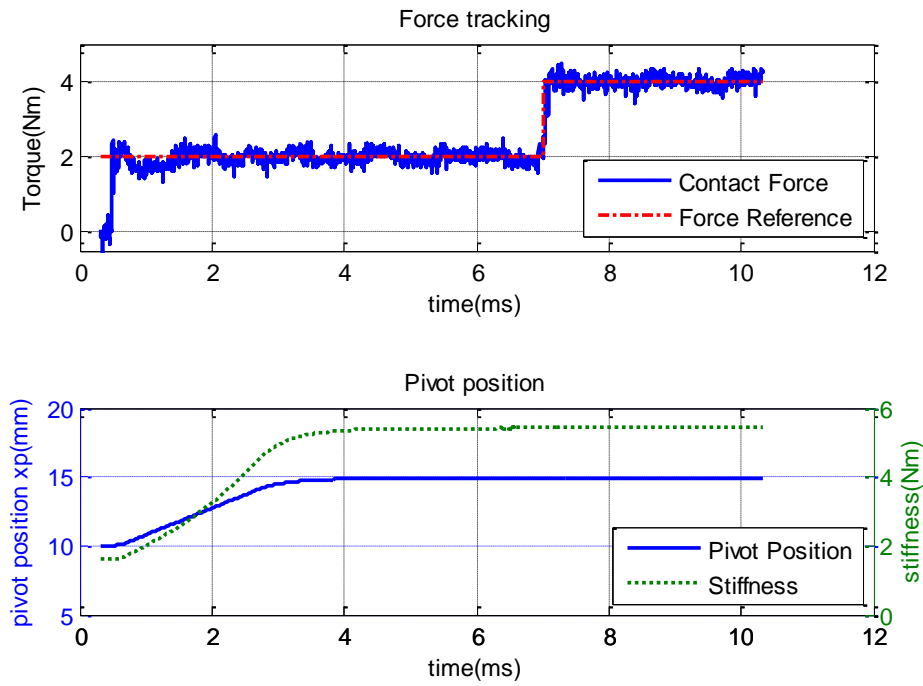
Figure 4.29: Force and pivot position during contact

From the result, it could be seen that no overshoot or vibration is observed during contact. After making contact, the pivot started to move away from the spring and stopped at $x_p=15mm$ in about 3 seconds. Another step input at t=7s was used as the reference and the sensor measured torque showed relatively fast response, same as the dotted line in Figure 4.23. This experiment has demonstrated how the variable stiffness property could be used to ensure a smooth contact and fast response.

In the experiment shown above, stiffness of $K=0.557Nm/deg$ and $K=1.84Nm/deg$ were used as an example to show the effectiveness of the

approach. In real implementation, the stiffness chosen should be based on several parameters, such as the spring stiffness, the targeted stiffness and the end-effector approaching speed. The results of using different stiffness setting and different approach speed have shown similar results and they are not shown in this thesis.

4.7 Summary

In this chapter, important characteristics that a variable stiffness joint needs to have in order to be used for various interactive tasks have been analyzed. Results showed that three characteristics, especially linear load-displacement are needed to perform force control, especially to handle unknown disturbance. Furthermore, to use a variable stiffness actuator in various applications, large achievable stiffness range is also necessary. Research shows that most variable stiffness joint mechanisms do not have all the characteristics. Therefore, a novel variable stiffness joint using a constrained lever mechanism is presented according to the needs. In this chapter, the working principle of the mechanism is explained with the aid of graphs. The CAD drawing of the design is shown to illustrate the mechanical realization of the concept. Then, experiments are performed to characterize the joint mechanism. Results have shown that the joint mechanism exhibits the desired characteristics as been specified in the design stage. Errors due to imperfection of the mechanical components such as backlash and hysteresis are also analyzed and improvements have been suggested to avoid or minimize them. After that, controller design for force control is shown. The closed loop response has proven the fact that higher stiffness will result in higher bandwidth but poorer disturbance rejection ability. Finally, a contact experiment to simulate the entire manipulation process, especially during contact is used to demonstrate how to control the variable stiffness joint for such applications. The result shows that the joint could maintain high bandwidth while not compromising the disturbance rejection ability.

Chapter 5

Conclusion

The main objective of this research is to improve robot force control through structure modification. In Chapter 1 and Chapter 2, the research in the field of robotics force control was introduced. The two commercially accepted approaches, force control through end-effector and force control through all joints were studied and presented. The main limitations in each method were analyzed and solutions are suggested to resolve the limitations. In Chapter 3, the dynamics of series macro-mini manipulator system was studied as an example of force control through end-effector approach. The focus of the research is on eliminating the internal vibration due to the low frequency resonant modes of the macro manipulator. The Zero Coupling Impedance criterion was introduced as a general design guideline for a series macro-mini manipulator system. In Chapter 4, a new variable stiffness joint mechanism was proposed to enhance force control performance at joint level. Since this novel mechanism was designed to according to design the requirements, high force control performance in interactive applications has become possible.

In the following section, the results obtained from the research will be summarized and discussed. The significance of the research will be explained. Finally, the limitations in the research will be discussed and recommendation for future research to resolve the limitations will be given.

5.1 Summary of Results

In Chapter 3, the dynamics of a series macro-mini manipulator was studied by building a mathematical model using simple linear components. The analysis of the model shows that the resonant modes in the macro manipulator at low frequency will form internal vibration in the macro manipulator. Through the coupling between the two manipulators, vibration will be transmitted to the

contact point. Therefore, force control performance will be compromised. A new method was proposed to suppress the vibration in the series macro-mini manipulator system by regulating the impedance of the coupling between the two manipulators. The proposed method, Zero Coupling Impedance criterion, describes a condition to eliminate vibration transmitted the contact point. Both simulation and experimental results proved that the effect due to the internal vibration of the macro manipulator could be removed from the contact force by satisfying the criterion. Therefore, a guideline to design a series macro-mini manipulator system without having the internal vibration affecting the force control performance is derived from the Zero Coupling Impedance criterion.

Chapter 4 presented the research work on developing a variable stiffness joint mechanism. Force control through all robot joints requires the robot joints to deliver the required force and handle disturbance while interacting with the environment. Analysis of a general manipulation process indicated three essential requirements that a robot joint should have to perform interactive tasks. However, most variable stiffness joint mechanisms do not have all the three characteristics. Therefore, a new variable stiffness joint mechanism that satisfies all the three requirements is proposed.

The challenges of designing a joint to meet all the three requirements are analyzed in Chapter 4. Maintaining constant force direction and lever arm ratio between input and output is the key to the required characteristics. A novel mechanism was proposed accordingly and the CAD drawing was shown to illustrate the implementation of the concept. Then, a prototype was built to prove the concept of the design. Experiments were conducted to verify the characteristics of the joint mechanism. Results showed that the prototype met the design requirements and further experiments were conducted to test the force control performance using this joint mechanism. The response of force control indicated that the joint is suitable for force control, especially with disturbance being present. Furthermore, demonstrative experiment showed promising result while the robot is searching for contact.

5.2   Significance of the Research

In research of series macro-mini manipulator system, it is commonly known that the bandwidth of the serially coupled manipulator is solely determined by the mini manipulator. However, the flexible macro manipulator will degrade the system performance if its resonant modes are excited. Several attempts have been made by researchers to resolve this limitation [40, 44-46]. Most methods suppress the vibration by designing controllers for the macro manipulator to damp out the resonant peaks, or utilizing external sensing to measure the vibration directly. These methods work well in laboratory environment but may not be easily implemented on commercial industrial robots. Most robot manufacturers do not provide access to the low level controller to modify the robot dynamics. Hence, the Zero Coupling Impedance criterion is an alternative solution to resolve the issue from a different perspective. This guideline states that the impedance of the coupling element between the macro and mini manipulator should be small and well identified. The controller should only use feedback from the coupling to cancel the mechanical impedance.

In general, the Zero Coupling Impedance criterion provides a simple method to eliminate vibration from the mini manipulator force control. It is more than a controller design since the problem is solved from the manipulator design stage. It indicates how to couple the mini manipulator to the macro manipulator to avoid the vibration problem. It also states the choice of sensory feedback before designing the controller. Therefore, this method is general and can be widely applied when designing a series macro-mini manipulator for force control, especially for machining.

The research work on developing the variable stiffness joint mechanism is another way to improve force control performance. Research in variable stiffness joint mechanism has become popular in the recent years. However, many of these mechanisms are designed for specific tasks. For example, variable stiffness actuators designed for robots to interact with human emphasize safety and put safety as the first design requirement. The stiffness may not need to be controlled precisely. Hence, the important characteristics

such as linear load-stiffness relationship are usually missing in those works. In this thesis, the proposed variable stiffness was designed to fit various applications due to its wide stiffness range. Stiffness is well handled by the specially designed mechanism to ensure easy and accurate control. The first prototype has shown the feasibility of implementing this mechanism using simple components. Testing results indicated that some challenging tasks such as searching for contact could be easily done with the proposed mechanism.

The variable stiffness design is a novel mechanism whose characteristics are purposely designed for machining tasks. Other variable stiffness mechanisms do not have all the identified properties, making them not ideal for force control machining. The results successfully demonstrated the potential of using this mechanism to construct a new generation of robot that is optimized for machining.

5.3 Limitations and Recommendations for Future Research

In this thesis, the research on the series macro-mini manipulator has used a direct drive motor due to the limited resource. However, in practice, the choose of the mini manipulator may also affect performance of the coupled system. Different types of mini manipulator may result in different new problems. Hence, other types of mini manipulator should be used to further verify the result. Furthermore, the grinding result shown in Chapter 3 only shows the contact force measured by the sensor. The correlation between the surface finishing and the contact is not analyzed. Although it is not covered by the scope of this thesis, it is worth studying to have a better understanding on force control machining.

For future research, it is recommended to test the Zero Coupling Impedance using more complex end effector module, for example, a SEA or a variable stiffness joint. Furthermore, the relationship between the contact force and the surface finishing quality need to be studied.

The work of the proposed variable stiffness mechanism used a DC brush motor coupled with planetary gear as the output motor. However, it is commonly known that the DC brush motor with planetary gear has many

problems such as backlash, non-backdrivable and low power rating, etc. Other source of power inputs are not tested in the thesis. Using different actuator may improve the force control performance further. Moreover, the size of the prototype could be reduced since all the components used to build it are not customized. A new joint that use customized components should be built so that the mechanism is optimized for the given task. Finally, in this thesis, only a joint with variable stiffness is designed. However, the dynamics of a single joint will be different from a complete robot arm. The performance of this joint should be further evaluated with a robot equipped with this joint.

In the future, it is recommended to test a few more different actuators as the power input to the system, for example, pneumatic system and hydraulic pump. In this thesis, a DC motor under position control mode was used to build the variable stiffness actuator. It was assumed to be a perfect position power source, i.e., it follows the command position with no delay or steady state error. Furthermore, the mechanical design should be revised such that the components are optimized for the design. Finally, a simple robot with multiple degree-of-freedom needs to be built to test the more complicated dynamic system.

Bibliography

1. Whitney, D.E., *Historical Perspective and State of the Art in Robot Force Control.* The International Journal of Robotics Research, 1987. **6**(1): p. 3-14.
2. Zeng, G. and Hemami, A., *An overview of robot force control.* Robotica, 1997. **15**(5): p. 473-482.
3. Albu-Schäffer, A., Haddadin, S., Ott, C., Stemmer, A., Wimböck, T., and Hirzinger, G., *The DLR lightweight robot: design and control concepts for robots in human environments.* Industrial Robot: An International Journal, 2007. **34**(5): p. 376-385.
4. Ulrich, N. and Kumar, V. *Passive mechanical gravity compensation for robot manipulators.* in *Robotics and Automation, 1991. Proceedings., 1991 IEEE International Conference on.* 1991: IEEE.
5. Townsend, W. and Salisbury, J.K., *Mechanical Design for Whole-Arm Manipulation*, in *Robots and Biological Systems: Towards a New Bionics?*, Dario, P., Sandini, G., and Aebischer, P., Editors. 1993, Springer Berlin Heidelberg. p. 153-164.
6. Sharon, A., Hogan, N., and Hardt, D.E. *High bandwidth force regulation and inertia reduction using a macro/micro manipulator system.* in *Robotics and Automation, 1988. Proceedings., 1988 IEEE International Conference on.* 1988.
7. Pratt, G.A. and Williamson, M.M. *Series elastic actuators.* in *Intelligent Robots and Systems 95.'Human Robot Interaction and Cooperative Robots', Proceedings. 1995 IEEE/RSJ International Conference on.* 1995: IEEE.
8. Sharon, A., Hogan, N., and Hardt, D.E., *The macro/micro manipulator: An improved architecture for robot control.* Robotics and Computer-Integrated Manufacturing, 1993. **10**(3): p. 209-222.
9. Cannon, D.W., Magee, D.P., Book, W.J., and Lew, J.Y. *Experimental study on micro/macro manipulator vibration control.* in *Robotics and Automation, 1996. Proceedings., 1996 IEEE International Conference on.* 1996.
10. Stevens, H. and How, J. *The limitations of independent controller design for a multiple-link flexible macro-manipulator carrying a rigid mini-manipulator.* in *Robotics for Challenging Environments.* 1996.
11. Salisbury, J.K. *Active stiffness control of a manipulator in cartesian coordinates.* in *Decision and Control including the Symposium on Adaptive Processes, 1980 19th IEEE Conference on.* 1980.
12. Hogan, N., *Impedance control: An approach to manipulation: Part illapplications.* Journal of dynamic systems, measurement, and control, 1985. **107**(2): p. 17.
13. Chee-Meng, C., Geok-Soon, H., and Wei, Z. *Series damper actuator: a novel force/torque control actuator.* in *Humanoid Robots, 2004 4th IEEE/RAS International Conference on.* 2004: IEEE.

14. Siciliano, B. and Khatib, O., *Springer handbook of robotics*. 2008: Springer.

15. Yoshida, K., *Engineering test satellite VII flight experiments for space robot dynamics and control: theories on laboratory test beds ten years ago, now in orbit.* The International Journal of Robotics Research, 2003. **22**(5): p. 321-335.

16. Ishikawa, H., Sawada, C., Kawasa, K., and Takata, M. *Stable compliance control and its implementation for a 6 dof manipulator*. in *Robotics and Automation, 1989. Proceedings., 1989 IEEE International Conference on*. 1989: IEEE.

17. Paul, R.P. and Shimano, B. *Compliance and control*. in *Proc. of the 1976 Joint Automatic Control Conference*. 1976.

18. Qian, H.P. and De Schutter, J. *Introducing active linear and nonlinear damping to enable stable high gain force control in case of stiff contact*. in *Robotics and Automation, 1992. Proceedings., 1992 IEEE International Conference on*. 1992.

19. Whitney, D.E., *Force Feedback Control of Manipulator Fine Motions.* J. Dyn. Sys., Meas., Control, 1977. **99**(2): p. 91.

20. Hogan, N., *Impedance Control: An Approach to Manipulation: Part I---Theory.* J. Dyn. Sys., Meas., Control, 1985. **107**(1): p. 7.

21. Neville, H., *Impedance Control: An Approach to Manipulation: Part I---Theory.* Journal of Dynamic Systems, Measurement, and Control, 1985. **107**(1).

22. Seraji, H. and Colbaugh, R., *Force Tracking in Impedance Control.* The International Journal of Robotics Research, 1997. **16**(1): p. 97-117.

23. Jung, S., Hsia, T.C., and Bonitz, R.G., *Force Tracking Impedance Control for Robot Manipulators with an Unknown Environment: Theory, Simulation, and Experiment.* The International Journal of Robotics Research, 2001. **20**(9): p. 765-774.

24. Seul, J., Hsia, T.C., and Bonitz, R.G., *Force tracking impedance control of robot manipulators under unknown environment.* Control Systems Technology, IEEE Transactions on, 2004. **12**(3): p. 474-483.

25. Seraji, H. *Adaptive admittance control: an approach to explicit force control in compliant motion*. in *Robotics and Automation, 1994. Proceedings., 1994 IEEE International Conference on*. 1994.

26. Seraji, H. *Adaptive admittance control: An approach to explicit force control in compliant motion*. in *Robotics and Automation, 1994. Proceedings., 1994 IEEE International Conference on*. 1994: IEEE.

27. Zeng, G. and Hemami, A., *An overview of robot force control.* Robotica, 1997. **15**(05): p. 473-482.

28. Mason, M.T., *Compliance and Force Control for Computer Controlled Manipulators.* Systems, Man and Cybernetics, IEEE Transactions on, 1981. **11**(6): p. 418-432.

29. Raibert, M.H. and Craig, J.J., *Hybrid position/force control of manipulators.* Journal of dynamic systems, measurement, and control, 1981. **103**(2): p. 126-133.

30. Anderson, R.J. and Spong, M.W., *Hybrid impedance control of robotic manipulators.* Robotics and Automation, IEEE Journal of, 1988. **4**(5): p. 549-556.

31. Carelli, R., Kelly, R., and Otrega, R., *Adaptive force control of robot manipulators.* International Journal of Control, 1990. **52**(1): p. 37-54.

32. Singh, S.K. and Popa, D.O., *An analysis of some fundamental problems in adaptive control of force and impedance behavior: Theory and experiments.* Robotics and Automation, IEEE Transactions on, 1995. **11**(6): p. 912-921.

33. Colgate, E. and Hogan, N., *Robust Control Dynamical Interacting Systems.* Int. J. of Contr, 1988. **48**(1).

34. Colgate, J.E. and Hogan, N., *Robust control of dynamically interacting systems.* International Journal of Control, 1988. **48**(1): p. 65-88.

35. Dawson, D., Lewis, F., and Dorsey, J., *Robust force control of a robot manipulator.* The International Journal of Robotics Research, 1992. **11**(4): p. 312-319.

36. Arimoto, S., Kawamura, S., and Miyazaki, F., *Bettering operation of robots by learning.* Journal of robotic systems, 1984. **1**(2): p. 123-140.

37. Jeon, D. and Tomizuka, M., *Learning hybrid force and position control of robot manipulators.* Robotics and Automation, IEEE Transactions on, 1993. **9**(4): p. 423-431.

38. Eppinger, S.D. and Seering, W.P. *Three dynamic problems in robot force control*. in *Robotics and Automation, 1989. Proceedings., 1989 IEEE International Conference on*. 1989: IEEE.

39. Eppinger, S. and Seering, W. *Understanding bandwidth limitations in robot force control*. in *Robotics and Automation. Proceedings. 1987 IEEE International Conference on*. 1987: IEEE.

40. Sharon, A. and Hardt, D. *Enhancement of robot accuracy using endpoint feedback and a macro-micro manipulator system*. in *American Control Conference, 1984*. 1984: IEEE.

41. Khatib, O. *Reduced effective inertia in macro-/mini-manipulator systems*. in *The fifth international symposium on Robotics research*. 1991: MIT Press.

42. Khatib, O., *Inertial properties in robotic manipulation: An object-level framework.* The International Journal of Robotics Research, 1995. **14**(1): p. 19-36.

43. Wernholt, E., *Multivariable frequency-domain identification of industrial robots.* 2007.

44. Lin, J., Huang, Z., and Huang, P., *An active damping control of robot manipulators with oscillatory bases by singular perturbation approach.* Journal of sound and vibration, 2007. **304**(1): p. 345-360.

45. Cheng, X. and Patel, R., *Neural network based tracking control of a flexible macro-micro manipulator system.* Neural Networks, 2003. **16**(2): p. 271-286.

46. Tso, S., Yang, T., Xu, W., and Sun, Z., *Vibration control for a flexible-link robot arm with deflection feedback.* International Journal of Non-Linear Mechanics, 2003. **38**(1): p. 51-62.

47. Pratt, G.A., Willisson, P., Bolton, C., and Hofman, A. *Late motor processing in low-impedance robots: impedance control of series-elastic actuators*. in *American Control Conference, 2004. Proceedings of the 2004*. 2004.

48. Jonathon, W.S. and Richard, F.f.W. *Improvements to Series Elastic Actuators*. in *Mechatronic and Embedded Systems and Applications,*

Proceedings of the 2nd IEEE/ASME International Conference on. 2006.

49. Vallery, H., Ekkelenkamp, R., van der Kooij, H., and Buss, M. *Passive and accurate torque control of series elastic actuators*. in *Intelligent Robots and Systems, 2007. IROS 2007. IEEE/RSJ International Conference on*. 2007.

50. Pratt, G.A. and Williamson, M.M. *Series elastic actuators*. in *Intelligent Robots and Systems 95. 'Human Robot Interaction and Cooperative Robots', Proceedings. 1995 IEEE/RSJ International Conference on*. 1995.

51. Robinson, D.W., Pratt, J.E., Paluska, D.J., and Pratt, G.A. *Series elastic actuator development for a biomimetic walking robot*. in *Advanced Intelligent Mechatronics, 1999. Proceedings. 1999 IEEE/ASME International Conference on*. 1999.

52. Morrell, J.B. and Salisbury, J.K. *Parallel coupled actuators for high performance force control: A micro-macro concept*. in *Intelligent Robots and Systems 95.'Human Robot Interaction and Cooperative Robots', Proceedings. 1995 IEEE/RSJ International Conference on*. 1995: IEEE.

53. Zinn, M., Khatib, O., Roth, B., and Salisbury, J.K., *Actuation methods for human-centered robotics and associated control challenges*, in *Control Problems in Robotics*. 2003, Springer. p. 105-119.

54. Wolf, S. and Hirzinger, G. *A new variable stiffness design: Matching requirements of the next robot generation*. in *Robotics and Automation, 2008. ICRA 2008. IEEE International Conference on*. 2008: IEEE.

55. Quy, H.V., Aryananda, L., Sheikh, F.I., Casanova, F., and Pfeifer, R. *A novel mechanism for varying stiffness via changing transmission angle*. in *Robotics and Automation (ICRA), 2011 IEEE International Conference on*. 2011: IEEE.

56. Schiavi, R., Grioli, G., Sen, S., and Bicchi, A. *VSA-II: A novel prototype of variable stiffness actuator for safe and performing robots interacting with humans*. in *Robotics and Automation, 2008. ICRA 2008. IEEE International Conference on*. 2008: IEEE.

57. Tonietti, G., Schiavi, R., and Bicchi, A. *Design and control of a variable stiffness actuator for safe and fast physical human/robot interaction*. in *Robotics and Automation, 2005. ICRA 2005. Proceedings of the 2005 IEEE International Conference on*. 2005: IEEE.

58. Migliore, S.A., Brown, E.A., and DeWeerth, S.P. *Biologically inspired joint stiffness control*. in *Robotics and Automation, 2005. ICRA 2005. Proceedings of the 2005 IEEE International Conference on*. 2005: IEEE.

59. Petit, F., Chalon, M., Friedl, W., Grebenstein, M., Schaffer, A., and Hirzinger, G. *Bidirectional antagonistic variable stiffness actuation: Analysis, design & implementation*. in *Robotics and Automation (ICRA), 2010 IEEE International Conference on*. 2010: IEEE.

60. Nam, K.-H., Kim, B.-S., and Song, J.-B., *Compliant actuation of parallel-type variable stiffness actuator based on antagonistic actuation*. Journal of mechanical science and technology, 2010. **24**(11): p. 2315-2321.

61. Wolf, S., Eiberger, O., and Hirzinger, G. *The DLR FSJ: Energy based design of a variable stiffness joint*. in *Robotics and Automation (ICRA), 2011 IEEE International Conference on*. 2011: IEEE.

62. Choi, J., Hong, S., Lee, W., Kang, S., and Kim, M., *A robot joint with variable stiffness using leaf springs*. Robotics, IEEE Transactions on, 2011. **27**(2): p. 229-238.

63. Morita, T. and Sugano, S. *Design and development of a new robot joint using a mechanical impedance adjuster*. in *Robotics and Automation, 1995. Proceedings., 1995 IEEE International Conference on*. 1995: IEEE.

64. Tsagarakis, N.G., Sardellitti, I., and Caldwell, D.G. *A new variable stiffness actuator (CompAct-VSA): Design and modelling*. in *Intelligent Robots and Systems (IROS), 2011 IEEE/RSJ International Conference on*. 2011: IEEE.

65. Jafari, A., Tsagarakis, N.G., and Caldwell, D.G. *AwAS-II: A new actuator with adjustable stiffness based on the novel principle of adaptable pivot point and variable lever ratio*. in *Robotics and Automation (ICRA), 2011 IEEE International Conference on*. 2011: IEEE.

66. Kim, B.-S. and Song, J.-B. *Hybrid dual actuator unit: A design of a variable stiffness actuator based on an adjustable moment arm mechanism*. in *Robotics and Automation (ICRA), 2010 IEEE International Conference on*. 2010: IEEE.

67. Erlbacher, E.A., *Force control basics*. Industrial Robot: An International Journal, 2000. **27**(1): p. 20-29.

Appendix: Controller Design for Decoupled Mini Manipulator

When designing force tracking controller, it is assumed that Zero Coupling Impedance criterion has been satisfied. Hence, the mini manipulator has been decoupled from the macro manipulator.

A fourth order linear time invariant system is used to model the mini manipulator with an end-effector, as shown in Figure A.1.
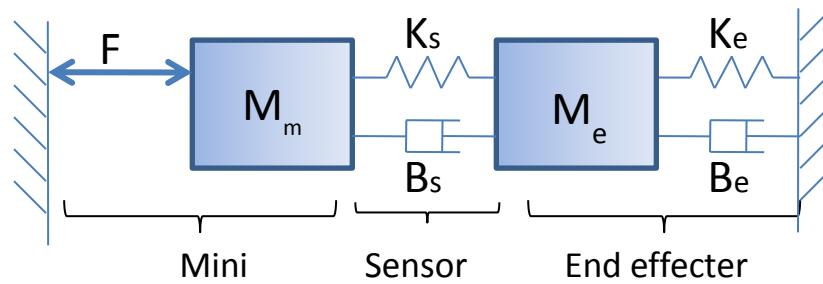

Figure A.1: Model of a mini manipulator with end effector

In this figure, M_e, B_e and K_e represent the mass of the end effector, damping and stiffness of the coupling between the robot and the environment, respectively. The objective of the controller design is to design a state feedback controller "*reg*" as shown in Figure A.2, such that the output "*y*" will track the input reference "*r*", with the presence of disturbance "*w*" and noise "*v*".
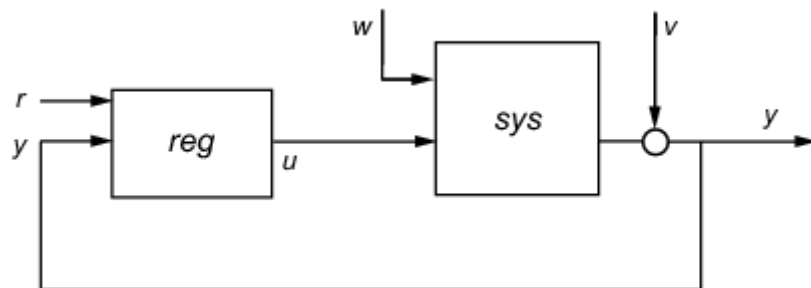

Figure A.2: Schematic of a feedback system

93

The "sys" in this figure is the model derived based on Figure A.1. It can be written as:

$$\dot{x} = Ax + Bu + Gw$$

$$y = Cx + Du + Hw + v$$

where,

$$A = \begin{bmatrix} 0 & 1 & 0 & 0 \\ -\dfrac{K_S}{M_m} & -\dfrac{B_S}{M_m} & \dfrac{K_S}{M_m} & \dfrac{B_S}{M_m} \\ 0 & 0 & 0 & 1 \\ \dfrac{K_S}{M_e} & \dfrac{B_S}{M_e} & -\dfrac{K_S + K_e}{M_e} & -\dfrac{B_S + B_e}{M_e} \end{bmatrix}$$

$$B = \begin{bmatrix} 0 & \dfrac{1}{M_m} & 0 & 0 \end{bmatrix}$$

$$C = \begin{bmatrix} K_S & 0 & -K_S & 0 \end{bmatrix}$$

$$D = 0$$

$$H = \begin{bmatrix} 0 & 0 \end{bmatrix}$$

$$G = \begin{bmatrix} 0 & 0 \\ 0 & 0 \\ 0 & 0 \\ \dfrac{K_e}{M_e} & \dfrac{B_e}{M_e} \end{bmatrix}$$

The system was first discretized with a sampling frequency *1ms*. The controller design consists of two parts: a tracking controller and an observer.

For the tracking controller, a Linear-Quadratic-Integral (LQI) control is used. The control law is to minimize the following cost function:

$$J(u) = \sum_{n=0}^{\infty} (z^T Q z + u^T R u)$$

where Q and R are the weighting matrices.

For the observer design, Kalman filter was used. With noise covariance data

$$E(w[n]w[n]^T = Q, E(v[n]v[n]^T), E(w[n]v[n]^T) = N$$

The estimator has the following state equation:

$$\hat{x}[n+1|n] = A\hat{x}[n|n-1] + Bu[n] + L(y[n] - C\hat{x}[n|n-1] - Du[n])$$

The gain matrix L is derived by solving a discrete Riccati equation to be

$$L = (APC^T + \bar{N})(CPC^T + \bar{R})^{-1}$$

where

$$\bar{R} = R + NH + N^T H^T + HQH^T$$

$$\bar{N} = G(QH^T + N)$$

The observer gain was calculated using the toolbox from MATLAB.